Unsymmetrical (1-lambda3)-1,2,4,6-thiatriazinyls with aryl and trifluoromethyl substituents: synthesis, crystal structures, EPR spectroscopy and voltammetry

Journal:	*Inorganic Chemistry*
Manuscript ID:	ic-2011-003996.R1
Manuscript Type:	Article
Date Submitted by the Author:	n/a
Complete List of Authors:	Boere, Rene; University of Lethbridge, Chemistry and Biochemistry Roemmele, Tracey; University of Lethbridge, Chemistry and Biochemistry Yu, Xin; University of Lethbridge, Chemistry and Biochemistry

Unsymmetrical 1λ³-1,2,4,6-thiatriazinyls with aryl and trifluoromethyl substituents: synthesis, crystal structures, EPR spectroscopy and voltammetry

René T. Boeré, Tracey L. Roemmele and Xin Yu*

Department of Chemistry and Biochemistry, University of Lethbridge, Lethbridge, AB Canada T1K 3M4

RECEIVED xxx

Keywords

Free radical; thiatriazinyl; electron paramagnetic resonance; cyclic voltammetry; ionization potential; electrochemistry; DFT calculations.

* To whom correspondence may be addressed. E-mail: boere@uleth.ca. Tel.: (403) 329-2045. Fax.: (403)329-2057.

Abstract

A general synthetic route to 3-trifluoromethyl-5-aryl-1λ^3-1,2,4,6-thiatriazinyl radicals was developed. X-ray structures were obtained for all five neutral radicals and show that they exist in the solid state as co-facial dimers linked by S···S contacts. X-ray structures were also obtained for two of the precursor chlorothiatriazines along with several aryl N-imidoylamidines, *p*-methoxybenzamidine and N-chlorosulfonyl-N,N'-benzamidine. Cyclic voltammetric studies were performed on the $[R_2C_2N_3S]^{\bullet}$ radicals in CH_3CN and CH_2Cl_2 with $[^nBu_4N][PF_6]$ as the supporting electrolyte under vacuum in an all-glass electrochemical cell. The results provide quasi-reversible formal potentials for the $[R_2C_2N_3S]^{-/0}$ process in the range of −0.61 to −0.47 V, irreversible peak potentials for the $[R_2C_2N_3S]^{0/+}$ process from 0.59 to 0.91 V at lower concentrations, and the appearance of a second, reversible oxidation process from 0.69 to 0.94 V at higher concentrations (versus the $Fc^{0/+}$ couple; Fc = Ferrocene). This behavior was indicative of monomer-dimer equilibrium in solution as ascertained from digital models of the voltammograms. There is a small but measurable trend in both the oxidation and reduction potentials with varying remote aryl substituents. EPR spectra were obtained for all five neutral radicals in CH_2Cl_2 solutions, which confirm concentration of the unpaired electron density on the heterocyclic core. Trends were also seen in the hyperfine splitting constants a_N with varying remote aryl substituents. Calculations were performed for all three oxidation states of the $[R_2C_2N_3S]^{-/\bullet/+}$ monomeric rings; the resulting theoretical redox energies correlate well with solution phase voltammetric data.

Introduction

There is strong continuing interest in the synthesis and structural chemistry of sulfur-nitrogen-carbon heterocyclic free radicals, with an emphasis on applications to the design of molecular conductors and molecular magnetism.[1] This interest extends to transition-metal coordination complexes that incorporate such radicals as ligands – including spin-active ligands.[2] We have contributed to the electrochemical characterization of the redox properties of this whole class of compounds, and in particular have characterized by solution electrochemistry the influence of aryl ring substituents on 5-aryl-1,2,3,4-dithiadiazolyls.[3]

In order to extend our approach to a new class of C,N,S radicals we have developed a general synthetic route to the asymmetrically substituted 3-trifluoromethyl-5-aryl-1λ^3-1,2,4,6-thiatriazinyls (Chart 1). We recently communicated the utility of such thiatriazinyl radicals as novel π-donor ligands to the organometallic moiety $CpCr(CO)_2$;[4] here we elaborate the chemistry of these heterocyclic free radicals, including structural characterization of novel intermediates and several final products in the solid state by X-ray crystallography, solution EPR spectroscopy, and a detailed electrochemical investigation interpreted in light of DFT calculations.

Chart 1. The 3-trifluoromethyl-5-aryl-1λ^3-1,2,4,6-thiatriazinyls

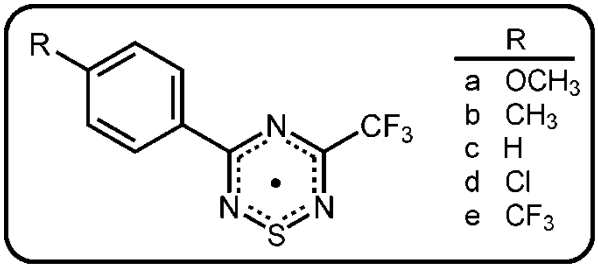

Results and Discussion

A primary goal of this work was the development of a more general route to 1,2,4,6-thiatriazinyl radicals which would allow for modification of the exocyclic substituents (Scheme 1). Various methods have been attempted to prepare both symmetric- and asymmetrically substituted thiatriazines.[5] Amidines have been reported to react with $S_3N_3Cl_3$ to form 1-chloro-1,2,4,6-thiatriazines.[5e,f] In this work, we first converted amidines into N-imidoylamidines and find that these, when passivated as hydrochlorides, afford 1-chloro-1,2,4,6-thiatriazines by direct reaction with sulfur dichloride in high yield.[5b,6] An established literature procedure was used to prepare the *para*-substituted benzamidine hydrochlorides,[7] but the free bases **1a–e** have not previously been reported. Full characterization of these useful intermediates is provided in the experimental section and the crystal structure of **1a** is presented in Figure S1.

Scheme 1. Synthetic route to the 3-trifluoromethyl-5-aryl-1,2,4,6-thiatriazines.

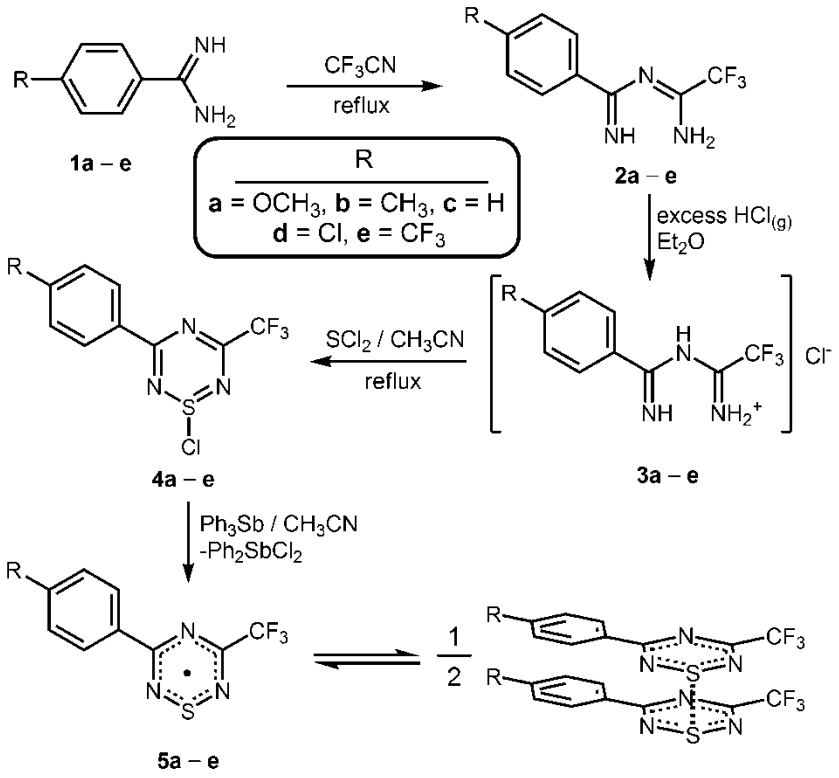

Aryl N-imidoylamidines. In contrast to amidine chemistry, aryl N-imidoylamidines have received less attention, although several preparative routes have been reported.[8] In this work it was found that direct reaction of trifluoroacetonitrile with the free-base amidines gave the desired imidoylamidines in high yields in accordance with the report by Schaeffer.[9] The colorless sublimed products were found to be pure by ^{1}H and ^{13}C NMR spectroscopy, MS and elemental analysis. The expected signals for hydrogen atoms attached to carbon were observed in ^{1}H NMR spectra recorded in $CDCl_3$ (Table S1). Three separate NH peaks are also observed (Figure S2), indicating non-equivalency of the hydrogen atom environments. The signals resonating around 11 and 6.7 ppm are noticeably broadened compared to the one near 9 ppm, indicating a higher rate of exchange between the former.

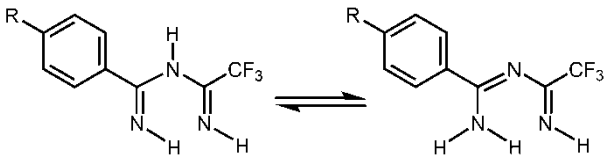

These results are consistent with either of the above tautomers, *i.e*. either with hydrogen attached to three different N atoms as at left, or as at right with one imino and two amino hydrogen atoms in which the latter are non-equivalent due to strong intramolecular hydrogen bonding. The solid-state structure (Figure 1) shows the dominance of the imino-amino tautomer, but also shows H-bonding of H1B to the backbone nitrogen atom N5 which, if exchange occurred, would interconvert it to the diimine. In the ^{13}C NMR spectra, seven distinct carbon peaks (Table S2) were observed, which are attributable to the seven different types of carbon atoms in **2a–e**.

X-ray structures of imidoylamidines are rare. In fact, no structures of unsubstituted imidoylamidines have been reported in the Cambridge Crystal Structure Database (CSD version 5.31 updated to Nov. 2009), and only one structure of an imidoylamidinium salt is known (with $[Se_2Cl_{10}]^{2-}$ as the counter ion).[10] However, crystal structures of imidoylamidinate anions

coordinated to various metals are known,[11] and the structure of the related parent biguanide has been reported.[12] Colorless crystalline plates of **2a**, **2c**, and **2e** were grown by sublimation in a three-zone tube furnace under dynamic vacuum and their structures were determined at low temperature by X-ray diffraction. All three crystal structures contain two crystallographically independent molecules which display very similar inter- and intramolecular hydrogen bonding [13] as shown by dashed lines in Figure 1 for compound **2c** as a representative example. The atom numbering scheme is the same for all three structures to facilitate comparison; the H-bonding data for **2a**, **2c**, and **2e** are discussed in the Supplementary Information (Table S3).

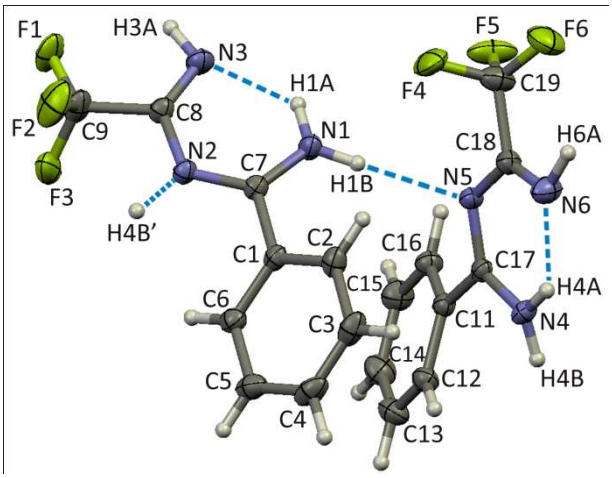

Figure 1. Thermal ellipsoids (30%) plot showing the two independent hydrogen-bonded molecules of **2c** as found in the crystal at −100(2) °C along with an additional H4B' atom to indicate how the chain propagates in the lattice. The H1B—N5 and H4B'—N2 bonds can be viewed as incipient tautomerism leading to the diimine isomer. Only the principal components of the disordered CF_3 groups are shown for clarity. (Figures S3 and S4 are plots of **2a** and **2e**.)

The average bond lengths and angles determined from all six crystallographically independent molecules of **2a**, **2c**, and **2e** are shown in Figure 2. This clearly shows that C8–N3 is short, characteristic of an imine, while C7–N1 and C7–N2 are identical within e.s.d. and of intermediate length, characteristic of a highly delocalized amidine. Aryl/CF_3 substitution

therefore leads to a rather unsymmetrical imidoyl amidine geometry, approximating to an imino-substituted amidine.

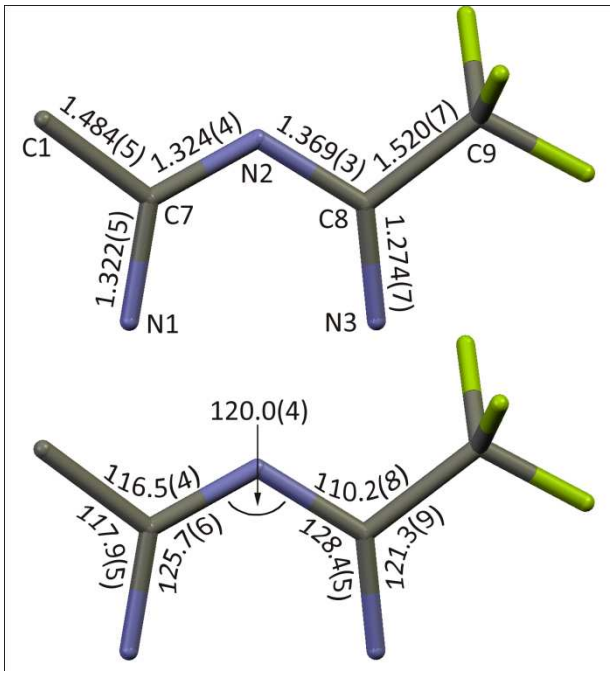

Figure 2. Average bond lengths (Å, top) and angles (°, bottom) from crystal structures of the six independent imidoylamidine molecules found in **2a**, **2c**, and **2e**. Errors are standard deviations.

Conversion to N-imidoylamidine hydrochlorides. Direct reaction between **2c** and sulfur dichloride to form **4c** resulted in low yields of product as an intractable oil that proved hard to purify. However, pacifying the reactive nitrogen base with HCl increased the yield of **4c** significantly and afforded a low-melting solid. Therefore all the imidoylamidines were converted with HCl(*g*) in dry diethyl ether to the corresponding hydrochloride salts **3a–e** which precipitated as white, insoluble solids that were characterized by infrared spectroscopy. Each adduct has a unique fingerprint region but similar broad bands in the 3300 cm^{-1} range characteristic for NH stretches involved in hydrogen bonding.

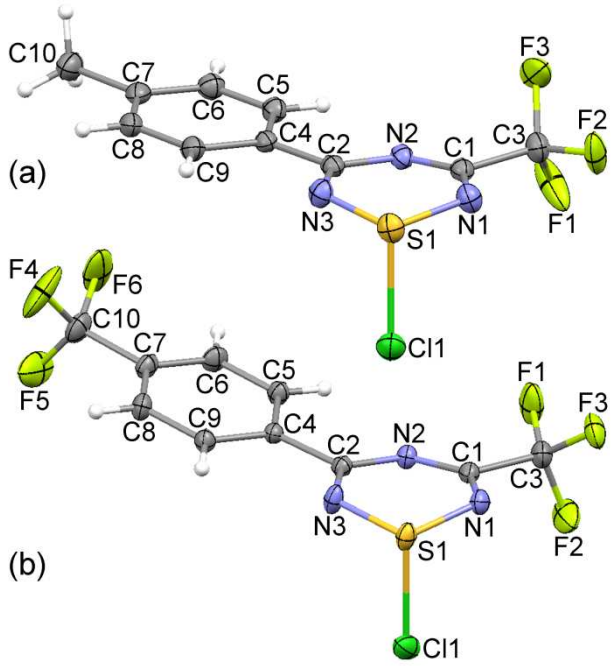

Figure 3. Thermal ellipsoids (30%) plots with atom numbering schemes showing the molecular structures of (a) **4b** and (b) **4e** as they are found within the crystal lattices at −100(2) °C. Only the principal components of the disordered CF_3 groups are shown.

1-chloro-3-trifluoromethyl-1,2,4,6-thiatriazines. An excess of SCl_2 was used to ensure the completion of the reaction of the imidoylamidine hydrochloride salts **3a–e** to the 1-chloro-thiatriazines **4a–e**. Crude yields were typically high (>80%), and these materials were used without further purification in the synthesis of the radicals. ^{1}H NMR spectra (Table S4) confirmed ring formation through absence of NH signals and only the phenyl and *para*-substituted hydrogen atoms appear in the spectra between 7.0 and 8.6 ppm. The signals of H_1, *meta* to the thiatriazine core, are weakly affected by heterocycle formation, shifting only ~0.10 ppm downfield compared to the imidoylamidines. However the signals of H_2, *ortho* to the heterocyclic core, are shifted downfield by ~0.60 ppm. This is diagnostic for formation of a thiazyl ring; for example, the chemical shifts of the *ortho* hydrogen atoms in comparably substituted 1,5-dithia-2,4,6,8-tetrazocine heterocycles are very similar to those of **4a–e**.[14] ^{13}C NMR was not obtained due to instability of the compounds to hydrolysis. However, extremely

moisture-sensitive X-ray quality crystals could be grown for **4b** and **4e** from acetonitrile solutions at −35 °C and the crystal structures were determined at low temperature. These structures confirm the formation of the six-membered ring with an almost perpendicular S–Cl bond, as shown in Figure 3. The C_2N_3 atoms are co-planar (maximum deviation 0.047(1) Å) with the sulfur atoms tipped slightly out of the plane (0.288(2) Å **4b** and 0.323(2) Å **4e**). The inter-atomic distances in **4b** and **4e** are quite comparable. Averaged bond lengths and angles from the two structures are presented in Figure 4. The phenyl rings in both structures have average C–C bond lengths of 1.389(10) Å and are essentially co-planar with the heterocyclic core. The packing of **4e** shows regular stacks aligned with the crystallographic *c* axis without any significant short contacts but **4b** has typical $S(\delta^+)$–$N(\delta^-)$ short contacts between pairs of rings (Figure S5).[1d]

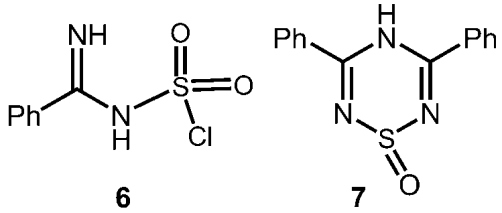

6 **7**

The sensitivity of **4** to moisture is highlighted by the hydrolysis of **4c** from adventitious H_2O in CH_3CN to give **6** as colorless blocks suitable for X-ray analysis (Figures S6-8). The hydrolysis product **6** surprisingly retains the S–Cl bond (unlike $\{PhCN\}_2\{NH\}S{=}O$, **7**),[15] but a $CF_3CH{=}NH$ moiety is eliminated while the sulfur is converted to oxidation state VI.

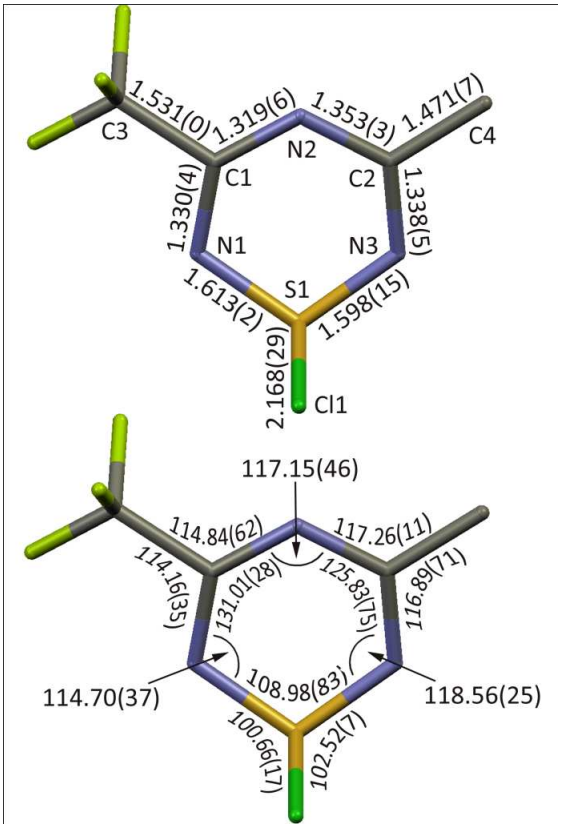

Figure 4. Average bond lengths (Å, top) and angles (°, bottom) with standard deviations from crystal structures of the 1-chlorothiatriazines **4b** and **4e**.

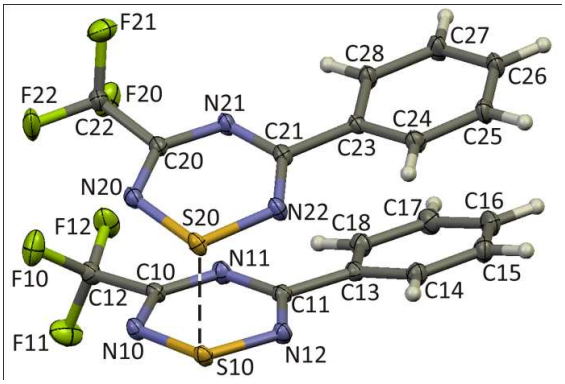

Figure 5. Thermal ellipsoids (30%) plot and atom numbering scheme showing the solid-state face-to-face and head-to-head dimerization of **5c**, which comprises the asymmetric unit in the lattice at −100(2) °C. The dashed line indicates the close contact between sulfur atoms, for which the S10···S20 distance is 2.625(1) Å. The structure of **5a** (Figure S9) is very similar with an S10···S20 distance of 2.6370(3) Å.

5-Aryl-3-trifluoromethyl-1,2,4,6-thiatriazinyls. Several reducing agents have been used previously to effect the reductive elimination of chloride ion from 1-chloro-1,2,4,6-thiatriazines. In early work, sodium verdazyl was often used.[5] Here we employed triphenylantimony because of its general utility in the reduction of thiazyl halides.[5e,f] A half-molar ratio of solid triphenylantimony was added by a solids-addition bulb to acetonitrile solutions of **4a–e** after careful removal of oxygen via freeze-thaw-degassing. Reduction to the radical was immediate in all cases, as the solution turned from a clear dark red to a dark purple (almost black) solution with precipitation of some solid. Precipitated crude products were purified by sublimation in a three zone tube furnace and produced X-ray quality plates of the radicals **5a–e**. Diffraction data was obtained at −100±2 °C and the structures solved and refined at this temperature; however in the case of **5b** persistent high R-factors were encountered and hence the structure was re-determined at RT with better results. Formation of a superlattice is suspected at the lower temperature. In each case, the solid-state structures display the same face-to-face and head-to-head (presumably diamagnetic) dimers obtained previously for bis(3,5-diphenyl-1,2,4,6-thiatriazinyl) **8**,[5e] despite the presence of the bulky CF_3 groups. For both **5a** and **5c**, one kind of crystallographically independent dimer is observed in their crystal lattices (Figure 5). For **5b** and **5d**, two sets of wedge-shaped dimers are found stacked back-to-front in the lattice (Figure 6).

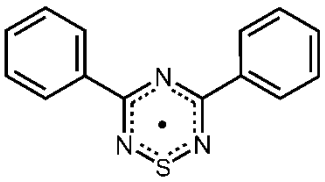

8

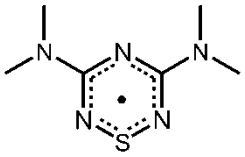

9

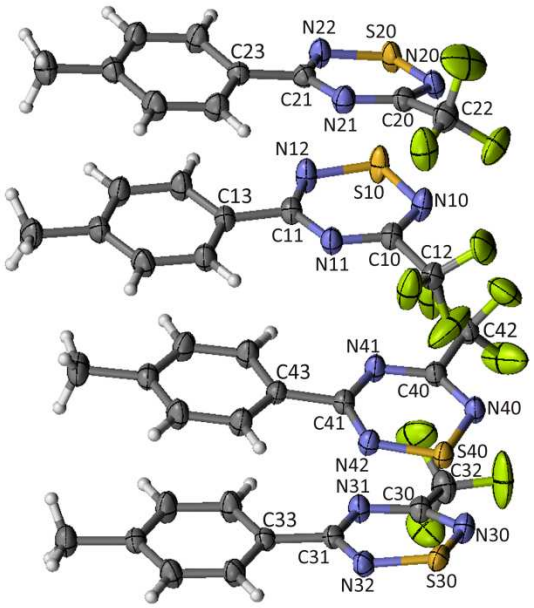

Figure 6. Thermal ellipsoids (30%) plot with atom numbering scheme showing the molecular structure of **5b** found within the crystal lattice at 23(2) °C. Four crystallographically independent molecules form into two distinct dimers. The S10···S20 distance is 2.684(1) Å and the S30···S40 distance is 2.6515(8) Å. A very similar arrangement is found in the lattice for **5d** (Figure S10) with S10···S20 and S30···S40 distances of 2.659(1) Å and 2.635(1) Å, respectively.

The shortest contact between C_2N_3S rings is always through the sulfur atoms, with an average distance of 2.643(21) Å. This is longer than a normal disulfide linkage but within range of other known thiatriazinyls such as **8**,[5e] whose shortest contact is 2.666(3) Å and 3,5-bis(dimethylamino)-1,2,4,6-thiatriazinyl **9**, whose shortest contact is again through the sulfur atoms at 2.5412(8) Å.[16] Average bond lengths and angles were calculated for the entire series **5a–e**, and the results are presented in Figure 7. The average S–N bond length over both bonds (SX0–NX0 and SX0–NX2, X=1–4) is 1.633(10) Å, which is shorter than the S–N single bond in $S_4N_4H_4$ (1.665 Å), and longer than the NAS bond in S_4N_4 (1.616 Å). The average C–N bond length in the ring is 1.332(16) Å, longer than an average C=N double bond (~1.270(15) Å),[17] and shorter than an average C–N single bond (1.472(5) Å). A typical heterocyclic CAN bond length is approximately 1.352(5) Å.[17] The asymmetric substitution pattern seen in **5a–e** allows for a

comparison of the bond lengths and angles with the symmetric diphenyl and dimethylamino analogues **8** and **9**. The C–N bond lengths are very similar, as are the S–N bond lengths with only the S–N bond closest to the CF_3 group averaging slightly longer than in **8**. The bond angles within the heterocyclic core are significantly less symmetrical with asymmetric substitution on the ring. Thus, the internal angles at the carbon of attachment of the CF_3 group are noticeably larger than in **8**.[5e] Correspondingly the average internal angles at sulfur are noticeably smaller than those in **8**.

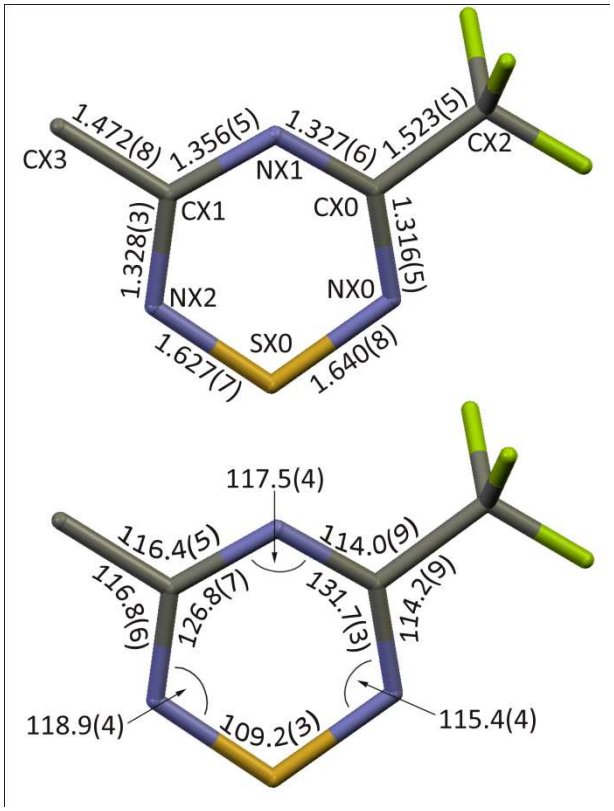

Figure 7. Comparison of bond lengths (Å, top) and angles (°, bottom) in 1,2,4,6-thiatriazinyls determined from five crystal structures. A common numbering scheme was used among crystallographically independent monomers (X = 1–4). The average intradimer short S···S contact distance is 2.643(21) Å.

In all five structures, the many independent C_2N_3S rings are almost planar (deviations in the range of 0.003 – 0.054 Å). The mean planes of each set of dimers are tipped towards each other such that the shortest contacts are always S···S, and the planes intersect with angles between normals in the range of 5–17°. Three distinct packing modes are found in the solid state amongst these five thiatriazinyl structures. In **5a** and **5c** there is a simple 2 + 2 mode, wherein two dimeric units (Figure 6) are centrosymmetrically associated through sideways $S(\delta^+)\cdots N(\delta^-)$ short contacts. However, the pairs of dimers are essentially co-planar in the case of **5a** (Figure S11), while in **5c** they are almost exactly out of register (Figure S12). These tetrameric units are isolated from other such units in the crystal lattice. Sideways S···N contacts range from 2.941(1) to 3.341(1) Å. In **5b** and **5d** there are four independent molecules that form two sets of typical dimers. However, the two sets of dimers are each associated with each other through $S(\delta^+)\cdots N(\delta^-)$ short contacts (Figures S13, S14). Interestingly, in each structure one such tetrameric unit is closer to the co-planarity that is observed in **5a**, while a second is out-of-register as in **5c**. The variation in sideways S···N contacts observed in these two structures is larger, from 3.025(2) to 3.551(2) Å. The final example is **5e** (Figure 8) for which four independent thiatriazinyls form *one* tetramer in the asymmetric unit. The sideways $S(\delta^+)\cdots N(\delta^-)$ interactions for this structure range from 3.034(2) to 3.199(2) Å and the association is out-of-register as in **5c**. This structure is particularly interesting because there is a further interaction between neighboring S40, N40 rings leading to a partial overlap of two adjacent tetramers (Figures S15, S16). Shortest atomic contacts are S40···C41' at 3.447(2) Å. This structure contains the most extensive set of interactions between thiatriazinyls ever reported but, although eight radicals are thereby associated, the interactions do not extend throughout the lattice.

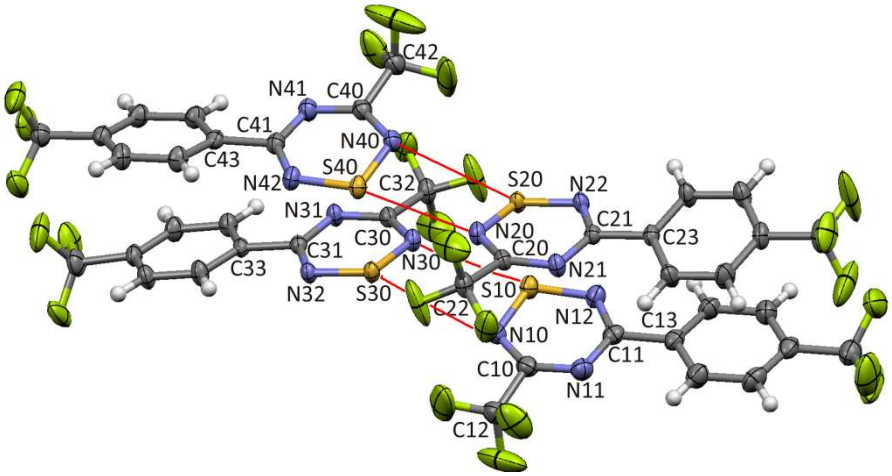

Figure 8. Thermal ellipsoids (30%) plot with atom numbering scheme showing the molecular structure of **5e** found within the crystal lattice at −100(2) °C. Four crystallographically independent molecules form into two distinct dimers with intra-dimer S10···S20 and S30···S40 distances of 2.6237(9) Å and 2.6255(8) Å, respectively. These dimers associate into a single tetrameric set through $S(\delta^+)$–$N(\delta^-)$ interactions (shown in red). The S20···N30 and S30···N20 distances are 3.169(2) Å and 3.199(2) Å, while S40···N20 and S10···N30 distances are 3.082(2) Å and 3.034(2) Å, respectively. The rings belonging to the dimers are out of register with each other as indicated by the different interaction lengths.

EPR Spectroscopy. The 1,2,4,6-thiatriazinyls are members of a larger class of unsaturated C,N,S compounds for which stable neutral free radicals can be generated.[1a] In this work, the trifluoromethyl thiatriazinyls **5a–e** were generated by dissolving high purity sublimed crystals in dichloromethane inside vacuum sealed EPR tubes. In all cases, well-defined EPR spectra with high signal-to-noise ratios were obtained displaying complex splitting patterns due to coupling to the three nonequivalent nitrogen nuclei in the thiatriazinyl ring along with three equivalent fluorine atoms of the directly attached CF_3 groups which cause each subpeak to split into small quartets. Excellent agreement was obtained between the experimental and simulated EPR spectra for all five compounds (Figure 9 shows a typical example; see also Figures S17-S20). However, the assignment of the hyperfine splitting (hfs) to the three nitrogen atoms required input from quantum calculations. The electronic structures of **5a–e** were determined from UB3LYP/6–31G(d) hybrid-DFT calculations (using Gaussian 98)[18] for the monomeric

radicals in the gas phase. Full geometry optimization was undertaken for each structure and frequency calculations confirmed the geometries to be minima. The experimental and calculated hfs constants are compiled in Table 1.

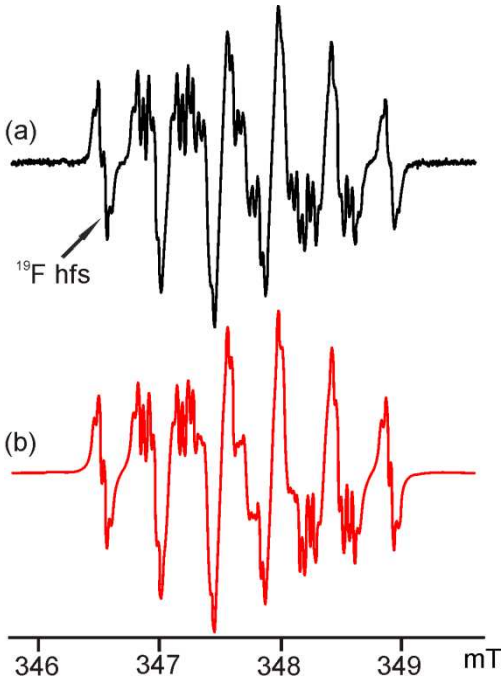

Figure 9. (a) Experimental and (b) simulated EPR spectra of **5d** in CH_2C1_2 at 18 °C, modulation amplitude 0.01 mT, modulation frequency 100 kHz. Simulations were performed with WinSim (version 0.98, 2002) [19] software using a 100% Lorentzian lineshape.

The unpaired electron occupies a π-SOMO which is delocalized over the heterocyclic core, a representation of which is shown in Figure 10 using **5b** as a typical example. The largest coefficient is on sulfur, but there is considerable unpaired electron density on each of the three nitrogen atoms and to a lesser extent on the carbon atoms in the ring. There are small coefficients on the fluorine atoms of the directly bound CF_3 group, as well as on the phenyl carbon atoms. There is, however, no experimental evidence for hyperfine coupling to the aryl ring hydrogen atoms and hfs from ^{19}F is likely to result mostly from spin polarization.

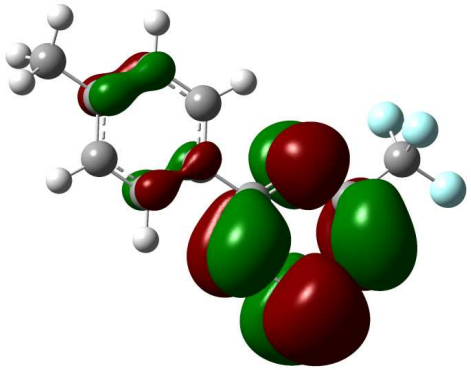

Figure 10. Kohn-Sham isosurface of the π-SOMO of **5b** from a UB3LYP/6–31G(d) calculation.

In each case there are three distinct a_N values, except for **5a** where two of the values are nearly identical. (Such accidental degeneracy of symmetry-non-equivalent nitrogen atoms has been reported for 3,5-bis(4-methoxyphenyl)-1,2,4,6-thiatriazinyl, for which all three nitrogen atoms appear to have identical hfs of 0.3927 mT).[20] The trends in the hfs with the remote *para* R-substituents on the phenyl ring are quite convincing. As controls we can cite the powerfully π-electron donating NMe_2 groups directly bound in 3,5-bis(dimethylamino)-1,2,4,6-thiatriazinyl **9**,[20] in which $a_{N2} = a_{N6}$ is twice as large as a_{N4}. Conversely, with two powerfully electron withdrawing CF_3 and CCl_3 groups directly attached in 3,5-bis(trifluoromethyl)-1,2,4,6-thiatriazinyl[24] and 3,5-bis(trichloromethyl)-1,2,4,6-thiatriazinyl,[5d,20b] a_{N4} is found to be larger by about 40% than a_{N2} and a_{N6}. The hyperfine splitting constants of **5a–e** are intermediate between these extremes, as expected. Nevertheless as the remote *para* substituents become more electron donating (from **e** to **a**), the a_{N6} value increases due to greater spin density on the N=S=N region of the ring. The spin density on the remaining nitrogen atoms decrease correspondingly, such that the sums of a_N values are found to be 1.190(5) for all five exemplars (standard deviation). Moreover, the variation in a_N values smoothly follow Hammet σ(p) coefficients (Figure S21). Thus EPR spectroscopy proves to be a very sensitive probe of the unpaired spin density on

thiatriazinyl rings. The directly bound CF_3 group causes further splitting of the EPR signals into quartets, implying rotational averaging of the three fluorine nuclei, but the a_F values are small. Similar a_F values have been reported for 3,5-bis(trifluoromethyl)-1,2,4,6-thiatriazinyl.[20]

Table 1. Experimental and calculated[a] EPR spectroscopic data for **5a–e**.

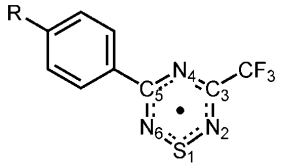

	a_{N2}		a_{N4}		a_{N6}		$a_{C3,5(avg)}$		a_{S1}	$a_{F(avg)}$	
cmpd	Expt (mT)	Calc (mT)	Expt (mT)	Calc (mT)	Expt (mT)	Calc (mT)	Expt (mT)	Calc (mT)	Calc [b] (mT)	Expt [c] (mT)	Calc (mT)
5a	0.310	0.297	0.435	0.409	0.436	0.460	0.705	–0.518	0.555	0.032	–0.063
5b	0.320	0.309	0.444	0.418	0.429	0.443	0.545	–0.531	0.555	0.036	–0.068
5c	0.325	0.313	0.445	0.422	0.425	0.437	0.675	–0.536	0.555	0.039	–0.069
5d	0.324	0.313	0.446	0.422	0.419	0.433	0.572	–0.534	0.558	0.040	–0.068
5e	0.332	0.319	0.454	0.428	0.404	0.423	0.666	–0.542	0.558	0.044	–0.070

[a] From UB3LYP calculations, multiplied by a scaling factor of 0.81. [b] Sulfur hfs was not observable due to the very small natural abundance of this isotope. [c] Hfs is to the three fluorine atoms in the directly bound CF_3 group.

Voltammetry. The study of redox active heterocycles requires handling of low concentrations of free radicals in solution which are highly susceptible to decomposition from oxygen or hydrolysis by adventitious moisture. An all-glass electrochemical cell sealed under vacuum which has been described previously was used in this work to avoid interferences.[21] Cyclic voltammetric studies were performed in both CH_2Cl_2 and CH_3CN solutions at temperatures of 20±2 °C and scan rates of $\nu = 0.1 - 10$ V s^{-1}. The voltammetric results at full concentration are summarized in Table 2.

Table 2. Voltammetry Data for compounds **5a–e** in CH_3CN and CH_2Cl_2 at full concentration. [a]

Cmpd	Conc. (mM)	E_p^{c1} (V)	E_p^{a1} (V)	E_m (V) [b]	E_p^{a2} (V) [c]	E_p^{c3} (V)	E_p^{a3} (V)	E_n (V) [d]	E_{cell} (V) [e]
CH_3CN solns with 0.1 M [^{n}Bu$_4$N][PF_6] supporting electrolyte									
5a [f]	7.3	–0.64	–0.51	–0.58	0.59	0.62	0.76	0.69	1.27
5b	6.3	–0.60	–0.51	–0.56	0.67	0.71	0.81	0.76	1.32
5c [g]	10.0	–0.60	–0.48	–0.54	0.73	0.74	0.89	0.82	1.36
5d [h]	11.0	–0.55	–0.45	–0.50	0.74	0.78	0.90	0.84	1.34
5e [i]	6.7	–0.51	–0.42	–0.47	0.84	0.85	0.96	0.91	1.38
CH_2Cl_2 solns with 0.4 M [^{n}Bu$_4$N][PF_6] supporting electrolyte									
5a [j]	10.0	–0.66	–0.55	–0.61	0.66	0.66	0.78	0.72	1.33
5b	8.7	–0.66	–0.54	–0.60	0.71	0.74	0.86	0.80	1.40
5c [k]	11.0	–0.64	–0.52	–0.58	0.76	0.78	0.92	0.85	1.43
5d [l]	9.0	–0.63	–0.47	–0.55	0.81	0.79	0.98	0.89	1.44
5e [m]	6.7	–0.55	–0.44	–0.50	0.91	0.87	1.01	0.94	1.44

[a] Reported vs. $Fc^{0/+}$ on a Pt working electrode, ν = 0.2 V s^{-1}, T = 20±2 °C. [b] $E_m = [E_p^{a1} + E_p^{c1}]/2 \approx E^{0/}$. [c] Irreversible wave observed. [d] $E_n = [E_p^{a3} + E_p^{c3}]/2 \approx E^{0/}$ [e] $E_{cell} = E_n - E_m$. [f] IRR oxidation wave at 1.75 V. [g] IRR reduction wave at −1.87 V. [h] IRR reduction wave at −1.80 V. [i] IRR reduction wave at −2.07 V. [j] IRR oxidation wave at 1.84 V. [k] IRR reduction wave at −1.78 V. [l] IRR reduction wave at −1.76 V. [m] IRR reduction wave at −1.65 V.

The 1,2,4,6-thiatriazinyls are very soluble in dichloromethane and moderately soluble in acetonitrile. In all cases the electrochemical response changed with analyte concentration, with the appearance of a new redox couple at more positive potentials as the solution became more concentrated (Figure 11). This change correlated with the color of the solution (from pale yellow to deep brown) as more analyte was added. From the current response of the CV data, the active concentrations from voltammetry taken when the solutions were pale yellow are estimated to be 10 – 20 times lower than the nominal concentration values listed in Table 2. At very low concentration (evidenced by a pale yellow color in solution) the peaks associated with reduction

of neutral material ($E_p^{c1/a1}$) have a large return wave over a range of scan rates, while that for oxidation (E_p^{a2}) shows no return wave at scan rates up to 10 V s^{-1}.

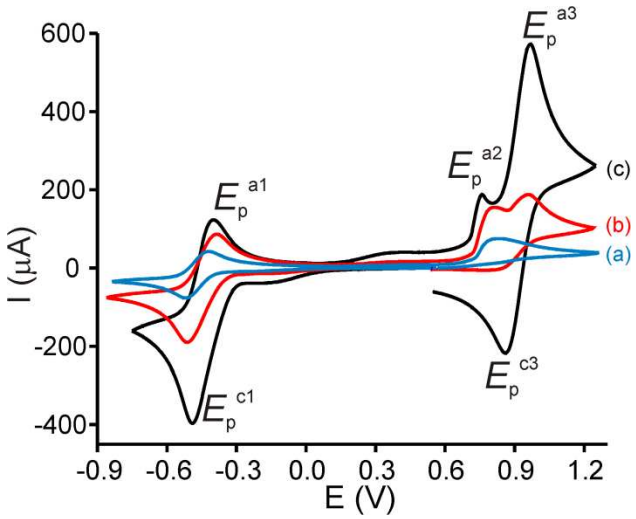

Figure 11. Overlapping CV's of the redox couples of **5e** in CH_3CN solution (0.1 M [^{n}Bu$_4$N][PF_6]) at: a) dilute concentration (blue), b) moderate concentration (red), and c) high concentration (black).

As the concentration increased (evidenced by development of brown color), a second oxidation process ($E_p^{a3/c3}$) appeared at a more positive potential and in the limit this process displayed return waves of comparable peak current height (I_p^{c3}/I_p^{a3} = 0.95 (**5a**), 0.96 (**5b**), 0.89 (**5c**), 0.93 (**5d**), 0.93 (**5e**)) under all the conditions used in this study. Figure 11 shows overlapping traces at three different concentrations of **5e**. At the highest concentration process E_p^{a2} is just a residual shoulder on the reversible wave at more anodic potential. Much the same thing occurred for all five compounds in both solvents. In each case, there was only a single potential associated with reduction of neutral material at all concentrations studied.

Table 3. CV Data for compounds **5a–e** in CH_3CN and CH_2Cl_2 at low concentration. [a]

Cmpd	E_p^{c1} (V)	E_p^{a1} (V)	E_m (V) [b]	E_p^{a2} (V) [c]	E_{cell} (V) [e]
CH_3CN solns with 0.1 M [^{n}Bu$_4$N][PF_6] supporting electrolyte					
5a	–0.60	–0.54	–0.57	0.59	1.13
5b	–0.59	–0.52	–0.56	0.67	1.19
5c	–0.57	–0.50	–0.54	0.73	1.23
5d	–0.53	–0.46	–0.50	0.74	1.20
5e	–0.51	–0.41	–0.46	0.84	1.25
CH_2Cl_2 solns with 0.4 M [^{n}Bu$_4$N][PF_6] supporting electrolyte					
5a	–0.54	–0.47	–0.51	0.66	1.13
5b	–0.53	–0.47	–0.50	0.71	1.18
5c	–0.50	–0.45	–0.48	0.76	1.21
5d	–0.49	–0.42	–0.46	0.81	1.23
5e	–0.45	–0.38	–0.42	0.91	1.29

[a] Reported vs. $Fc^{0/+}$ on a Pt working electrode, ν = 0.2 V s^{-1}, T = 20±2 °C. [b] $E_m = [E_p^{a1} + E_p^{c1}]/2 \approx E^{0/}$. [c] Irreversible wave observed. [d] $E_{cell} = E_p^{a2} - E_p^{a1}$.

When the solutions are at the full indicated concentration (Table 2) the potential range for the "reduction" process is from –0.58 to –0.47 V vs. $Fc^{0/+}$ in CH_3CN and –0.61 to –0.50 V vs. $Fc^{0/+}$ in CH_2Cl_2, and has an overall change of 0.11 V in both solvents. The potential range for the "oxidation" process is from 0.69 to 0.91 V vs. $Fc^{0/+}$ in CH_3CN and 0.72 to 0.94 V vs. $Fc^{0/+}$ in CH_2Cl_2, and has an overall change of 0.22 V. The average E_{cell} values ($E_{cell} = E_n - E_m$) are 1.33±0.04 V in CH_3CN and 1.41±0.05 V in CH_2Cl_2, with a small but notable increase (0.11 V in both solvents) as the substituent R moves from electron donating to electron withdrawing. Values for **5d** are slightly lower than expected in both solvents, although the individual E_m and E_n values for **5d** still follow the expected trend.

At lower concentrations (Table 3) the potential range for the "reduction" process is from –0.57 to –0.46 V vs. $Fc^{0/+}$ in CH_3CN (change of 0.11 V) and –0.51 to –0.42 V vs. $Fc^{0/+}$ in CH_2Cl_2 (change of 0.09 V). The potential range for the irreversible "oxidation" process is from 0.59 to 0.84 V vs. $Fc^{0/+}$ in CH_3CN and 0.66 to 0.91 V vs. $Fc^{0/+}$ in CH_2Cl_2 for an overall change of 0.25 V in both solvents. Average E_{cell} values (where $E_{cell} = E_p^{a2} - E_p^{a1}$) are 1.20±0.05 V in CH_3CN and 1.21±0.06 V in CH_2Cl_2, which are essentially identical for both solvents. This contrasts with the small but notable change in E_{cell} values (~100 mV) at higher concentrations between the two solvents. For a monomeric neutral thiatriazinyl radical, the redox process is assumed to involve removal from, or addition to the π-SOMO, and can be represented as:

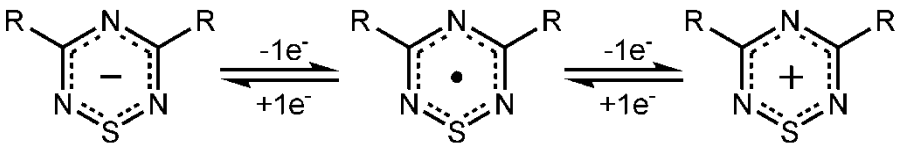

[1]

Since the same redox orbital is involved in the electrochemical oxidation and reduction reactions, one expects the substituents R to influence both redox processes by the same amount, so long as the influence is purely inductive. Exactly this has been observed in electrochemical investigations of more than twenty 1,2,3,5-dithiadiazolyls.[3] However, unlike the dithiadiazolyls, the redox orbital of the thiatriazinyls (the SOMO, Figure 10) does not have a node at the substituent-bearing carbon atoms. It is to be expected, therefore, that resonance effects can have a significant influence. These are expected to affect the oxidation and reduction processes differently.

Another factor that cannot be discounted is the effect of dimer formation on the redox processes since thiatriazinyls form strong dimers (d(S···S = 2.643(21) Å) compared to 1,2,3,5-

dithiadiazolyls (mean d(S···S = 3.03 – 3.16 Å).[3c,22] In a dimeric thiatriazine the redox process can be represented as:

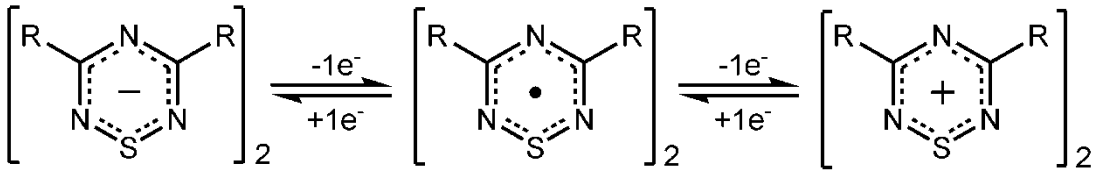

[2]

The formation of thiatriazinyl dimers has been convincingly interpreted as the result of diffuse side-on overlap of the $3b_1$ π-orbital of the individual thiatriazinyl rings (Figure 12) in a face-to-face dimeric arrangement similar to that found in the solid state for dithionite salts.[5e,23] This overlap represents the only net "bonding" interaction between the rings; that it is centered on a single sulfur atom which has the largest share of the unpaired spin density leads to relatively strong bonding. The dimer is a diamagnetic species and hence oxidation occurs from a different orbital (the in-phase combination) than reduction (the out-of-phase combination). It is therefore to be expected that the substituents influence these distinct orbitals by different amounts.

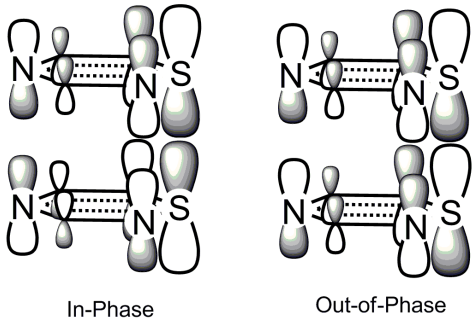

Figure 12. The in-phase and out-of-phase combinations of the $3b_1$ SOMO of model 3,5-dihydro-1,2,4,6-thiatriazinyls.

Digital Modeling of CVs of the 1,2,4,6-thiatriazinyls. In order to further probe the effect of monomer-dimer equilibrium on the voltammetry we turned to digital modeling of the voltammograms at both low and high concentrations using DigiElch software.[24] Starting with lower concentrations of the radical in solution (~1/10 the values listed in Table 2), we established

a plausible model for the monomer undergoing both a chemically irreversible oxidation and a reversible reduction. The resultant CV is shown as the blue trace in Figure 13. In this case, the model assumes that following a one-electron oxidation of the thiatriazinyl radical (abbreviated as $[TTA]^{\bullet}$ in Scheme 2) there is a chemically irreversible first-order decay step ($K_{eq4}= 10^6$, $k_{f4} = 5$ s^{-1}). No chemical step is associated with the one-electron reduction. Then, at higher concentrations the model which fit most closely to the experimental CVs follows the "ladder" scheme shown in Scheme 2.[25] The favorable formation of the dimer $[TTA_2]$ at higher concentrations (K_{eq1} = 400–800, k_{f1} = 1 M^{-1} s^{-1}) and the unfavorable formation of the dication dimer $[TTA_2]^{2+}$ ($K_{eq2} < 1$, k_{f2} = 0.01 M^{-1} s^{-1}) results in very satisfactory simulations (they are a good visual match to experimental data, see black trace in Figure 13) when the oxidation of the $[TTA_2]$ dimer is a two-electron process. Assuming a one-electron oxidation for this step does not result in a good match. The formation of the monoanionic dimer $[TTA_2]^{\bullet-}$ from $[TTA]^{\bullet}$ + $[TTA]^{-}$ was also favored (K_{eq3} = 271, $k_{f3} < 10$ M^{-1} s^{-1}).

The value for K_{eq1} of 400–800 is in reasonable agreement with previously derived equilibrium constants for association of diphenyl thiatriazinyls and selenatriazinyls by Oakley *et al.* from EPR experiments (K_{eq} = 33 for sulfur and K_{eq} = 2000 for selenium).[6] Similar investigations into the monomer-dimer equilibrium for 4-(2'-pyridyl)-1,2,3,5-dithiadiazolyl (K_{eq} ≅ 0.05 at RT) have been undertaken using absorption spectroscopy.[2e] The self-consistent fit of these data to the "ladder" scheme is thus satisfying and chemically reasonable in view of the large association constants expected for thiatriazinyls. That the dication favors monomers fits well with removal of the very electrons involved in the association. The only surprise is the apparent "decomposition" of monomeric cation under inert conditions where these 6π Hückel

species are expected to be thermally stable.[5i] We propose that the irreversibility of this electrode process may involve electron self-exchange.[26] Thus a rapid pseudo first order cascade reaction:

$$[TTA]^+ + [TTA]^\bullet \leftrightarrow [TTA]^\bullet + [TTA]^+ \quad [3]$$

could remove the cation from the electrode surface when the dominant species in solution is $[TTA]^\bullet$. On the other hand, when $[TTA_2]$ is the dominant species, the driving force for the self-exchange reaction weakens and this reaction may become sluggish. While we believe that this mechanism is a plausible proposal, detailed testing in which actual voltammograms are fit to theory will be required to obtain precise values for the kinetic parameters. Such an undertaking is beyond the scope of the current project.

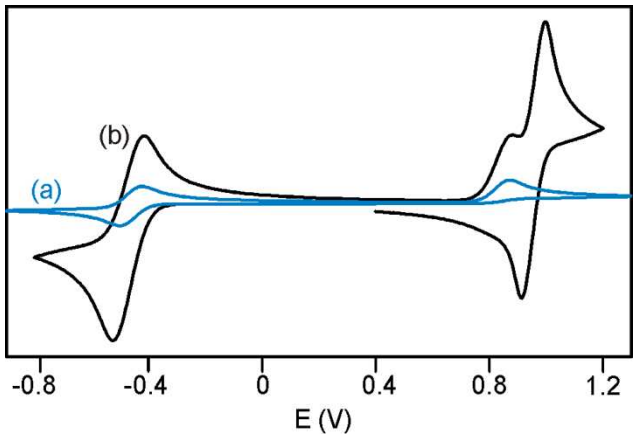

Figure 13. Calculated CVs for both (a) monomeric (blue line) and (b) dimeric (black line) solutions of **5e** resulting from the input of kinetic parameters listed in the text and following the "ladder" scheme shown in Scheme 2. These CVs follow the specific case of $\nu = 0.2$ V s^{-1}, K_{eq1} = 400, $k_{f1} = 1$ M^{-1} s^{-1}, $K_{eq2} = 0.0766$, $k_{f2} = 0.01$ M^{-1} s^{-1}, $K_{eq3} = 271$, $k_{f3} = 1$ M^{-1} s^{-1}, $K_{eq4} = 10^6$, k_{f4} = 5 s^{-1} (first-order decay of $[TTA]^+$), $k_{s1} = k_{s2} = k_{s3} = k_{s4} = 0.03$ cm s^{-1}, conc. dimer = 0.01 mol L^{-1}, conc. monomer 0.001 mol L^{-1}. The potential was first swept in the cathodic direction starting from 0.4 V.

Correlation of redox potentials with gas phase calculations. Previous studies have shown that quantum calculations, when used judiciously, can provide corroboration of electrochemical results.[3] Fully geometry optimized calculations at the (U)B3LYP/6–31G(d) level of theory were performed for the monomeric cation, anion, and neutral thiatriazine derivatives.

No attempt was made to model the weakly bound dimeric molecules. The energies of these optimized molecules were then used to define the theoretical redox reactions:

$$0/+1 \text{ process: } E_{cation} - E_{radical} = E_{oxidation} \quad [4]$$

$$-1/0 \text{ process: } E_{anion} - E_{radical} = E_{reduction} \quad [5]$$

Scheme 2. Proposed "Ladder" Scheme interrelating the voltammetric behavior of thiatriazinyls at lower and higher concentrations.

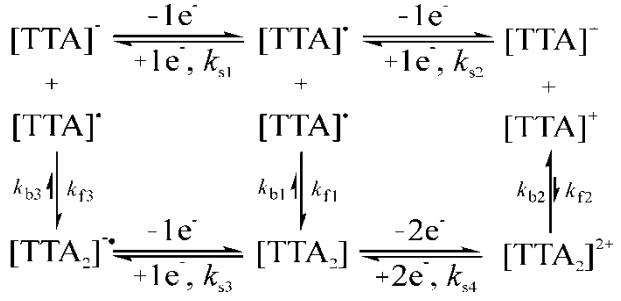

Table 4 lists the calculated and experimental redox potentials for **5a–e** from the experimental CV data at low concentrations taken from Table 3, and correlation curves are presented in Figure 14. The results are graphed by process type and each graph includes results for both solvents.

Table 4. Calculated and experimental redox potentials of **5a–e** for the monomeric radical.

	−1/0 process			0/+1 process		
Cmpd	Calc (eV)	E_m (V) CH_3CN	E_m (V) CH_2Cl_2	Calc (eV)	E_p^{a1} (V) CH_3CN	E_p^{a1} (V) CH_2Cl_2
5a	−1.89	−0.57	−0.51	7.29	0.59	0.66
5b	−1.94	−0.56	−0.50	7.50	0.67	0.71
5c	−1.99	−0.54	−0.48	7.65	0.73	0.76
5d	−2.16	−0.50	−0.46	7.72	0.74	0.81
5e	−2.25	−0.46	−0.42	7.90	0.84	0.91
Δ	0.36	0.11	0.09	0.61	0.25	0.25

Excellent correlation is obtained between the calculated gas phase and experimental solution phase oxidation and reduction potentials of the monomeric radicals **5a–e**, which is particularly noteworthy for the 0/+1 process which uses peak potentials from an irreversible process in both solvents.[3b] The reliability of the electrochemical data for this series obtained from CV is confirmed by this correlation. The solution oxidation and reduction potentials also correlate well with Hammett σ_p substituent constants (Figures S22, S23).[27]

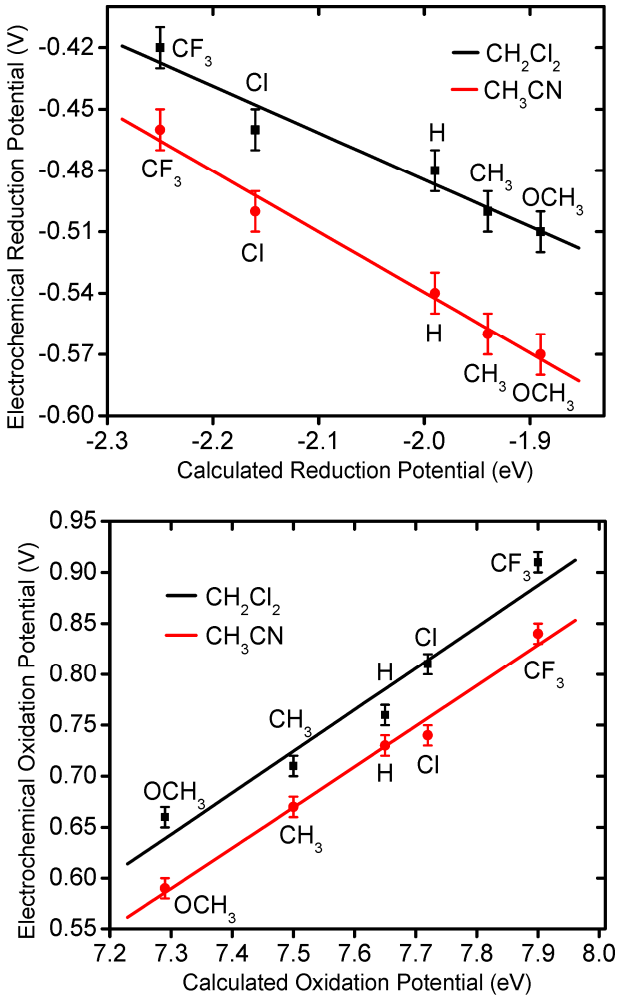

Figure 14. Plot of the calculated vs. experimental monomer reduction potentials (top) and oxidation potentials (bottom) of **5a–e** as measured by cyclic voltammetry in CH_2Cl_2 (black line, R = 0.975, top and R = 0.975, bottom), and (b) CH_3CN (red line, R = 0.993, top and R = 0.994, bottom) solution. Error bars express an estimated error in measured potential of ±0.01 V.

Conclusions

This paper reports a comprehensive investigation of a complete series of unsymmetrical aryl/trifluoromethyl-substituted thiatriazinyls. The synthetic work has elaborated new and versatile imidoylamidine reagents and demonstrated their ability to form the ring compounds through direct condensation with sulfur halides. Conversion to the neutral thiatriazinyls was successful for all five exemplars. All the synthetic results are supported by thorough structural studies that provide extremely reliable mean parameters from high-quality, low-temperature diffraction data. The complex EPR spectral data are shown to fit to well-defined substituent trends even though the variation in hfs values is small. Finally, complex voltammetric behavior involving the first reliably-detected monomer-dimer equilibria in the history of the electrochemistry of thiazyl rings has been modeled using sophisticated digital software to provide a convincing interpretation that is consistent with the predicted chemical nature of the various redox products. Further work on thiatriazinyls including detailed fitting of monomer-dimer equilibria to voltammetric data is in progress in our laboratory and will be reported at a future time.

Experimental

General procedures. Trifluoroacetonitrile (PCR Inc.) was obtained commercially and used as received. SCl_2 (Aldrich) was distilled from PCl_3 with $CaCl_2$ moisture protection. Triphenylantimony (Aldrich) and HCl(g) (Praxair) were obtained commercially and used as received. The substituted aryl amidine hydrochlorides were prepared according to the literature method.[7] Unless otherwise indicated, all procedures were performed under an atmosphere of purified N_2 using a drybox, Schlenkware, and vacuum-line techniques. Solvents used were reagent-grade or better. Acetonitrile (HPLC grade) was double-distilled from P_2O_5 and CaH_2;

dichloromethane was distilled from CaH_2; *n*-Heptane was dried by distillation over $LiAlH_4$; toluene over sodium; anhydrous diethyl ether was dried by distillation from sodium wire.

Spectroscopic methods. Infrared spectra were obtained as KBr plates and were recorded on a Bomem MB102 Fourier transform spectrometer. Melting points were determined on an Electrothermal melting point apparatus (capillaries) and are uncorrected. EPR spectra (X band) were recorded on a Bruker EMX-113/12 spectrometer as solutions in dichloromethane in 4 mm Pyrex glass tubes sealed under vacuum. NMR spectra were acquired at 250.13 (^{1}H) and 62.90 (^{13}C) MHz on a Bruker/Tecmag AC250 spectrometer using $CDCl_3$ as the solvent and thus as reference. Mass spectra were recorded by the Mass Spectrometry Center, University of Alberta, Edmonton. Microanalyses were performed by M-H-W Laboratories in Phoenix, AZ.

Electrochemical methods and procedures. Crystals of high purity **5a–e** were collected, weighed, and loaded into individual break-seal tubes and attached to the electrochemical cell by fusing the glass along with a known mass of ferrocene in a separate break seal.[25] The electrodes are all platinum and were sealed into the glass and cleaned in between experiments using conc. HNO_3. Cyclic voltammograms (CVs) were obtained at temperatures of 21±2 °C in CH_3CN and CH_2Cl_2 solutions containing 0.1 M and 0.4 M [^{n}Bu$_4$N][PF_6], respectively, as the supporting electrolyte. The electrolyte was loaded into the cell and dried under vacuum in an oil bath set at 80 °C overnight prior to transfer of the solvent. Both CH_2Cl_2 and CH_3CN were distilled and stored over molecular sieves prior to use. The solvents were freeze thaw degassed at least five times prior to their transfer into the cell over a vacuum line. For CVs all measurements were recorded at room temperature (22±2 °C), and the scan rates were varied between 0.1 – 10 V s^{-1}.

In a typical experiment, the electrolyte solution is scanned to obtain a background current and determine the effective electrochemical window. Next the seal to analyte is broken and a

small amount is dissolved until a signal with satisfactory S/N is obtained. The concentration of analyte is incrementally increased while obtaining CV traces. Finally, all the analyte is thoroughly mixed with the electrolyte solution to establish a known "full" concentration. After all CV data is satisfactorily recorded, the seal to the reference is broken and a sufficient quantity of ferrocene is added to the cell to obtain an accurate reference for the voltage scale.

X-ray crystallography. Crystals were selected and mounted in Paratone™ on the ends of thin glass capillaries and cooled on the goniometer head to –100 °C with the Bruker low-temperature accessory attached to the APPEX-II diffractometer. Mo Kα radiation (λ = 0.71073 Å) was used throughout. Multi-scan absorption corrections were applied to all the data sets, and refinement was conducted with full-matrix least-squares on F^2 using SHELXTL 6.14.[28] In the case of **5b**, data sets collected at –100 °C solve and refine but are stuck at $R_1 = 0.14$ due to a suspected superlattice formation. Therefore another crystal was selected, covered in epoxy cement, and glued to the end of a glass fiber. Diffraction data collected at 23 °C refined to a low R-factor and provided a fully acceptable structure. Details of the refinements and disorder models for typical rotational disorder of CF_3 groups are provided in the electronic Crystallographic Information File. Crystal data and refinement parameters are also summarized in Table 5. Structures of **2c** and **5c** determined at room temperature as the same as at –100 °C.

Computational details. DFT calculations undertaken for this study employed geometry optimization at the (U)B3LYP/6-31G(d) level. Harmonic vibrational frequencies were calculated for all optimized geometries to confirm that they are stationary points. Calculation of energies and EPR hyperfine splitting (hfs) constants used the same level of theory. All calculations were performed using the Gaussian 98 suite of programs.[18]

Synthesis of amidines 1a–e. $C_6H_4C(NH)NH_2$ **1c.** Benzamidine hydrochloride hydrate (26.3 g, 0.173 mol) and KOH (32.4 g, 0.576 mol) were added to 175 mL distilled water. CH_2Cl_2 (2 × 200 mL) was used to extract the product. The solvent was rotary evaporated leaving a pale yellow oil which solidified overnight in the freezer. The solid was sublimed at 80 °C under vacuum to give 12.79 g (61.9% yield) of pure white **1c**. ^{1}H NMR ($CDCl_3$): δ 5.28 (s, 3H, NH), 7.42 – 7.62 (m, 5H, phenyl).

$CH_3OC_6H_4C(NH)NH_2$ **1a.** 4-methoxybenzonitrile (15.08 g, 0.1133 mol) was added to $Et_2O{\cdot}LiN(SiMe_3)_2$ (27.26 g, 0.1129 mol) in 200 mL distilled diethyl ether and stirred for 20 h with a drying tube attached. A 1:1 mixture of ethanol and conc. HCl (30 mL) was added slowly through a dropping funnel leaving a white precipitate. The solid was recovered by filtration and dried in air. It was then re-dissolved in distilled water and treated with excess NaOH solution affording a pale purple solid. This was sublimed at 91 °C under vacuum to give 3.72 g (22.2% yield) pure **1a**. Plate shaped X-ray quality crystals were collected on a cold finger following vacuum sublimation. ^{1}H NMR ($CDCl_3$): δ 3.85 (s, 3H, CH_3), 4.99 (s, 3H, NH), 6.93 (d, 2H, $J_{H\text{-}H}$ = 9.0 Hz, $C_{Ar}H$), 7.57 (d, 2H, $J_{H\text{-}H}$ = 8.4 Hz, $C_{Ar}H$).

$CH_3C_6H_4C(NH)NH_2$ **1b.** *p*-Tolunitrile (6.356 g, 0.05425 mol) was added to $Et_2O{\cdot}LiN(SiMe_3)_2$ (12.47 g, 0.05165 mol) in 200 mL distilled diethyl ether and stirred for 22 hrs with a drying tube attached. A 1:1 mixture of ethanol and conc. HCl (30 mL) was added slowly through a dropping funnel to give a pink precipitate. The solid was recovered by filtration and dried in air. It was then redissolved in distilled water and treated with excess KOH. CH_2Cl_2 (2 × 200 mL) was used to extract the product. The solvent was rotary evaporated and the solution was dried using andrydrous sodium sulfate to give a yellow solid. The solid was sublimed at 70 °C

under vacuum to give 1.51 g (21.8% yield) pure **1b**. ^{1}H NMR ($CDCl_3$): δ 2.40 (s, 3H, CH_3), 4.83 (s, 3H, NH), 7.23 (d, 2H, $J_{H\text{-}H}$ = 8.1 Hz, $C_{Ar}H$), and 7.51 (d, 2H, $J_{H\text{-}H}$ = 8.4 Hz, $C_{Ar}H$).

$ClC_6H_4C(NH)NH_2$ **1d.** Prepared by the same method reported for **1a** using 4-chlorobenzonitrile (7.69 g, 0.0559 mol) and $Et_2O{\cdot}LiN(SiMe_3)_2$ (12.7 g, 0.0524 mol) in 200 mL distilled diethyl ether. The pale pink color solid was sublimed at 91 °C under vacuum to give 4.33 g (53.7% yield) pure **1d**. ^{1}H NMR ($CDCl_3$): δ 3.88 (s, 3H, NH), 7.41 (d, 2H, $J_{H\text{-}H}$ = 8.4 Hz, $C_{Ar}H$), and 7.75 (d, 2H, $J_{H\text{-}H}$ = 8.7 Hz, $C_{Ar}H$).

$CF_3C_6H_4C(NH)NH_2$ **1e.** Prepared by the same method reported for **1a** using *α,α,α*-trifluoro-p-tolunitrile (8.94 g, 52.2 mmol) and $Et_2O{\cdot}LiN(SiMe_3)_2$ (12.4 g, 51.5 mmol) in 200 mL distilled diethyl ether. After the solid was collected by filtration and air dried it was sublimed at 85 °C under vacuum to give 5.61 g (57.9% yield) pure **1e**. ^{1}H NMR ($CDCl_3$): δ 4.90 (s, 3H, NH), 7.75 (d, 2H, $J_{H\text{-}H}$ = 8.4 Hz, $C_{Ar}H$), 7.70 (d, 2H, $J_{H\text{-}H}$ = 8.4 Hz, $C_{Ar}H$). ^{19}F NMR ($CDCl_3$): δ –62.02 (CF_3).

Synthesis of trifluoromethyl imidoylamidines 2a–e. $C_6H_5C_3N_3H_3F_3$ **2c**. Trifluoroacetonitrile (2.06 g, 21.7 mmol) was measured on a vacuum line by PVT methods and added to 2.53 g (21.1 mmol) of benzamidine **1c** in 20 mL acetonitrile in a 300 x 25 mm heavy-wall Pyrex™ reactor fitted with a Rotaflow™ stopcock equipped with a small magnetic stirring bar at −196 °C. The mixture was warmed to RT, heated to 60 °C with stirring for 10 min and then cooled to RT and evaporated, leaving a clear oil. Upon refrigeration this solidified to leave 4.37 g of white solid (20.3 mmol, 96% yield), mp 42–45 °C. ^{1}H NMR (δ, $CDCl_3$): 6.8 (s, NH), 7.38–7.54 (m, 3H, phenyl), 7.83–7.88 (m, 2H, $C_{Ar}H$), 9.1 (s, NH), 11.0 (s, NH); ^{13}C NMR (δ, $CDCl_3$): 117.8 (q, 281 Hz), 127.4 (s), 129.0 (s), 132.2 (s), 135.2 (s), 163.5 (q, 33 Hz), 165.9 (s). Mass spectrum (*m/e*) 214 ($PhC_2N_3H_2CF_3^+$, 100%), 169 ($PhC_2N_2H_2F_2^+$, 4%), 146 ($PhC_2N_3H_3^+$, 12%), 129 ($PhC_2N_2^+$,

6%), 104 ($PhCNH^+$, 48%). Analysis calculated (found): 50.24 (50.35) % C, 3.75 (4.01) % H, 19.53 (19.37) % N.

4–$CH_3OC_6H_5C_2N_3H_3CF_3$ **2a**. Prepared as **2c** using CF_3CN (1.09 g, 11.5 mmol) and **1a** (1.58 g, 10.5 mmol) in 10 mL acetonitrile. A white solid remained which was sublimed *in vacuo* at 46 °C to leave 1.43 g of pure white crystals (5.8 mmol, 56% yield), mp 41–45°C. ^{1}H NMR (δ, $CDCl_3$): 3.9 (s, OCH_3), 6.7 (s, NH), 6.9 (d, 2H, $C_{Ar}H$), 7.9 (d, 2H, $C_{Ar}H$), 9.0 (s, NH), 11.0 (s, NH). ^{13}C NMR (δ, $CDCl_3$): 55.7 (s), 114.3 (s), 117.9 (q, 281 Hz), 127.3 (s), 129.3 (s), 163.1 (s), 163.4 (q, 33 Hz), 165.3 (s). Mass spectrum (*m/e*) 244 ($CH_3OPhC_2N_3H_2CF_3^+$, 42%), 199 ($CH_3OPhC_2N_2H_2F_2^+$, 4%), 176 ($CH_3OPhC_2N_3H_3^+$, 20%), 159 ($CH_3OPhC_2N_2^+$, 13%), 134 ($CH_3OPhCNH^+$, 100%). Analysis calculated (found): 48.98 (48.85) %C, 4.11 (4.22) %H, 17.14 (17.32) %N.

4–$CH_3C_6H_5C_2N_3H_3CF_3$ **2b**. Prepared as **2c** using CF_3CN (1.34 g, 14.1 mmol) and **1b** (1.96 g, 14.6 mmol) in 15 mL acetonitrile. A pink solid remained which was sublimed in vacuo at 48 °C to leave 2.48 g of white crystals (10.8 mmol, 77% yield), mp 54–57 °C. ^{1}H NMR (δ, $CDCl_3$): 2.4 (s, CH_3), 6.7 (s, NH), 7.3 (d, 2H, $C_{Ar}H$), 7.8 (d, 2H, $C_{Ar}H$), 9.1 (s, NH), 11.0 (s, NH). ^{13}C NMR (δ, $CDCl_3$): 21.7 (s), 117.8 (q, 281 Hz), 127.6 (s), 129.7 (s), 132.4 (s), 142.8 (s), 163.6 (q, 33 Hz), 165.8 (s). Mass spectrum (*m/e*) 228 ($CH_3PhC_2N_3H_2CF_3^+$, 100%), 183 ($CH_3PhC_2N_2H_2F_2^+$, 2%), 160 ($CH_3PhC_2N_3H_3^+$, 7%), 143 ($CH_3PhC_2N_2^+$, 4%), 118 (CH_3PhCNH^+, 30%). Analysis calculated (found): 52.40 (52.34) % C, 4.40 (4.60) % H, 18.33 (18.50) % N.

4–$ClC_6H_5C_2N_3H_3CF_3$ **2d**. Prepared as **2c** using trifluoroacetonitrile (2.07 g, 21.8 mmol) and **1d** (3.25 g, 21.0 mmol) in 20 mL acetonitrile. A white solid remained which was sublimed *in vacuo* at 49 °C to leave 4.72 g of pure white crystals (18.9 mmol, 90% yield); mp 45–48 °C. ^{1}H NMR (δ, $CDCl_3$): 6.7 (s, NH), 7.4 (d, 2H, $C_{Ar}H$), 7.8 (d, 2H, $C_{Ar}H$), 9.2 (s, NH), 11.0 (s, NH).

^{13}C NMR (δ, $CDCl_3$): 117.7 (q, 281 Hz), 128.8 (s), 129.3 (s), 133.6 (s), 138.6 (s), 163.3 (q, 34 Hz), 164.8 (s). Mass spectrum (*m/e*) 248 ($ClPhC_2N_3H_2CF_3^+$, 42%), 180 ($ClPhC_2N_3H_3^+$, 10%), 163 ($ClPhC_2N_2^+$, 13%), 138 ($ClPhCNH^+$, 100%). Analysis calculated (found): 43.31 (43.50) %C, 2.83 (3.00) %H, 16.83 (17.06) %N.

4–$CF_3C_6H_5C_2N_3H_3CF_3$ **2e**. Prepared as **2c** using trifluoroacetonitrile (1.02 g, 10.7 mmol) and **1e** (1.98 g, 10.5 mmol) in 10 mL acetonitrile. A white solid remained which was sublimed *in vacuo* at 60 °C to leave 2.52 g of white crystals (8.9 mmol, 85% yield); mp 80–83 °C. ^{1}H NMR (δ, $CDCl_3$): 6.8 (s, NH), 7.7 (d, 2H, $C_{Ar}H$), 8.0 (d, 2H, $C_{Ar}H$), 9.3 (s, NH), 11.1 (s, NH). ^{13}C NMR (δ, $CDCl_3$): 117.7 (q, 281 Hz), 123.9 (q, 273 Hz), 126.0 (q, 4 Hz), 127.9 (s), 133.9 (q, 33 Hz), 138.6 (s), 163.2 (q, 34 Hz), 164.7 (s). Mass spectrum (*m/e*) 282 ($CF_3PhC_2N_3H_2CF_3^+$, 100%), 237 ($CF_3PhC_2N_2H_2F_2^+$, 5%), 214 ($CF_3PhC_2N_3H_3^+$, 13%), 197 ($CF_3PhC_2N_2^+$, 3%), 172 (CF_3PhCNH^+, 45%). Analysis calculated (found): 42.42 (42.32) %C, 2.49 (2.39) %H, 14.84 (14.88) %N.

Synthesis of trifluoromethyl imidoylamidine hydrochlorides 3a–e. $C_6H_5C_3N_3H_3F_3$.HCl **3c**. Anhydrous HCl was bubbled through a suspension of **2c** (2.04 g, 9.5 mmol) in diethyl ether. The white precipitate was filtered in air and dried to leave 2.34 g of crude solid (9.3 mmol, 98% yield), mp (dec.) 174–175 °C. For FTIR data, see the Supplemental Information.

4-$CH_3OC_6H_4C_3N_3H_3F_3$.HCl **3a**. Prepared as **3c** from **2a** (1.01g, 4.1mmol) providing 1.09 g of crude white solid (3.9 mmol, 94% yield), mp (dec.) 213–215 °C.

4–$CH_3C_6H_4C_3N_3H_3F_3$.HCl **3b**. Prepared as **3c** from **2b** (1.59 g, 6.9 mmol), providing 1.50 g of solid **3b** (5.7 mmol, 82% yield), mp (dec.) 198–200 °C.

4–$ClC_6H_4C_3N_3H_3F_3$.HCl **3d**. Prepared as **3c** from **2d** (2.40 g, 9.6 mmol) providing 2.65 g of white solid (9.3 mmol, 97% yield), mp (dec.) >244 °C.

4–$CF_3C_6H_4C_3N_3H_3F_3$.HCl **3e**. Prepared as **3c** from **2e** (2.37 g, 8.4 mmol) providing 2.65 g of white solid (8.3 mmol, 99% yield), mp (dec.) 181–183 °C.

Synthesis of 1-chloro-5-aryl-3-trifluoromethyl-1,2,4,6-thiatriazines 4a–e. $C_6H_5C_2N_3SClCF_3$ **4c**. Freshly distilled SCl_2 (2.8 mL, 44.1 mmol) in 10 mL acetonitrile was added dropwise to a suspension of imidoylamidine.HCl **3c** (2.24 g, 8.9 mmol) in 30 mL acetonitrile. The yellow mixture was heated to reflux for 1.5 h giving an orange-red color. After filtering to remove any solids, the solvent was removed *in vacuo* to leave an orange oil (2.23 g, 8.0 mmol, 90% yield). ^{1}H NMR (δ, $CDCl_3$): 7.52–7.58 (m, 2H, $C_{Ar}H$), 7.67–7.74 (m, H, $C_{Ar}H$), 8.45–8.48 (m, 2H, $C_{Ar}H$).

4–$CH_3OC_6H_5C_2N_3SClCF_3$ **4a**. Prepared as **4c** using SCl_2 (1.6 mL, 25.1 mmol) in 10 mL acetonitrile added dropwise to **3a** (1.45 g, 5.1 mmol) in 25 mL acetonitrile. The solvent was removed in vacuo, leaving a dark orange oil. Recrystallization with hot toluene followed by hot acetonitrile left an orange oil (1.29 g, 81% yield). ^{1}H NMR (δ, $CDCl_3$): 3.94 (s, CH_3O), 7.02 (d, 2H, $C_{Ar}H$), 8.45 (d, 2H, $C_{Ar}H$).

4–$CH_3C_6H_5C_2N_3SClCF_3$ **4b**. Prepared as **4c** using SCl_2 (1.8 mL, 28.3 mmol) in 10 mL acetonitrile and **3b** (1.47 g, 5.5 mmol) in 25 mL acetonitrile. The solvent was removed in vacuo, leaving an orange-red solid (1.77 g, 97% yield). ^{1}H NMR (δ, $CDCl_3$): 2.49 (s, CH_3), 7.35 (d, 2H, $C_{Ar}H$), 8.37 (d, 2H, $C_{Ar}H$).

4–$ClC_6H_5C_2N_3SClCF_3$ **4d**. Prepared as **4c** using SCl_2 (2.2 mL, 34.6 mmol) in 10 mL and **3d** (2.54 g, 8.9 mmol) in 40 mL acetonitrile. The solvent was removed in vacuo, leaving a dark orange oil. This was recrystallized with hot heptane to leave an orange solid (2.78 g, 99% yield). ^{1}H NMR (δ, $CDCl_3$): 7.53 (d, 2H, $C_{Ar}H$), 8.41 (d, 2H, $C_{Ar}H$).

4–$CF_3C_6H_5C_2N_3SClCF_3$ **4e**. Prepared as **4c** using SCl_2 (2.2 mL, 34.6 mmol) in 10 mL and **3e** (2.13 g, 6.7 mmol) in 40 mL acetonitrile. The solvent was removed in vacuo, leaving a dark orange oil. (2.50 g, 98% yield). ^{1}H NMR (δ, $CDCl_3$): 7.82 (d, 2H, $C_{Ar}H$), 8.59 (d, 2H, $C_{Ar}H$).

Synthesis of 3-trifluoromethyl-5-aryl-1,2,4,6-thiatriazinyls 5a–e. $C_6H_5C_2N_3SCF_3$ **5c**. A pear-shaped solids addition funnel was loaded with triphenylantimony (1.42 g, 4.0 mmol) and attached to a side-arm flask containing **4c** (2.23 g, 8.0 mmol) and 25 mL acetonitrile. After degassing the solvent by three freeze-thaw cycles and warming to RT, while still under vacuum, the Ph_3Sb was added with stirring. A fine dark purple precipitate formed, and the crystals were vacuum filtered under nitrogen to give 1.14 g of crude product (4.7 mmol, 59% yield), mp. (dec.) 110–3 °C. Purification was achieved by vacuum sublimation in a three-zone tube furnace. Mass spectrum (*m/e*) 245 ($PhC_3N_3SF_3^+$, 43%), 149 ($PhCN_2S^+$, 6%), 129 ($PhC_2N_2^+$, 3%), 104 ($PhCN^+$, 100%). Analysis calculated (found): 44.26 (44.12) %C, 2.06 (2.24) %H, 17.21 (17.13) %N.

4–$CH_3OC_6H_5C_2N_3SCF_3$ **5a**. Prepared as **5c** from **4a** (1.25 g, 4.0 mmol) and Ph_3Sb (0.79 g, 2.2 mmol) in 20 mL acetonitrile to give 0.41 g of dark purple solids (1.5 mmol, 37% yield), mp (dec.) 135–40 °C. Purification was achieved by vacuum sublimation in a three-zone tube furnace. Mass spectrum (*m/e*) 274 ($CH_3OPhC_3N_3SF_3^+$, 65%), 255 ($CH_3OPhC_3N_3SF_2^+$, 4%), 179 ($CH_3OPhCN_2S^+$, 3%), 117 (CH_3OPhCN^+, 100%). Analysis calculated (found): 43.80 (43.90) %C, 2.57 (2.71) %H, 15.32 (15.18) %N.

4–$CH_3C_6H_5C_2N_3SCF_3$ **5b**. Prepared as **5c** from **4b** (1.05 g, 3.6 mmol) and Ph_3Sb (0.64 g, 1.8 mmol) in 15 mL acetonitrile to give 0.46 g of dark purple solids (1.8 mmol, 50% yield), mp (dec.) 140–2 °C. Purification was achieved by vacuum sublimation in a three-zone tube furnace. Mass spectrum (*m/e*) 258 ($CH_3PhC_3N_3SF_3^+$, 100%), 239 ($CH_3PhC_3N_3SF_2^+$, 4%), 163

($CH_3PhCN_2S^+$, 24%), 117 (CH_3PhCN^+, 45%). Analysis calculated (found): 46.51 (46.67) % C, 2.73 (2.96) % H, 16.27 (16.41) % N.

4–$ClC_6H_5C_2N_3SCF_3$ **5d**. Prepared as **5c** from **4d** (2.78 g, 8.9 mmol) and Ph_3Sb (1.71 g, 4.8 mmol) in 30 mL acetonitrile to give 1.36 g of dark purple solids (4.9 mmol, 55% yield), mp (dec.) 131–4 °C. Purification was achieved by vacuum sublimation in a three-zone tube furnace. Mass spectrum (*m/e*) 278 ($ClPhC_3N_3SF_3^+$, 100%), 259 ($ClPhC_3N_3SF_2^+$, 5%), 183 ($ClPhCN_2S^+$, 18%), 137 ($ClPhCN^+$, 47%). Analysis calculated (found): 38.79 (38.72) % C, 1.45 (1.41) % H, 15.08 (15.08) % N.

4–$CF_3C_6H_5C_2N_3SCF_3$ **5e**. Prepared as **5c** from **4e** (2.32 g, 6.7 mmol) and Ph_3Sb (1.31 g, 3.7 mmol) in 25 mL acetonitrile to give 0.45 g of dark purple product (1.4 mmol, 20% yield), mp (dec.) 101–5°C. Purification was achieved by vacuum sublimation in a three-zone tube furnace. Mass spectrum (*m/e*) 312 ($CF_3PhC_3N_3SF_3^+$, 100%), 197 ($CH_3PhC_2N_2^+$, 24%), 171 (CF_3PhCN^+, 30%). Analysis calculated (found): 38.47 (38.52) % C, 1.29 (1.53) % H, 13.46 (13.34) % N.

Isolation of N-chlorosulfonyl-N,N'-benzamidine 6. Attempts to grow crystals of **4** by slow cooling (−30 °C) in anhydrous CH_3CN were successful only for **4b** and **4e**; in the case of **4c** colorless crystals of a hydrolysis product **6** were obtained which could be identified as N-chlorosulfonyl-N,N'-benzamidine by a single-crystal X-ray diffraction structure determination. Further characterization of this material was not undertaken.

Acknowledgement. We thank the University of Lethbridge and the Natural Sciences and Engineering Research Council of Canada for financial support of this work. Some preliminary groundwork for this project was undertaken by Russell J. Goodman. We thank Meg O'Shea for performing DFT calculations and WestGrid for access to computational facilities and Dr. Gotthelf Wolmershäuser for determining RT X-ray structures of **2c** and **5c**.

Supporting Information Available. Supplemental crystal structure information; a representative NMR spectrum of imidoylamidine; infra-red spectral data; tables of hydrogen-bonds; graphs showing correlation of hfs and solution redox potentials with Hammett parameters; additional EPR spectra; data from Gaussian calculations; electronic crystallographic data in CIF format.

References.

1. (a) Chivers, T. *A Guide to Chalcogen-Nitrogen Chemistry*, World Scientific Publishing Co. Singapore, 2005. (b) Hicks, R. G. *Stable Radicals: Fundamentals and Applied Aspects of Odd-Electron Compounds*, Wiley, N.Y., 2010. (c) Torroba, T. *J. Prakt. Chem.* **1999**, *341*, 99–113. (d) Lekin, K.; Winter, S. M.; Downie, L. E.; Bao. X.; Tse, John S.; Desgreniers, S.; Secco, R. A.; Doube, P.A.; Oakely, R.T. *J. Am. Chem. Soc.* **2010**, *132*, 16212-16224. (e) Winter, S. M.; Cvrkalj, K.; Dube, P. A.; Robertson, C. M.; Probert, M. R.; Howard, J. A. K.; Oakley, R. T. *Chem. Commun*. **2009**, 7306–7308. (f) Fujita, W.; Awaga, K. *Science*, **1999**, *286*, 261–262. (g) Leitch, A. A.; Oakley, R. T.; Reed, R. W.; Thompson, L. K. *Inorg. Chem*. **2007**, *46*, 6261–6270. (h) Gilroy, J.B.; Joe B.; Lemaire, M.T.; Patrick, B.O.; Hicks, R.G. *Cryst. Eng. Comm.* **2009**, *11*, 2180-2184. (i) Decken, A.; Mailman, A.; Passmore, J *Chem. Commun.* **2009**, 6077-6079. (j) Vasilieva, N. V.; Irtegova, I.G.; Gritsan, N. P.; Lonchakov, A. V.; Makarov, A. Y.; Shundrin, L. A.; Zibarev, A.V. *J. Phys. Org. Chem.* **2010**, *23*, 536-543. (k) Semenov, N.A.; Pushkarevsky, N. A.; Lonchakov, A. V.; Bogomyakov, A. S.; Pritchina, E. A.; Suturina, E. A.; Gritsan, N. P.; Konchenko, S. N.; Mews, R.; Ovcharenko, V.I.; Zibarev, A.V.; *Inorg. Chem.* **2010**, *49*, 7558-7564. (l) Kanai, K.; Yoshida, H.; Noda, Y.; Iwasaki, A.; Suizu, R., Tsutumi, J.; Imabayashi, H.; Ouchi, Y.; Sato, N.; Seki, K.; Awaga, K. *Phys. Chem. Chem. Phys.* **2009**, *11*, 11432-11436. (m)

Cordes, A. W.; Haddon, R. C.; Oakley, R. T. *Adv. Mater*. **1994**, *6*, 798–802. (n) Cordes, A. W.; Haddon, R. C.; Oakley, R. T.; *Phosphorus, Sulfur, Silicon Relat. Elem*. **2004**, *179*, 673–684. (o) Barclay, T. M.; Cordes, A. W.; Haddon, R. C.; Itkis, M. E.; Oakley, R. T.; Reed, R. W.; Zhang, H. *J. Am. Chem. Soc*. **1999**, *121*, 969–976. (p) Brusso, J. L.; Clements, O. P.; Haddon, R. C.; Itkis, M. E.; Leitch, A. A.; Oakley, R. T.; Reed, R. W.; Richardson, J. F. *J. Am. Chem. Soc*. **2004**, *126*, 8256–8265. (q) Alberola, A.; Less, R. J.; Pask, C. M.; Rawson, J. M.; Palacio, F.; Oliete, P.; Paulsen, C.; Yamaguchi, A.; Farley, R. D.; Murphy, D. M. *Angew. Chem., Int. Ed*., **2003**, *42*, 4782–4785. (r) Rawson, J. M.; Alberola, A.; Whalley, A. *J. Mater. Chem*. **2006**, *16*, 2560–2565. (s) Benin, V.; Kaszynski, P. *J. Org. Chem.* **2000**, *65*, 8086–8088.

2. (a) Preuss, K. E. *Dalton Trans*. **2007**, 2357–2369. (b) Hearns, N. G. R.; Preuss, K. E.; Richardson, J. F.; Bin-Salamon, S. *J. Am. Chem. Soc*. **2004**, 126, 9942–9943. (c) Awaga, K.; Tanaka, T.; Shirai, T.; Fujimori, M.; Suzuki, Y.; Yoshikawa, H.; Fujita, W. *Bull. Chem. Soc. Jpn*. **2006**, *79*, 25–34. (d) Jennings, M.; Preuss, K. E.; Wu, J. *Chem. Commun*. **2006**, 341–343. (e) Britten, J.; Hearns, N. G. R.; Preuss, K. E.; Richardson, J. F.; Bin-Salamon, S. *Inorg. Chem*. **2007**, *46*, 3934–3945. (f) Hearns, N. G. R.; Clérac, R.; Jennings, M.; Preuss, K. E. *Dalton Trans*. **2009**, 3193–3203. (g) Hearns, N. G. R.; Fatila, E. M.; Clérac, R.; Jennings, M.; Preuss, K. E. *Inorg. Chem*. **2008**, *47*, 10330–10431.

3. (a) Boeré, R. T.; Roemmele, T. L. *Coord. Chem. Rev*. **2000**, *210*, 369–445. (b) Boeré, R. T.; Moock, K. H. *J. Am. Chem. Soc.* **1995**, *117*, 4755–4760. (c) Boeré, R. T.; Moock, K. H.; Parvez, M. *Z. anorg. allg. Chem*. **1994**, *620*, 1589–1598.

4. Ang, C. Y.; Boeré, R. T.; Goh, L. Y.; Koh, L. L.; Kuan, S. L.; Tan, G. K.; Yu, X. *Chem. Comm*. **2006**, 4735–4737.

5. (a) Geevers, J.; Hackmann, T.; Trompen, W. P. *J. Chem. Soc. C* **1970**, 875–878. (b) Kornuta, P. P.; Derii, L. I.; Romanenko, E. A. *Chemistry of Heterocyclic Compounds* **1978**, *273*, 226. (c) Kornuta, P. P.; Derii, L. I.; Markovskii, L. N. *Zh. Org. Khim*. **1980**, *16*, 1308–1313. (d) Markovskii, L. N.; Kornuta, P. P.; Katchkovskaya, L. S.; Polumbrik, P. M. *Sulfur Lett.* **1983**, *1*, 143–145. (e) Hayes, P. J.; Oakley, R. T.; Cordes, A. W.; Pennington, W. T. *J. Am. Chem. Soc*. **1985**, *107*, 1346–1351. (f) Cordes, A. W.; Hayes, P. J.; Josephy, P. D.; Koenig, H.; Oakley, R. T.; Pennington, W. T. *J. Chem. Soc., Chem. Commun*. **1984**, 1021–1022. (g) Cordes, A. W.; Craig, S. L.; Condren, M. S.; Oakley, R. T.; Reed, R. W. *Acta Cryst.* **1986**, *C42*, 922–923. (h) Ramakrishna, T. V. V.; Elia, A. J.; Vij, A. *Inorg. Chem*. **1999**, *38*, 3022–3026. (i) Boeré, R. T.; Cordes, A. W.; Hayes, P. J.; Oakley, R. T.; Reed, R. W.; Pennington, W. T. *Inorg. Chem*. **1986**, *25*, 2445–2450. (j) Knapp, C.; Watson, P. G.; Lork, E.; Friese, D. H.; Mews, R.; Decken, A. *Inorg. Chem*. **2008**, *47*, 10618–10625. (k) Chen, S.-J.; Behrens, U.; Fischer, E.; Mews, R.; Pauer, F.; Sheldrick, G. M.; Stalke, D.; Stohrer, W.-D. *Chem. Ber*. **1993**, *126*, 2601–2607. (l) Cordes, A. W.; Oakley, R. T. *Acta Cryst*. **1987**, *C43*, 1645–1646. (m) Farrar, J.M.; Patel, M.K.; Kaszynski, P.; Young, V.G., Jr. *J. Org. Chem.* **2000**, *65*, 931–940. (n) Kaszynski, P. *J. Phys. Chem. A* **2001**, *105*, 7615–7625. (o) Kaszynski, P. *J. Phys. Chem. A* **2001**, *105*, 7626–7633.

6. Oakley, R. T.; Reed, R. W.; Cordes, A. W.; Craig, S. L.; Graham, J. B. *J. Am. Chem. Soc*. **1987**, *109*, 7745–7749.

7. Boeré, R. T.; Oakley, R. T.; Reed, R. W. *J. Organomet. Chem.* **1987**, *331*, 161–167.

8. (a) Peak, D. A. *J. Chem. Soc.* **1952**, 215–226. (b) Oto, K.; Ichikawa, E. Patent Japan JP 48003811, 1973; *Chem. Abstr.* **1973**, *79*, 18443. (c) Liebscher, J.; Knoll, A.; Berger, A.; Krenzke, A. Patent East Ger. DD 219,479, 1985; *Chem. Abstr.* **1985**, *103*, 195834. (d)

Brown, H. C.; Schuman, P. D. *J. Org. Chem.* **1963**, *28*, 1122–1127. (e) Schaeffer, F.C.; Hechenbleikner, I.; Peters, G. A.; Wystrach, V.P. *J. Am. Chem. Soc.* **1958**, *81*, 1466–1470.

9. Peters, G. A.; Schaeffer, F.C. Patent: *Ger* 1,175,684; *Chem. Abstr.* **1964**, 61:14694*c*.

10. Privett, A. J.; Craig, S. L.; Jeter, D. Y.; Cordes, A. W.; Oakley, R. T.; Reed, R. W. *Acta Cryst*. **1987**, *C43*, 2023–2025.

11. (a) Kopylovich, M. N.; Pombeiro, A. J. L.; Fischer, A.; Kloo, L.; Kukushkin, V. Y. *Inorg. Chem*. **2003**, *42*, 7239–7248. (b) Gushchin, P. V.; Tyan, M. R.; Bokach, N. A.; Revenco, M. D.; Haukka, M.; Wang, M.-J.; Lai, C.-H.; Chou, P.-T.; Kukushkin, V. Y. *Inorg. Chem*. **2008**, *47*, 11487–11500. (c) Norrestam, R. *Acta Cryst*. **1984**, *C40*, 955–957. (d) Robinson, V.; Taylor, G. E.; Woodward, P.; Bruce, M. I.; Wallis, R. C. *J. Chem. Soc., Dalton Trans.* **1981**, 1169–1173. (e) Barker, J.; Kilner, M.; Mahmoud, M.M.; Wallwork, S. C. *J. Chem. Soc., Dalton Trans.* **1989**, 837–841. (f) Hursthouse, M. B.; Mazid, M. M.; Robinson, S. D.; Sahajpal, A. *J. Chem. Soc., Dalton Trans.* **1994**, 3615–3620. (i) Aris, D. R.; Barker, J.; Phillips, P. R.; Alcock, N. W.; Wallbridge, M. G. H. *J. Chem. Soc., Dalton Trans.* **1997**, 909–910.

12. Pinkerton, A.A.; Schwarzenbach, D. *J. Chem.Soc., Dalton Trans.* **1978**, 989–996.

13. Greenwood, N. N.; Earnshaw, A. *Chemistry of the Elements, 2nd Edition*; Reed Educational and Professional Publishing Ltd.: Oxford, 1997; p 60.

14. (a) Boeré, R. T.; Moock, K. H.; Derrick, S.; Hoogerdijk, W.; Preuss, K.; Yip, J. *Can. J. Chem.* **1993**, *71*, 473–486. (b) Boeré, R. T.; Fait, J.; Larsen, K.; Yip, J. *Inorg. Chem.* **1992**, *31*, 1417–1423.

15. Cordes, A. W.; Oakley, R. T. *Acta Cryst., Section C: Cryst. Struct. Commun.* **1987**, *C43*, 1645–1646.

16. Boeré, R. T. unpublished data.

17. *CRC Handbook of Chemistry and Physics, 70th Edition*; Weast, R. C.; CRC Press: Boca Raton, FL, 1989; p F–188.

18. Frisch, M. J.; Trucks, G. W.; Schlegel, H. B.; Scuseria, G. E.; Robb, M. A.; Cheeseman, J. R.; Zakrzewski, V. G.; Montgomery Jr., J. A.; Stratmann, R. E.; Burant, J. C.; Dapprich, S.; Millam, J. M.; Daniels, A. D.; Kudin, K. N.; Strain, M. C.; Farkas, O.; Tomasi, J.; Barone, V.; Cossi, M.; Cammi, R.; Mennucci, B.; Pomelli, C.; Adamo, C.; Clifford, S.; Ochterski, J.; Petersson, G. A.; Ayala, P. Y.; Cui, Q.; Morokuma, K.; Malick, D. K.; Rabuck, A. D.; Raghavachari, K.; Foresman, J. B.; Cioslowski, J.; Ortiz, J. V.; Baboul, A. G.; Stefanov, B. B.; Liu, G.; Liashenko, A.; Piskorz, P.; Komaromi, I.; Gomperts, R.; Martin, R. L.; Fox, D. J.; Keith, T.; Al-Laham, M. A.; Peng, C. Y.; Nanayakkara, A.; Gonzalez, C.; Challacombe, M.; Gill, P. M. W.; Johnson, B.; Chen, W.; Wong, M. W.; Andres, J. L.; Gonzalez, C.; Head-Gordon, M.; Replogle, E. S.; and Pople, J. A. *Gaussian 98*, Revision A.7; Gaussian Inc.: Pittsburgh, PA, 1998.

19. Duling, D. R. *J. Magn. Reson., Ser. B* **1994**, *104*, 105–110.

20. (a) Boeré, R. T.; Oakley, R. T.; Reed, R. W.; Westwood, N. P. C. *J. Am. Chem. Soc*. **1989**, *111*, 1180–1185. (b) Boeré, R. T.; Roemmele, T. L. *Phosphorus, Sulfur, and Silicon* **2004**, *179*, 875–882.

21. Moock, K. H.; Rock, M. H. *J. Chem. Soc., Dalton Trans.* **1993**, 2459-2463.

22. (a) Lau, H. F.; Ang, P. C. Y.; Ng, V. W. L.; Kuan, S. L.; Goh, L. Y.; Borisov, A. S.; Hazendonk, P.; Roemmele, T. L.; Boeré, R. T.; Webster, R. D. *Inorg. Chem.* **2008**, *47*, 632–644. (b) Beekman, R. A.; Boeré, R. T.; Moock, K. H.; Parvez, M. *Can. J. Chem.* **1998**, *76*, 85–93.

23. Oakley, R.T. *Prog. Inorg. Chem.* **1988**, 36, 299-391.

24. (a) Rudolph, M. *J. Electroanal. Chem*. **2003**, *543*, 23. (b) Rudolph, M. *J. Electroanal. Chem*. **2004**, 571, 289. (c) Rudolph, M. *J. Electroanal. Chem*. **2003**, *558*, 171. (d) Rudolph, M. *J. Comput. Chem.* **2005**, *26*, 619. (e) Rudolph, M. *J. Comput. Chem*. **2005**, *26*, 1193.

25. (a) Evans, D. H. *Chem. Rev*. **1990**, *90*, 739–751. (b) Evans, D. H. *Chem. Rev*. **2008**, *108*, 2113–2144.

26. K. Izutsu, *Electrochemistry in Nonaqueous Solutions*, 2nd ed. Weinheim: Wiley-VCH, 2009, p.100ff.

27. Boeré, R. T.; Bond, A. M.; Chivers, T.; Feldberg, S.W.; Roemmele, T.L. *Inorg. Chem.* **2007**, *46*, 5569-5607.

28. Sheldrick, G. M. *Acta Cryst., Section A*. **2008,** *A64*, 112–122.

TOC SYNOPSIS

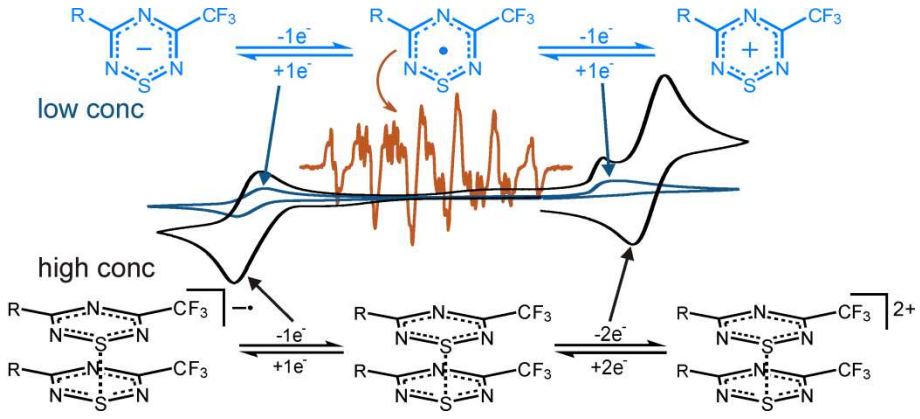

Complex concentration-dependence of the cyclic voltammograms of the title compounds in solution can be explained by monomer-dimer equilibria and the data fit a ladder scheme. EPR spectra on very dilute solutions unambiguously identify the monomeric radicals in solution.

Table 5. Crystallographic Data and Refinement Parameters for Compounds **1–6.**

complex	**1a**	**2a**	**2c**	**2e**	**4b**	**4e**
empirical formula	$C_8H_{10}N_2O$	$C_{10}H_{10}F_3N_3O$	$C_9H_8F_3N_3$	$C_{10}H_7F_6N_3$	$C_{10}H_7ClF_3N_3S$	$C_{10}H_4ClF_6N_3S$
M_r	150.18	245.21	215.18	283.19	293.70	347.67
Cryst size (mm^3)	0.25×0.15×0.12	0.45×0.37×0.20	0.401×0.208×0.116	0.652×0.429×0.310	0.31×0.16×0.16	0.17×0.14×0.14
cryst syst	Triclinic	Triclinic	Monoclinic	Monoclinic	Orthorhombic	Monoclinic
space group	*P*1	*P*1	$P2_1/n$	$P2_1/n$	$P2_12_12$	$P2_1/c$
a (Å)	5.005(10)	9.2967(19)	8.8135(17)	11.2481(8)	14.507(3)	14.5920(14)
b (Å)	10.15(2)	10.538(2)	16.356(3)	14.6690(10)	17.395(3)	11.8343(11)
c (Å)	15.54(3)	11.787(3)	14.069(3)	14.3328(10)	4.7852(8)	7.4331(7)
(deg)	86.58(2)	93.783(2)	90.00	90.00	90.00	90.00
(deg)	87.40(2)	105.567(2)	101.503(2)	93.7750(10)	90.00	94.7720(10)
(deg)	79.77(2)	97.335(2)	90.00	90.00	90.00	90.00
V ($Å^3$)	775(3)	1097.2(4)	1987.3(7)	2359.8(3)	1207.6(3)	1279.1(2)
Z	4	4	8	8	4	4
D_c ($Mg·m^{-3}$)	1.287	1.484	1.438	1.594	1.615	1.805
μ (mm^{-1})	0.088	0.134	0.130	0.165	0.511	0.530
θ range	2.04-27.89	1.80-27.00	1.93-27.42	1.99-26.36	1.83-29.59	2.22-28.83
coll. reflns	8956	12270	28147	24664	12307	14808
obsd reflns	3580	4750	4532	4826	2987	3137
no. of param	219	333	345	404	192	217
F(000)	320	504	880	1136	592	688
T (K)	173(2)	173 (2)	173(2)	173(2)	173(2)	173(2)
R1, wR2 [$I > \sigma 2(I)$]	0.0410, 0.0959	0.0338, 0.0842	0.0370, 0.0859	0.0468, 0.1217	0.0379, 0.0965	0.0327, 0.0843
R1, wR2 [all data]	0.0695, 0.1053	0.0420, 0.0896	0.0496, 0.0934	0.0538, 0.1298	0.0550, 0.1026	0.0414, 0.0895
GOF	0.978	1.038	1.041	1.038	1.031	1.056

[a] $wR2 = [\sum\{w (F_o^2 - F_c^2)^2\}/\sum w (F_o^2)^2]^{1/2}$; $R1 = \sum||F_o| - |F_c||/\sum|F_o|$. [b] $F_o > 4\sigma (F_o)$. [c] $GOF = [\sum\{w (F_o^2 - F_c^2)^2\}/(n - p)]^{1/2}$ where n = number of reflections and p = number of refined parameters.

Table 5 (cont'd). Crystallographic Data and Refinement Parameters for Compounds **1–6.**

complex	**5a**	**5b**	**5c**	**5d**	**5e**	**6**
empirical formula	$C_{10}H_7F_3N_3OS$	$C_{10}H_7F_3N_3S$	$C_9H_5F_3N_3S$	$C_9H_4ClF_3N_3S$	$C_{10}H_4F_6N_3S$	$C_7H_7ClN_2O_2S$
M_r	274.25	258.25	244.22	278.66	312.22	218.66
Cryst size (mm^3)	0.476×0.192×0.118	0.185×0.171×0.153	0.287×0.215×0.086	0.29×0.22×0.14	0.311×0.155×0.06	0.13×0.12×0.12
cryst syst	Triclinic	Triclinic	Triclinic	Triclinic	Triclinic	Tetragonal
space group	*P*1	*P*1	*P*1	*P*1	*P*1	$P4_12_12$
a (Å)	7.1075(8)	11.5126(12)	9.136(4)	11.1851(15)	10.7943(6)	9.4879(9)
b (Å)	11.5130(13)	14.7539(15)	10.728(4)	14.799(2)	13.3162(8)	9.4879(9)
c (Å)	13.3832(15)	15.0498(15)	11.016(5)	14.806(2)	16.7910(10)	21.584(4)
(deg)	88.0000(10)	111.2160(10)	84.652(4)	110.9450(10)	94.0420(10)	90.00
(deg)	86.2810(10)	99.9130(10)	69.663(4)	103.210(2)	107.4760(10)	90.00
(deg)	80.4830(10)	107.6770(10)	68.715(3)	106.5720(10)	96.1190(10)	90.00
V ($Å^3$)	1077.5(2)	2153.0(4)	942.6(7)	2038.8(5)	2275.6(2)	1943.0(5)
Z	4	8	4	8	8	8
D_c ($Mg·m^{-3}$)	1.691	1.593	1.721	1.816	1.823	1.495
μ (mm^{-1})	0.333	0.321	0.362	0.600	0.358	0.576
θ range	1.79-27.42	1.96-26.59	1.97-27.45	1.61-28.49	1.90-28.73	2.34-26.86
coll. reflns	15562	23211	13575	22885	26627	21297
obsd reflns	4872	8841	4267	9467	10697	2076
no. of param	327	729	577	629	777	124
F(000)	556	1048	492	1112	1240	896
T (K)	173(2)	296(2)	173(2)	173(2)	173(2)	173(2)
R1, wR2 [$I > \sigma\ 2(I)$]	0.0273, 0.0732	0.0379, 0.1035	0.0368, 0.0976	0.0426, 0.0893	0.0440, 0.1137	0.0421, 0.1102
R1, wR2 [all data]	0.0302, 0.0757	0.0572, 0.1127	0.0444, 0.1036	0.0825, 0.1054	0.0689, 0.1256	0.0610, 0.1166
GOF	1.032	1.026	1.047	1.022	1.036	0.984

[a] $wR2 = [\sum\{w (F_o^2 - F_c^2)^2\}/\sum w (F_o^2)^2]^{1/2}$; $R1 = \sum||F_o| - |F_c||/\sum|F_o|$. [b] $F_o > 4\sigma (F_o)$. [c] $GOF = [\sum\{w (F_o^2 - F_c^2)^2\}/(n - p)]^{1/2}$ where n = number of reflections and p = number of refined parameters.

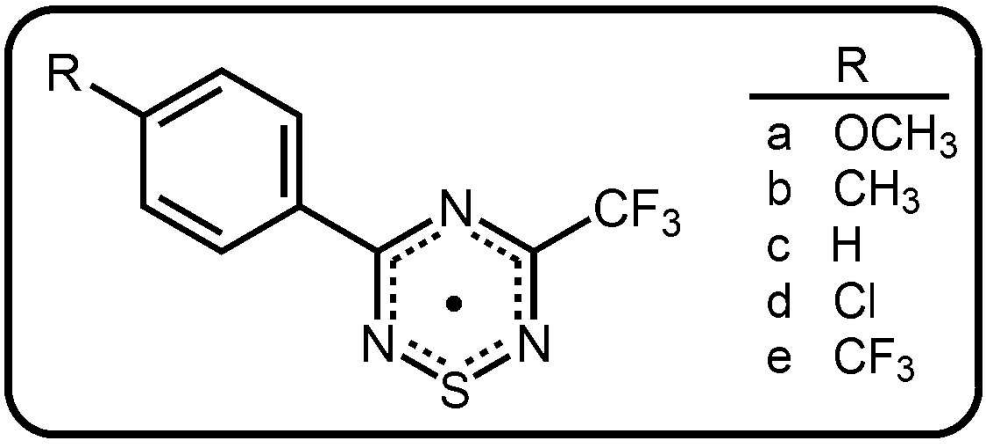

The 3-trifluoromethyl-5-aryl-1lambda3-1,2,4,6-thiatriazinyls
96x43mm (300 x 300 DPI)

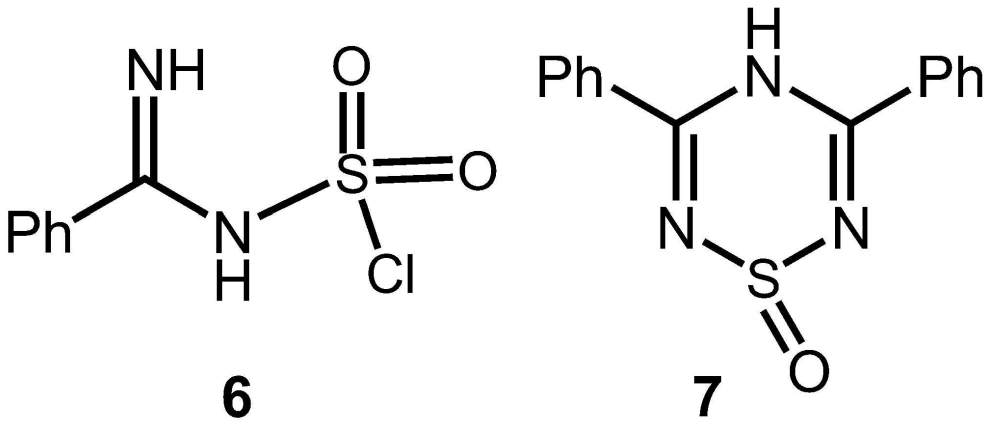

6 **7**

no caption
86x38mm (600 x 600 DPI)

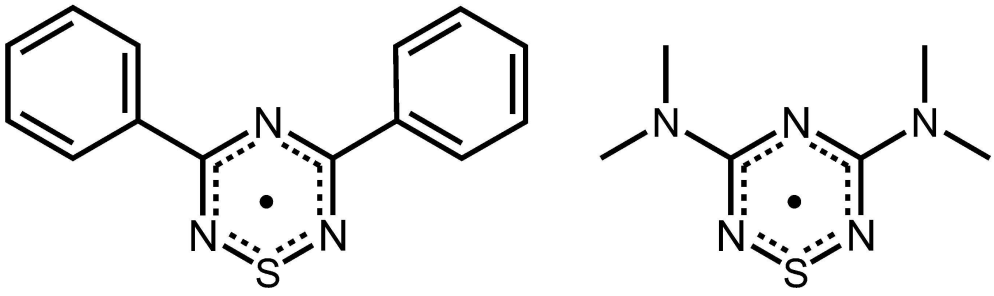

8 **9**

no caption
115x48mm (600 x 600 DPI)

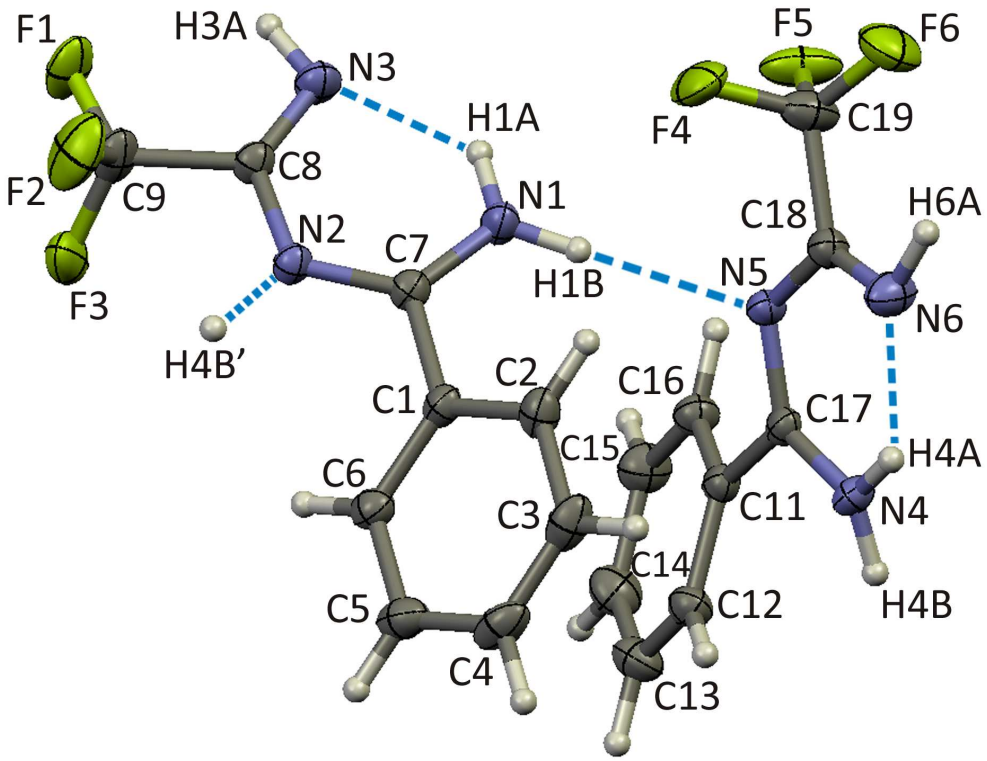

Thermal ellipsoids (30%) plot showing the two independent hydrogen-bonded molecules of 2c as found in the crystal at −100(2) °C along with an additional H4B' atom to indicate how the chain propagates in the lattice. The H1B—N5 and H4B'—N2 bonds can be viewed as incipient tautomerism leading to the diimine isomer. Only the principal components of the disordered CF3 groups are shown for clarity. (Figures S3 and S4 are plots of 2a and 2e.)
80x61mm (600 x 600 DPI)

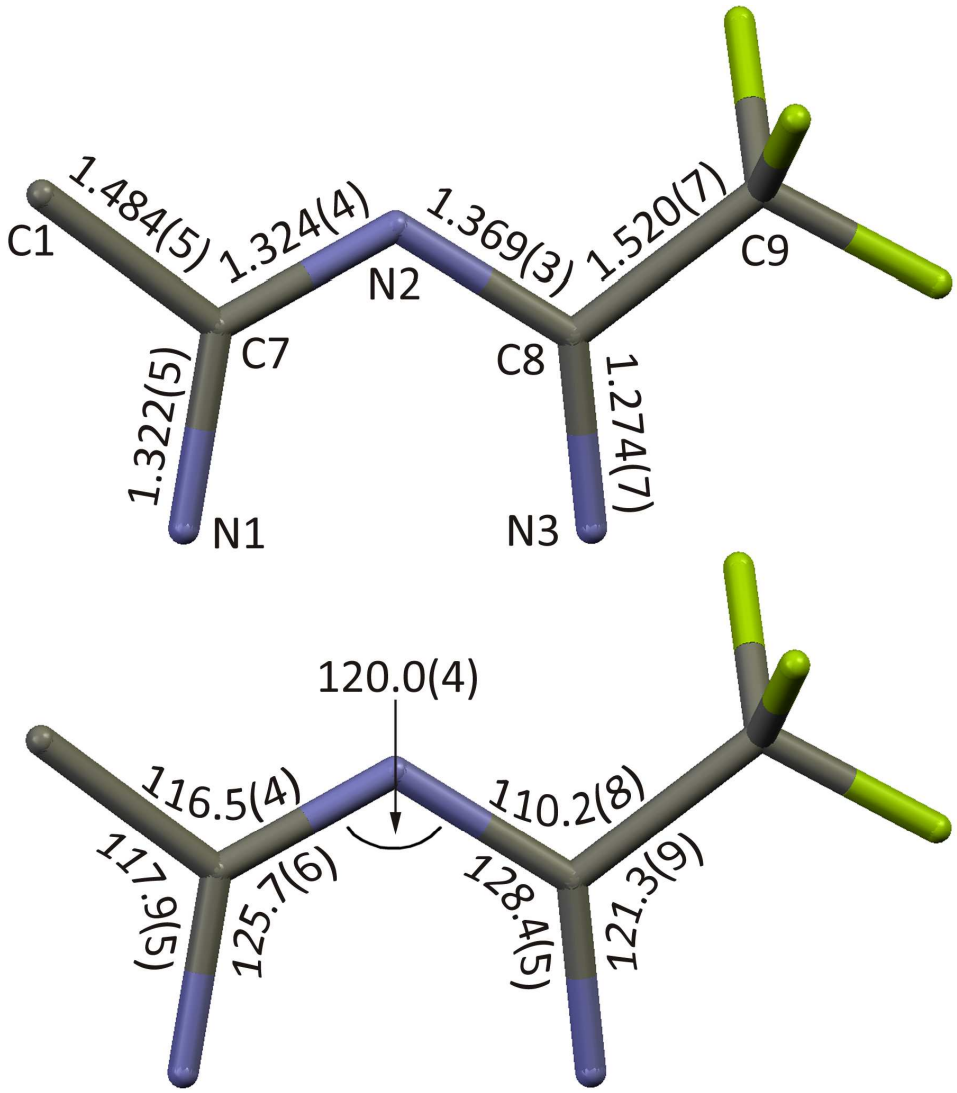

Average bond lengths (Å, top) and angles (°, bottom) from crystal structures of the six independent imidoylamidine molecules found in 2a, 2c, and 2e. Errors are standard deviations.
80x88mm (600 x 600 DPI)

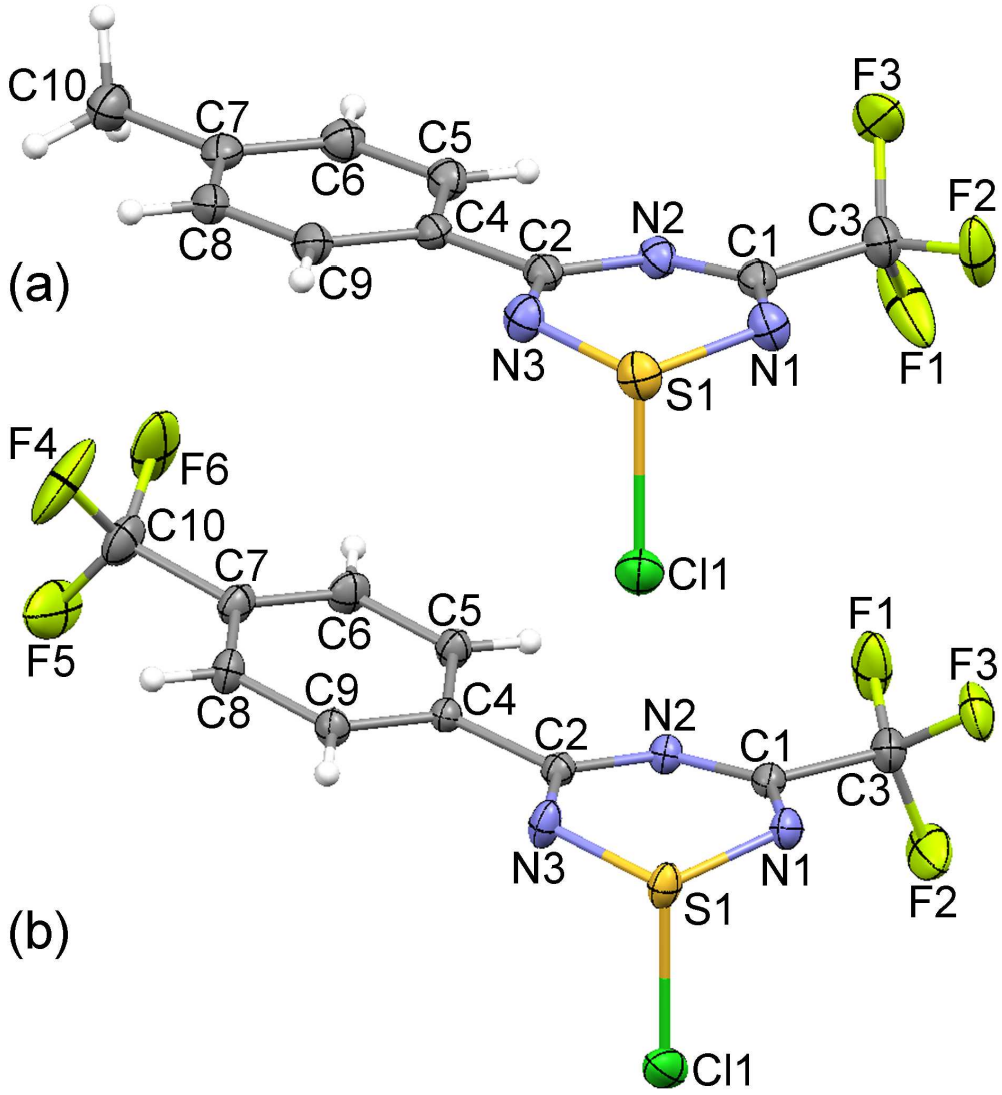

Thermal ellipsoids (30%) plots with atom numbering schemes showing the molecular structures of (a) 4b and (b) 4e as they are found within the crystal lattices at −100(2) °C. Only the principal components of the disordered CF3 groups are shown.
80x89mm (600 x 600 DPI)

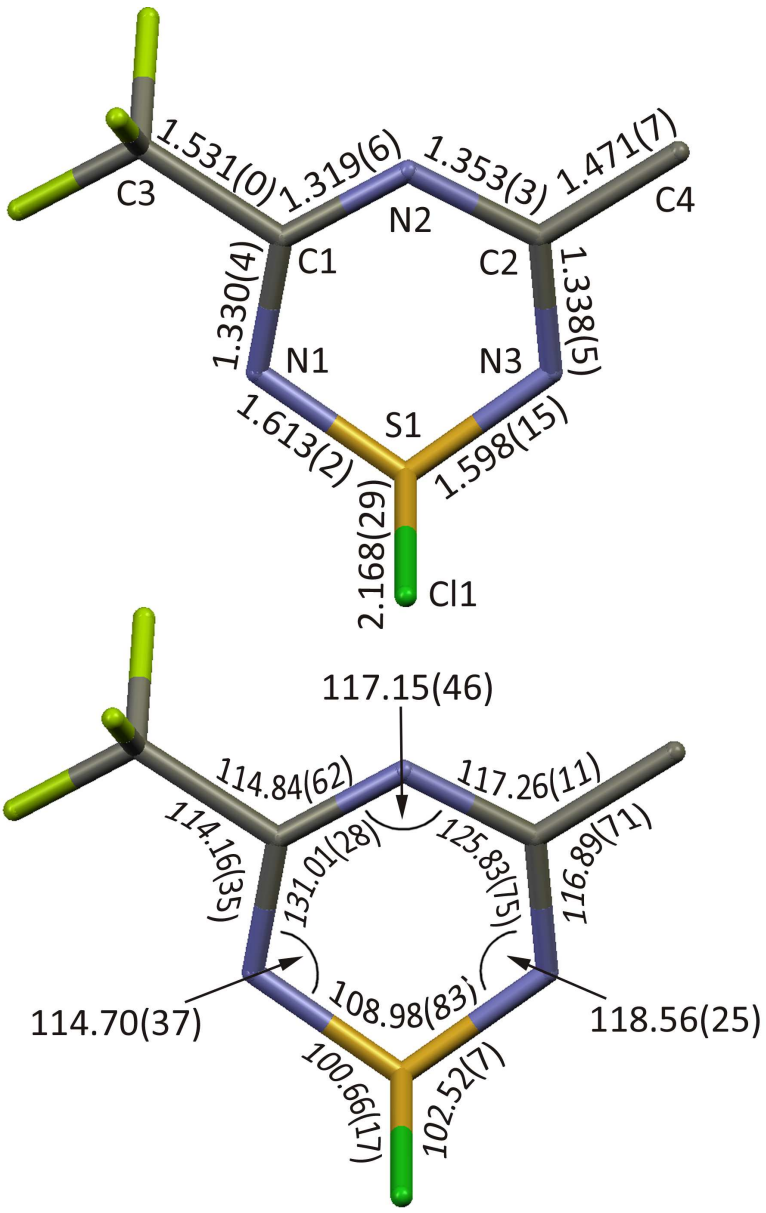

Average bond lengths (Å, top) and angles (°, bottom) with standard deviations from crystal structures of the 1-chlorothiatriazines 4b and 4e.
80x118mm (600 x 600 DPI)

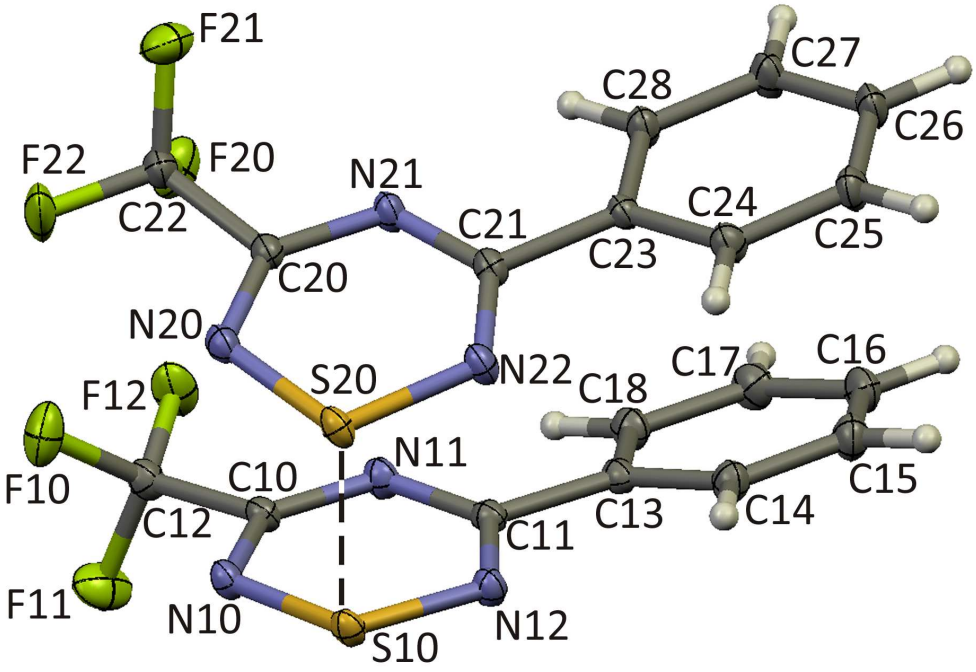

Thermal ellipsoids (30%) plot and atom numbering scheme showing the solid-state face-to-face and head-to-head dimerization of 5c, which comprises the asymmetric unit in the lattice at −100(2) °C. The dashed line indicates the close contact between sulfur atoms, for which the S10···S20 distance is 2.625(1) Å. The structure of 5a (Figure S9) is very similar with an S10···S20 distance of 2.6370(3) Å.
80x53mm (600 x 600 DPI)

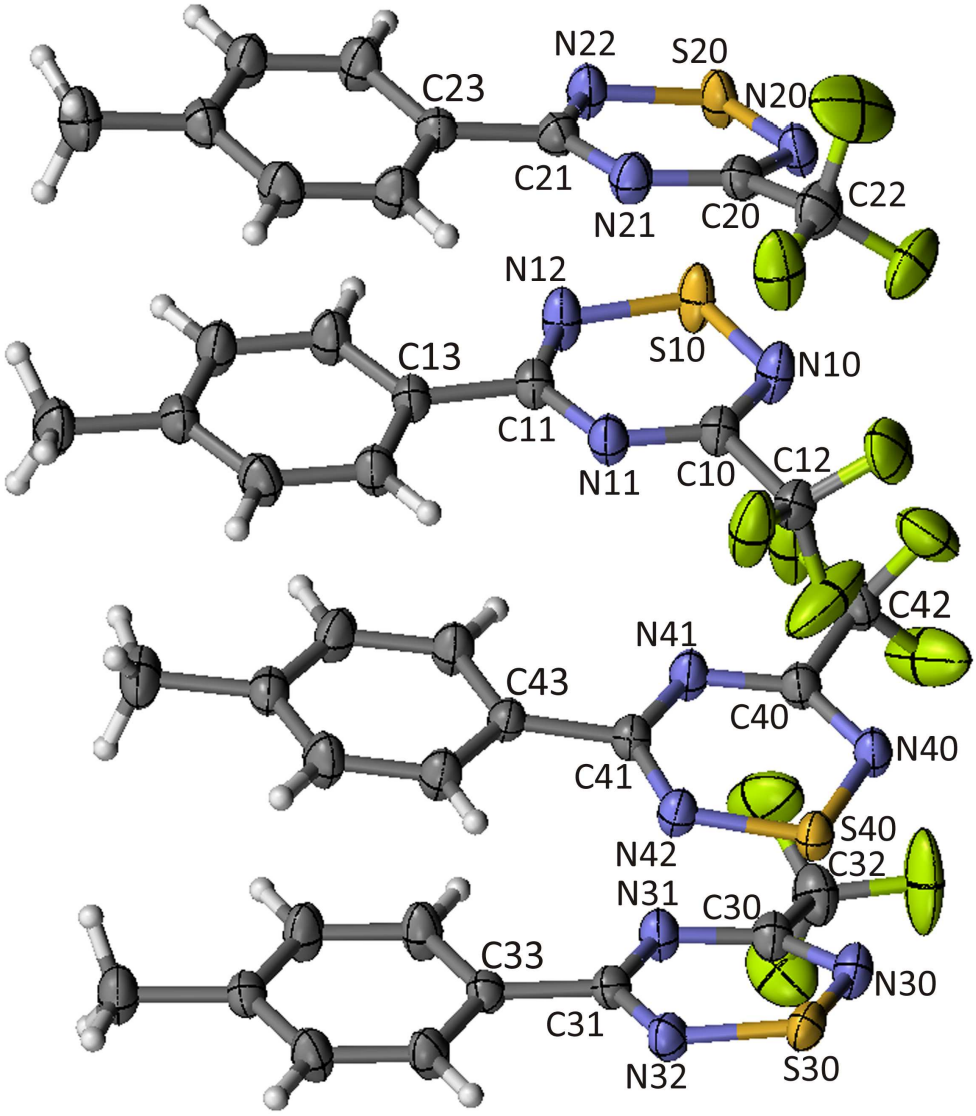

Thermal ellipsoids (30%) plot with atom numbering scheme showing the molecular structure of 5b found within the crystal lattice at 23(2) °C. Four crystallographically independent molecules form into two distinct dimers. The S10···S20 distance is 2.684(1) Å and the S30···S40 distance is 2.6515(8) Å. A very similar arrangement is found in the lattice for 5d (Figure S10) with S10···S20 and S30···S40 distances of 2.659(1) Å and 2.635(1) Å, respectively.
99x119mm (600 x 600 DPI)

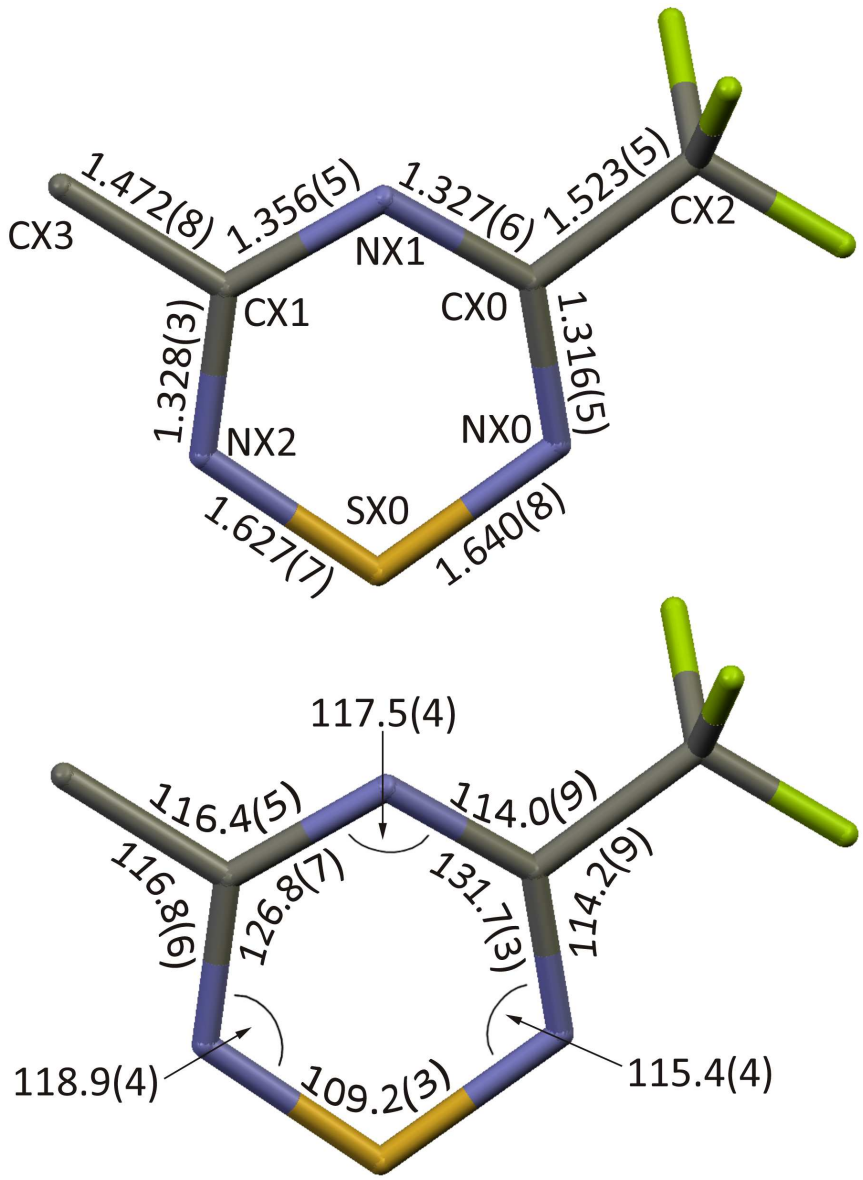

Comparison of bond lengths (Å, top) and angles (°, bottom) in 1,2,4,6-thiatriazinyls determined from five crystal structures. A common numbering scheme was used among crystallographically independent monomers (X = 1–4). The average intradimer short S···S contact distance is 2.643(21) Å.

80x106mm (600 x 600 DPI)

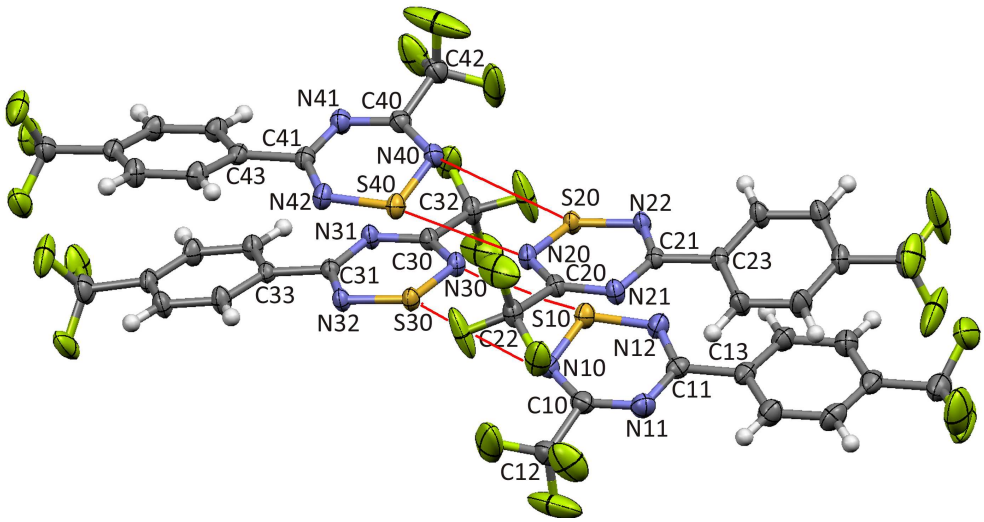

Thermal ellipsoids (30%) plot with atom numbering scheme showing the molecular structure of 5e found within the crystal lattice at −100(2) °C. Four crystallographically independent molecules form into two distinct dimers with intra-dimer S10···S20 and S30···S40 distances of 2.6237(9) Å and 2.6255(8) Å, respectively. These dimers associate into a single tetrameric set through S(δ+)–N(δ−) interactions (shown in red). The S20···N30 and S30···N20 distances are 3.169(2) Å and 3.199(2) Å, while S40···N20 and S10···N30 distances are 3.082(2) Å and 3.034(2) Å, respectively. The rings belonging to the dimers are out of register with each other as indicated by the different interaction lengths.
120x62mm (600 x 600 DPI)

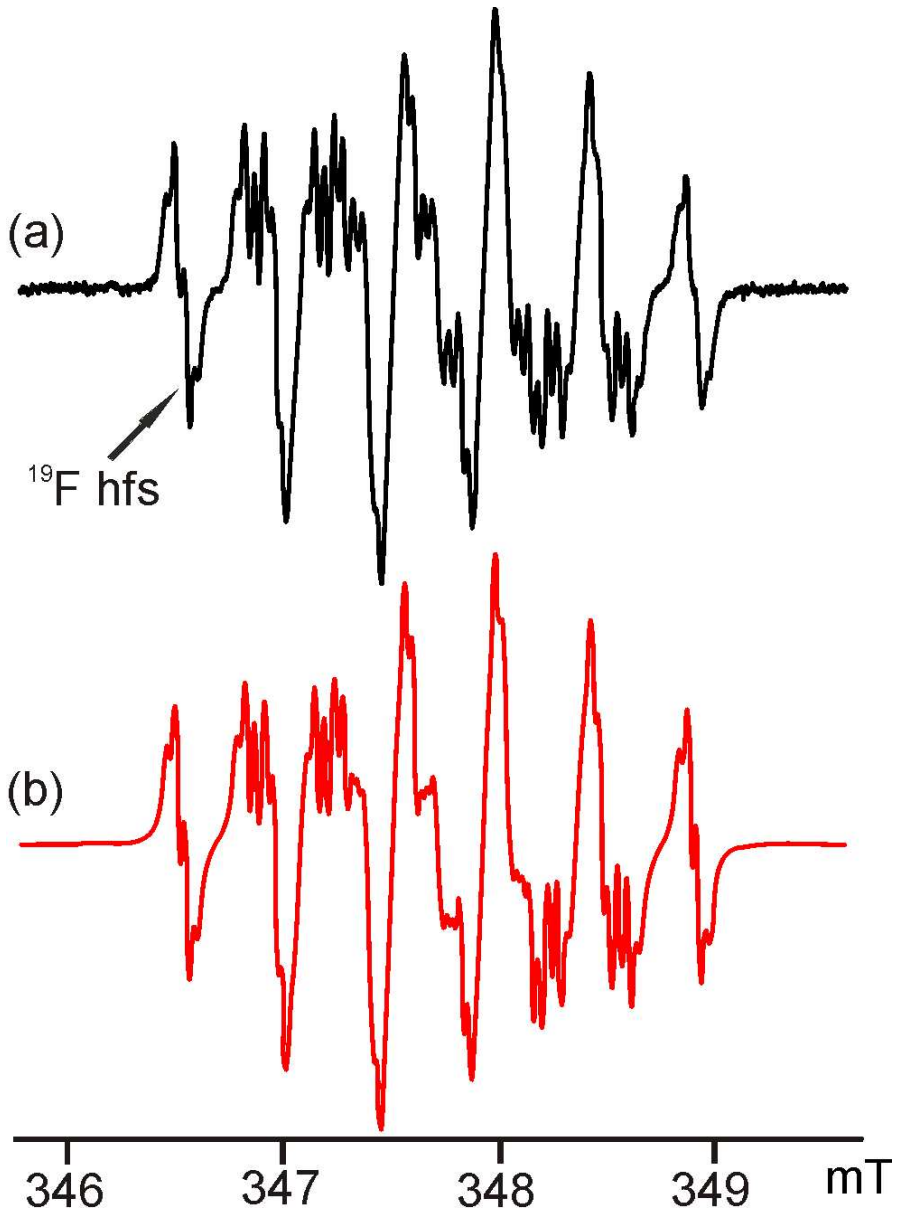

(a) Experimental and (b) simulated EPR spectra of 5d in CH2C12 at 18 °C, modulation amplitude 0.01 mT, modulation frequency 100 kHz. Simulations were performed with WinSim (version 0.98, 2002) 19 software using a 100% Lorentzian lineshape.
83x112mm (300 x 300 DPI)

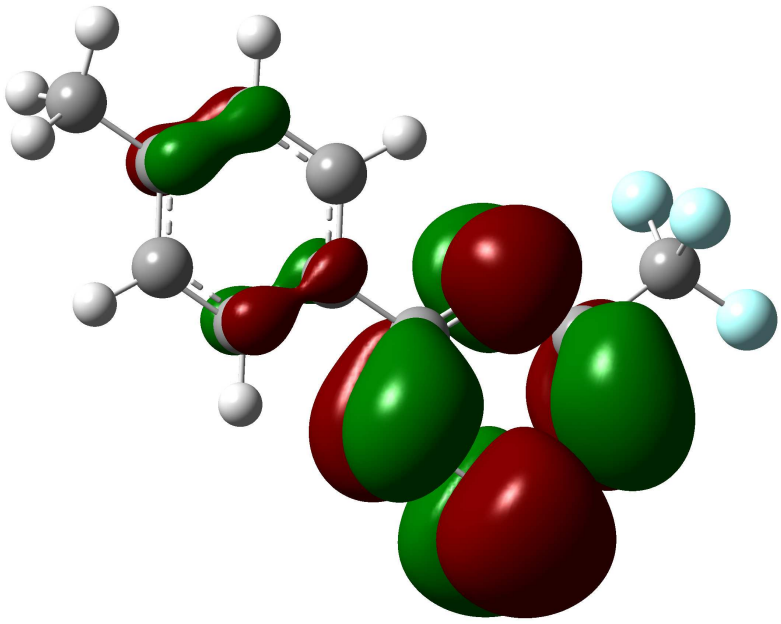

Kohn-Sham isosurface of the π-SOMO of 5b from a UB3LYP/6–31G(d) calculation.
956x690mm (72 x 72 DPI)

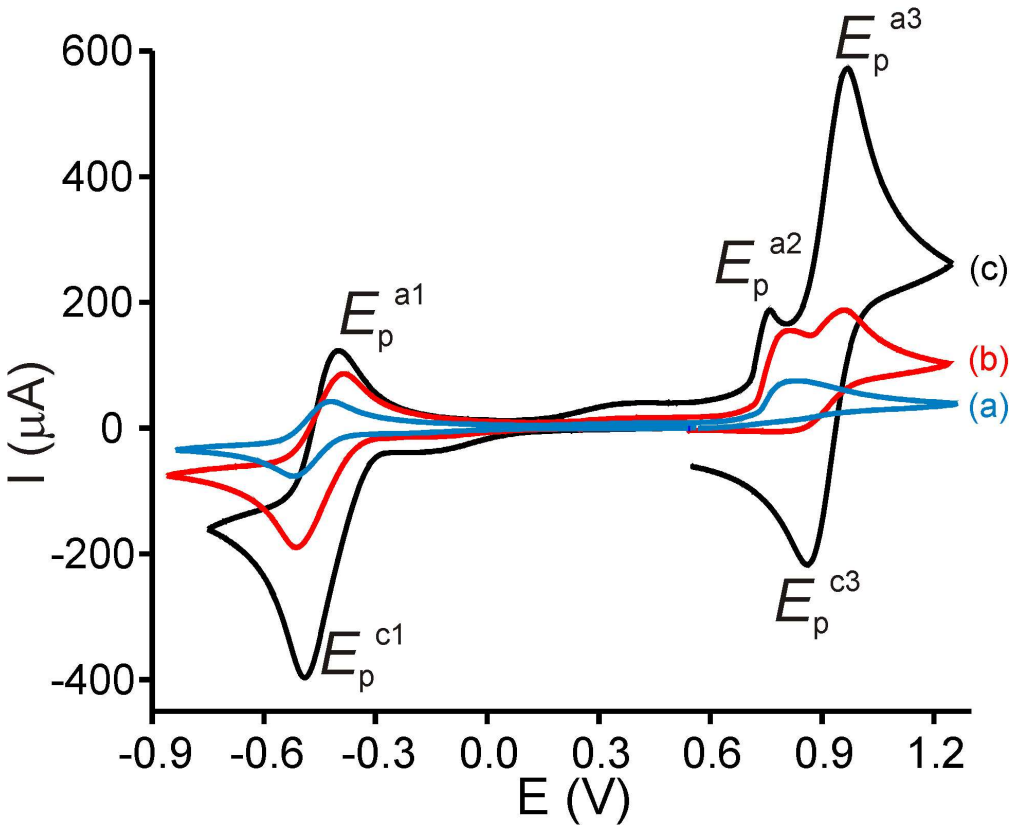

Overlapping CV's of the redox couples of 5e in CH3CN solution (0.1 M [nBu4N][PF6]) at: a) dilute concentration (blue), b) moderate concentration (red), and c) high concentration (black).
82x67mm (600 x 600 DPI)

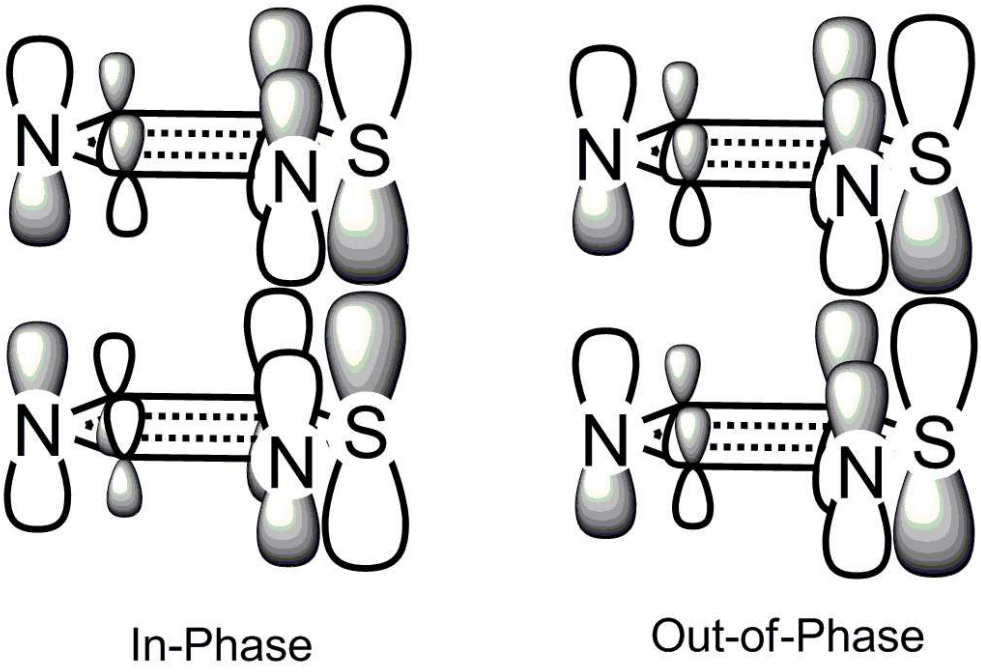

The in-phase and out-of-phase combinations of the 3b1 SOMO of model 3,5-dihydro-1,2,4,6-thiatriazinyls.
87x60mm (300 x 300 DPI)

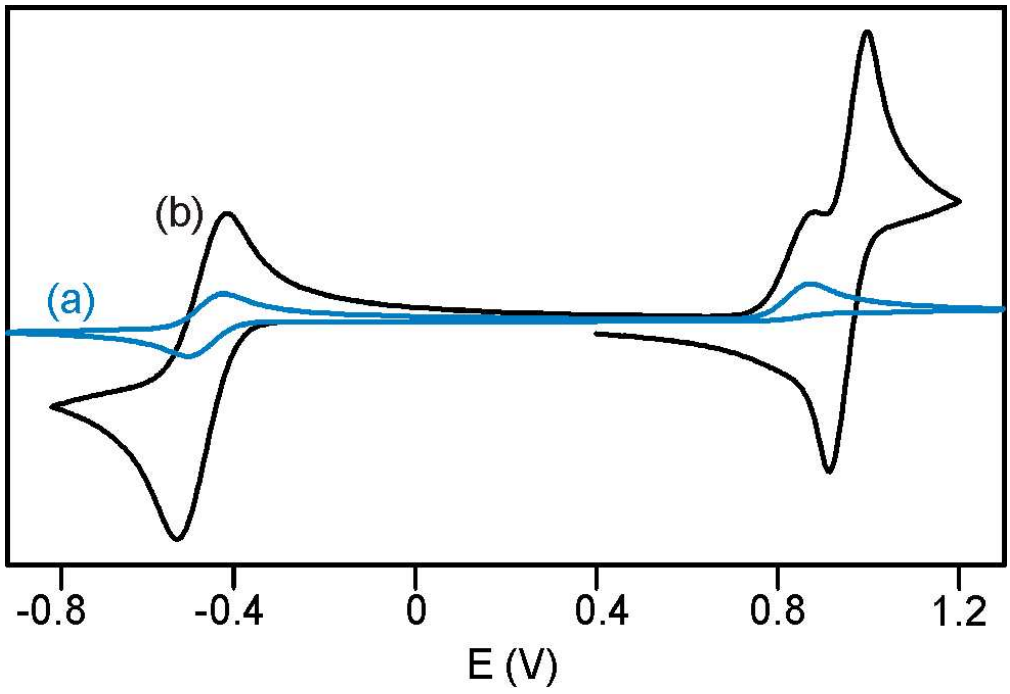

Calculated CVs for both (a) monomeric (blue line) and (b) dimeric (black line) solutions of 5e resulting from the input of kinetic parameters listed in the text and following the "ladder" scheme shown in Scheme 2. These CVs follow the specific case of v = 0.2 V s−1, Keq1 = 400, kf1 = 1 M−1 s−1, Keq2 = 0.0766, kf2 = 0.01 M−1 s−1, Keq3 = 271, kf3 = 1 M−1 s−1, Keq4 = 106, kf4 = 5 s−1 (first-order decay of [TTA]+), ks1 = ks2 = ks3 = ks4 = 0.03 cm s−1, conc. dimer = 0.01 mol L−1, conc. monomer 0.001 mol L−1. The potential was first swept in the cathodic direction starting from 0.4 V.
82x56mm (300 x 300 DPI)

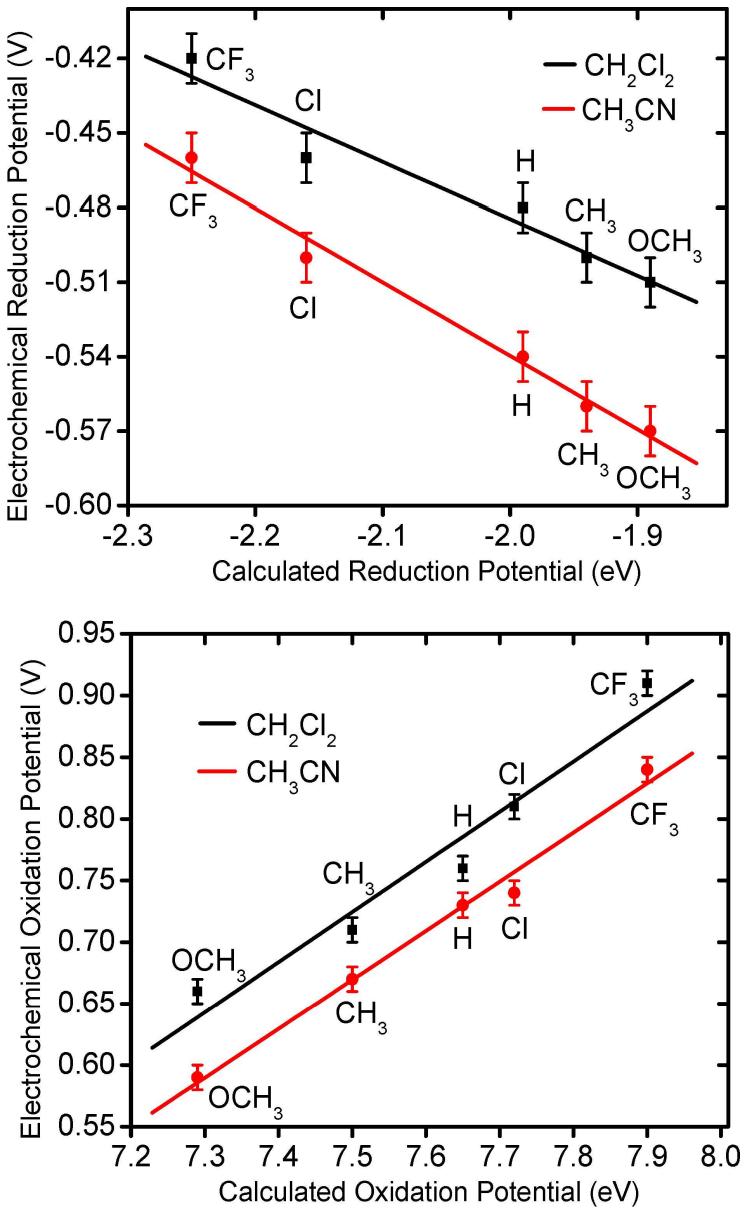

Plots of the calculated vs. experimental monomer reduction potentials (top) and oxidation potentials (bottom) of 5a–e as measured by cyclic voltammetry in CH2Cl2 (black line, R = 0.975, top and R = 0.975, bottom), and (b) CH3CN (red line, R = 0.993, top and R = 0.994, bottom) solution. Error bars express an estimated error in measured potential of ±0.01 V.
79x130mm (600 x 600 DPI)

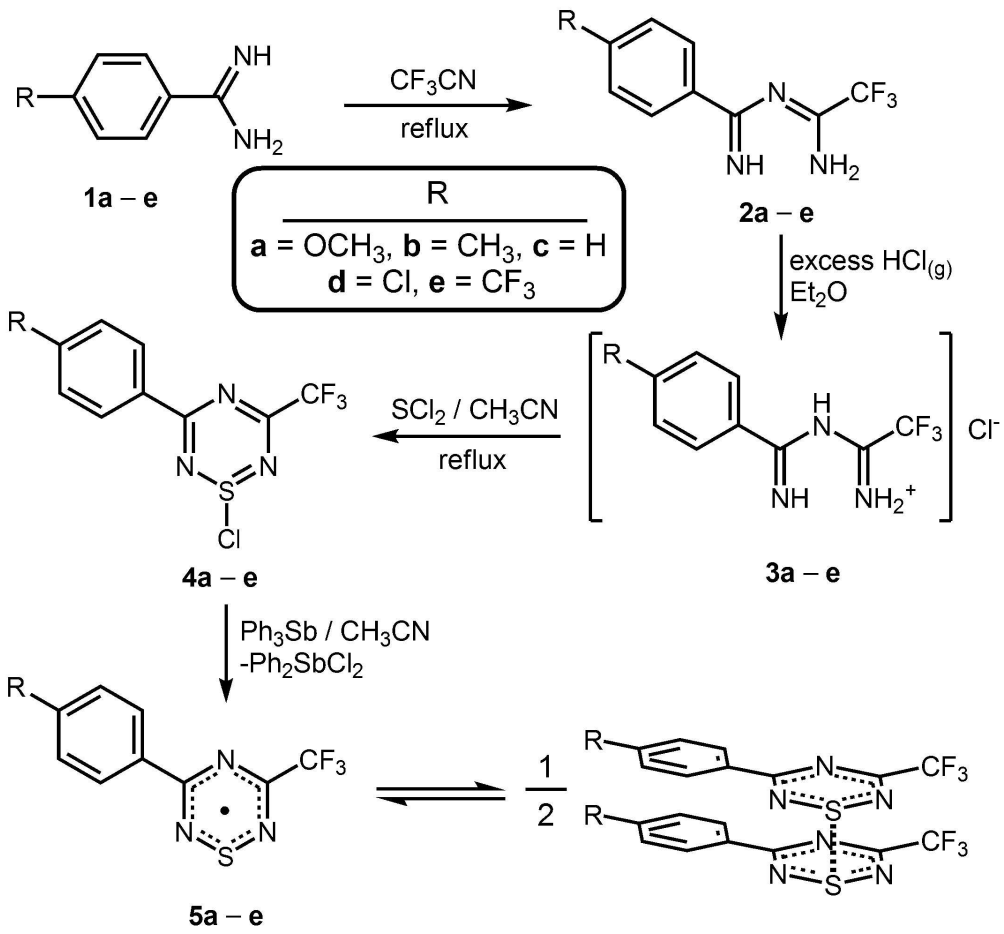

Synthetic route to the 3-trifluoromethyl-5-aryl-1,2,4,6-thiatriazines.
181x167mm (300 x 300 DPI)

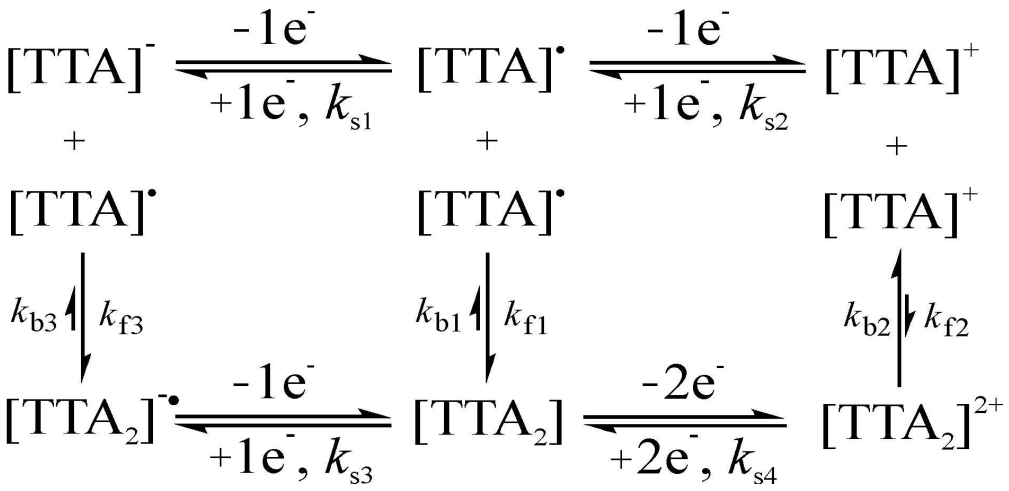

Proposed "Ladder" Scheme interrelating the voltammetric behavior of thiatriazinyls at lower and higher concentrations.
79x37mm (600 x 600 DPI)

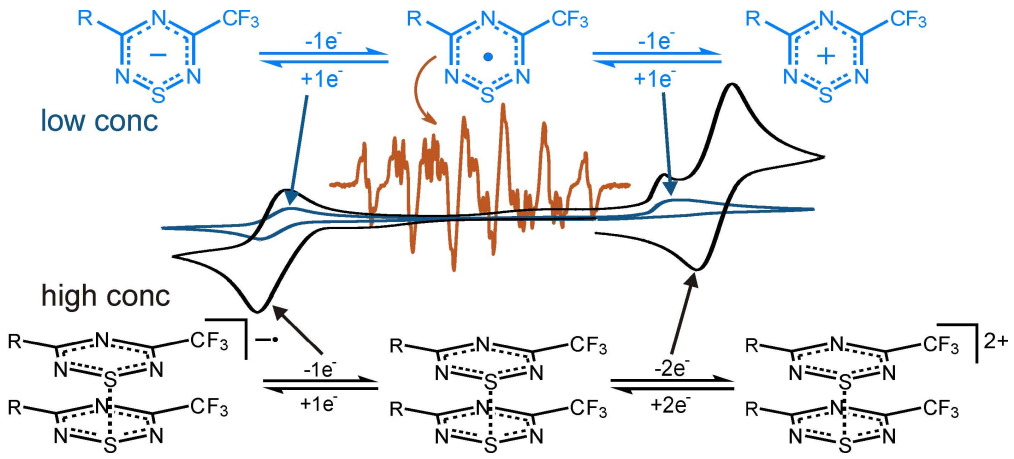

Complex concentration-dependence of the cyclic voltammograms of the title compounds in solution can be explained by monomer-dimer equilibria and the data fit a ladder scheme. EPR spectra on very dilute solutions unambiguously identify the monomeric radicals in solution.
119x53mm (600 x 600 DPI)

Unsymmetrical 1λ³-1,2,4,6-thiatriazinyls with aryl and trifluoromethyl substituents: synthesis, crystal structures, EPR spectroscopy and voltammetry

René T. Boeré, Tracey L. Roemmele and Xin Yu*

Department of Chemistry and Biochemistry, University of Lethbridge, Lethbridge, AB Canada T1K 3M4

* To whom correspondence may be addressed. E-mail: boere@uleth.ca. Tel.: (403) 329-2045. Fax.: (403)329-2057

IC-2011-003996

Supplementary Information

Crystallographic characterization of benzamidine 1a

Hydrogen bonding in the crystal structures of imidoylamidines 2a-e

Infra-red spectra of 2a-e and 3a-e

Crystallographic Characterization of *para*-substituted benzamidine 1a

Amidine chemistry is of interest due to the multifaceted bonding modes of these compounds as complex-ligands and their widespread use as synthons for subsequent chemical transformations.[1] This compound was characterized by X-ray crystallography as an example of an aryl benzamidine. No structure of this derivative has yet been reported in the Cambridge Crystallographic Database (2010 edition.) Plate shaped X-ray quality crystals of **1a** were collected on a cold finger following vacuum sublimation and its structure was determined by crystallography (Figure 1). The unit cell contains two independent hydrogen-bonded centrosymmetric dimers of a type previously determined for amidines.[2] The C–N distances in the amidine unit are indicative of partial single (C1–N1 = 1.358(3) Å) and partial double bond (C1–N2 = 1.294(3) Å) character, and are consistent with previously known values for aryl amidines.[3]

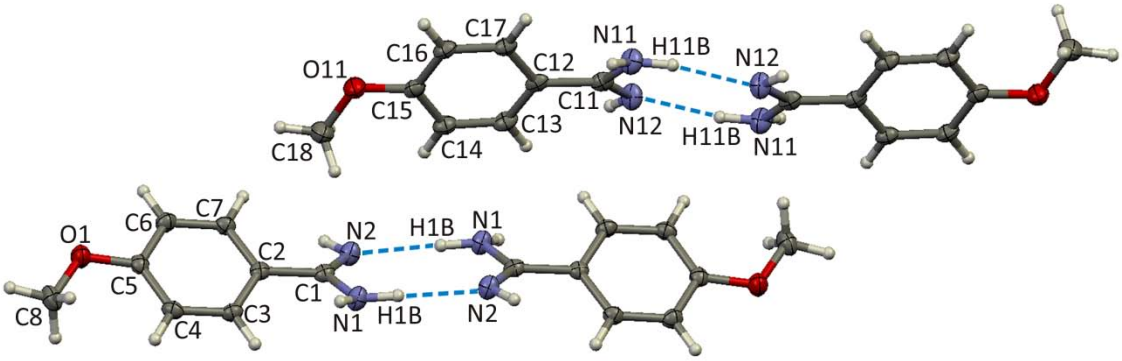

Figure S1. Thermal ellipsoids (30%) plot showing the two independent hydrogen-bonded dimers of **1a** found within the crystal lattice at −100(2) °C. Each dimeric pair is connected in ribbons to adjacent dimers of the same type through additional H bonding between N2 and H1A.The molecules that are fully-labelled comprise the asymmetric unit of the cells, each related to another molecule of the same type by inversion symmetry as required by the $P\bar{1}$ space group.

Table S1. ^{1}H NMR spectral data for the aryl N-imidoylamidines **2a–e**.[a]

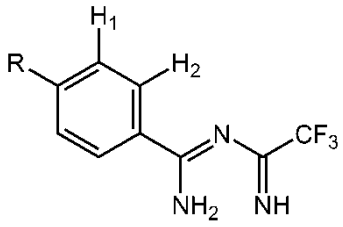

cmpd	R	H_1	H_2	J_{AB} (Hz)	R	NH	NH	NH
2a	CH_3O	6.93	7.87	9.0	3.85	11.0	9.0	6.7
2b	CH_3	7.26	7.81	8.1	2.41	11.0	9.1	6.7
2c	H	m 7.38– 7.54	m 7.83 – 7.88	—	m 7.38 – 7.54	11.0	9.1	6.8
2d	Cl	7.42	7.84	8.8	—	11.0	9.2	6.7
2e	CF_3	7.73	8.02	8.1	—	11.1	9.3	6.8

[a] All values are in ppm, with reference to TMS.

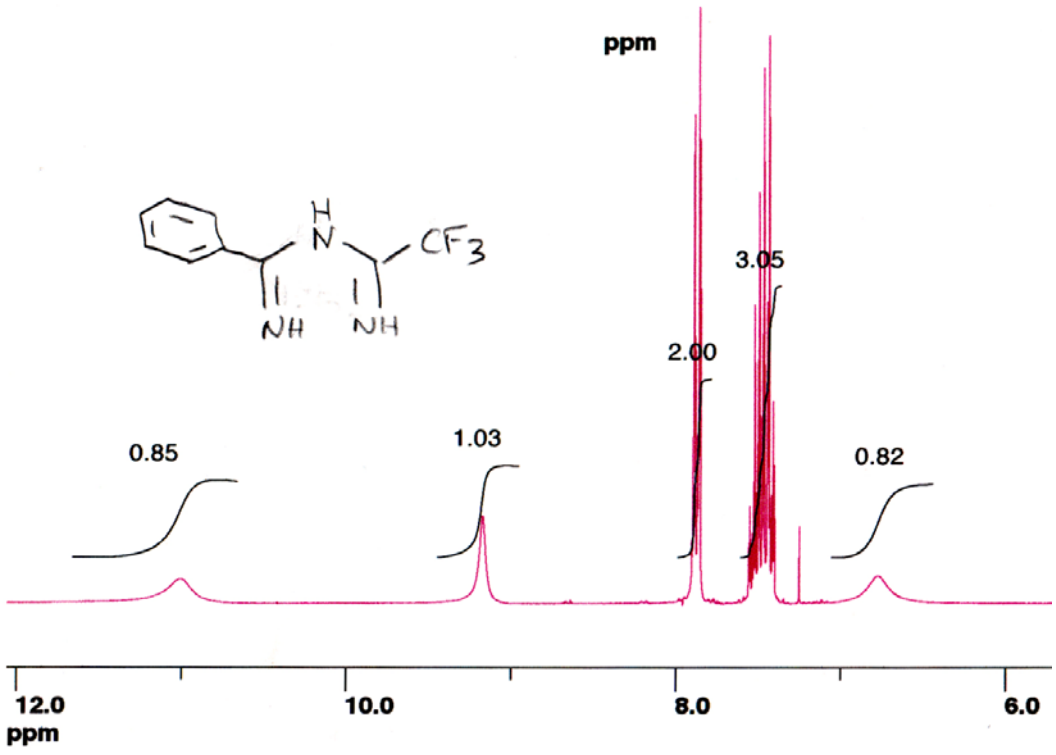

Figure S2. ^{1}H NMR Spectrum (250MHz, $CDCl_3$) of compound **2c** which is entirely typical of all the imidoylamidines prepared in this work. The three kinds of NH peaks have very distinct chemical shifts and linewidths.

Table S2. ^{13}C NMR of aryl imidoylamidines **2a–e**.[a]

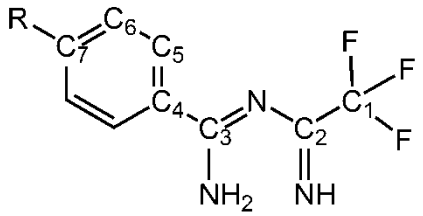

cmpd	C_1	C_2	C_3	C_4	C_5	C_6	C_7	R
2a	117.86[b]	163.41[c]	165.33	127.33	129.25	114.32	163.09	55.66
2b	117.84[b]	163.55[c]	165.83	132.37	127.64	129.70	142.84	21.65
2c	117.80[b]	163.51[c]	165.92	135.22	127.44	129.02	132.20	—
2d	117.70[b]	163.31[c]	164.76	133.60	128.83	129.28	138.62	—
2e	117.67[b]	163.23[c]	164.65	138.55	127.91	125.98[d]	133.91[c]	123.91[e]

[a] All values are in ppm, with reference to TMS. [b] q, $^3J_{(F,C)}$ = 281 Hz [c] q, $^3J_{(F,C)}$ = 33 Hz. [d] q, $^3J_{(F,C)}$ = 3.9 Hz. [e] q, $^3J_{(F,C)}$ = 273 Hz.

Hydrogen bonding in the crystal structures of imidoylamidines 2a-e

Strong intramolecular hydrogen bonding (Table S3) is found from N3 to H1A and N6 to H4A in all cases, leading to *pseudo* six-membered rings with N··N distances in the range 2.6350(18) – 2.6928(18) Å. There are also weaker (2.9765(15) – 3.1934(16) Å) intermolecular H-bonds which link N1 and N4 to the backbone nitrogen atoms (N2, N5) of the next molecule in **2c** and **2e** (compared to the typical N··N distance range 2.94 – 3.15 Å for H-bonding between nitrogen.)[4] However, **2a** differs from the others by having additional short contacts between both N3 and H4A and N6 and H3A. In this case all the intermolecular N··N distances are rather long, ranging from 3.1832(16) to 3.2342(17) Å. The N–H···N angles range between 124.9(13) and 175.1(14)°, normal for this class.[4] Interestingly, in the case of **2c** and **2e** one NH atom from each imidoylamidine is not involved in any H-bonding (H3A, H6A).

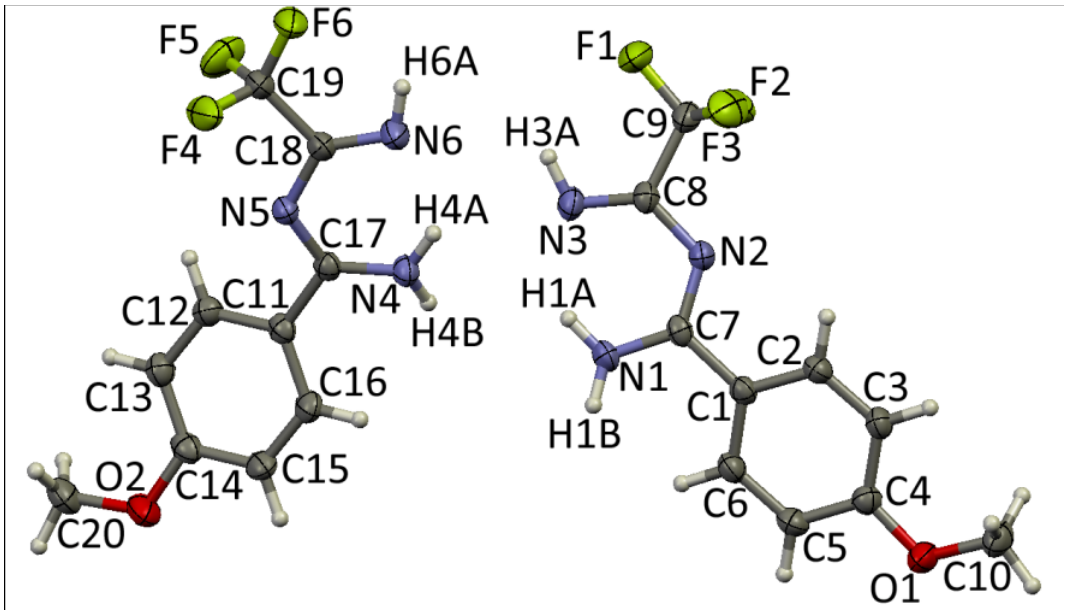

Figure S3. Thermal ellipsoids (30%) plot showing the two independent molecules of **2a** found within the crystal lattice at −100(2) °C. There are short contacts between both N4 and N6 with N3, but N4 to N6 is slightly beyond the range of a normal H-bond at −100(2) °C.

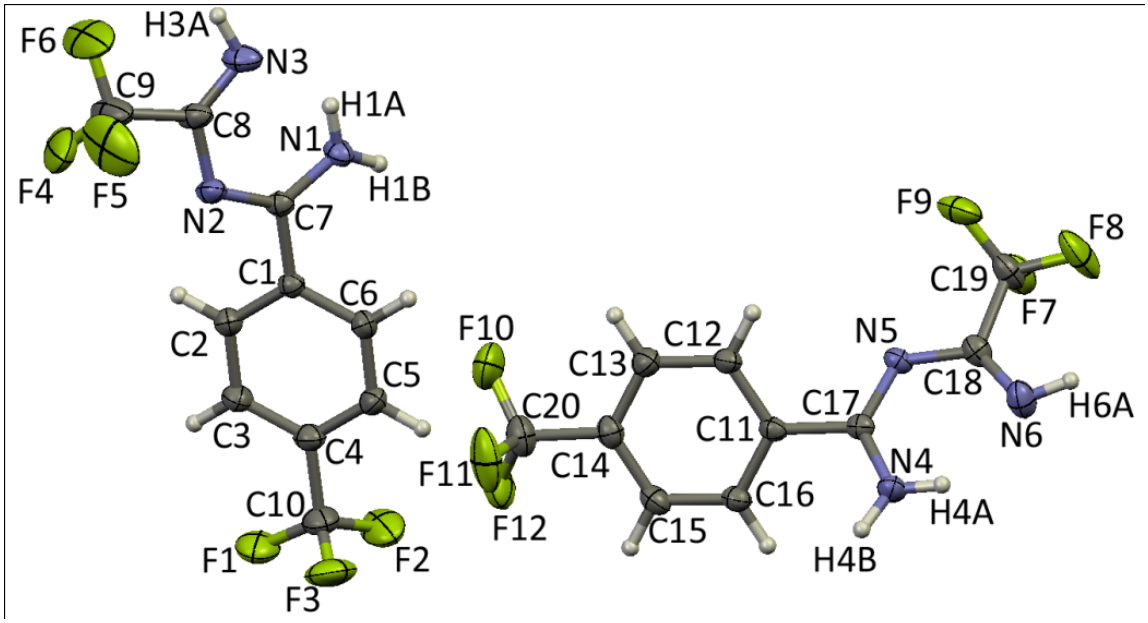

Figure S4. Thermal ellipsoids (30%) plot showing the two independent hydrogen-bonded molecules of **2e** found within the crystal lattice at −100(2) °C.

Table S3. Hydrogen bonds [Å] and angles [°] for imidoylamidines **2a**, **2c**, and **2e**.

Bond Type	D–H...A	Cmpd	d(D...A)	<(DHA)
Inter	N1–H1B...N5	**2a**	3.1832(16)	139.2(14)
		2c	3.0868(16)	175.1(14)
		2e	2.994(2)	170.2(19)
Inter	N4–H4B...N2	**2a**	3.1869(16)	136.3(14)
		2c	2.9765(15)	153.3(13)
		2e	3.099(2)	172(2)
Intra	N1–H1A...N3	**2a**	2.6448(18)	133.9(14)
		2c	2.6712(17)	131.4(13)
		2e	2.660(2)	134.5(18)
Intra	N4–H4A...N6	**2a**	2.6928(18)	129.3(14)
		2c	2.6350(18)	133.5(13)
		2e	2.643(2)	132.0(18)
Inter	N4–H4A...N3	**2a**	3.1934(16)	139.5(13)
Inter	N3–H3A...N6	**2a**	3.2342(17)	124.9(13)

Infra-red spectra of 2a-e and 3a-e

(KBr pellets; recorded on a Bomem MB102 FTIR spectrometer)

2a: 3383 (m), 3325 (m), 3178 (w), 1601 (s), 1572 (s), 1485 (s), 1466 (sh), 1438 (m), 1423 (m), 1399 (m), 1311 (m), 1261 (s), 1233 (s), 1221 (s), 1174 (vs), 1141 (vs), 1113 (sh), 1094 (m), 1029 (m), 998 (m), 837 (s), 815 (w), 786 (m), 758 (w), 745 (w), 729 (w), 708 (w), 689 (w), 642 (w), 614 (w), 588 (w), 563 (m), 514 (w), 479 (w), 433 (w) cm^{-1}.

2b: 3455 (m), 3345 (m), 3330 (m), 1612 (s), 1571 (m), 1524 (m), 1486 (s), 1400 (m), 1289 (w), 1231 (s), 1175 (s), 1154 (vs), 1111 (sh), 1019 (m), 998 (m), 954 (w), 867 (w), 842 (m), 831 (m), 820 (m), 781 (m), 734 (m), 687 (m), 670 (w), 593 (w), 543 (m), 513 (m), 466 (w), 441 (w) cm^{-1}.

2c: 3330 (m), 3118 (w), 1631 (s), 1600 (s), 1579 (s), 1513 (s), 1481 (s), 1449 (s), 1420 (m), 1320 (w), 1300 (w), 1224 (s), 1164 (s), 1144 (vs), 1076 (w), 1031 (m), 1000 (s), 932 (w), 878 (m), 826 (m), 800 (w), 775 (m), 715 (m), 695 (s), 614 (w), 602 (w), 583 (m), 516 (w), 448 (w), 421 (w) cm^{-1}.

2d: 3333 (s), 3257 (m), 3102 (m), 1644 (s), 1600 (s), 1572 (w), 1515 (m), 1475 (m), 1428 (w), 1395 (w), 1300 (w), 1226 (s), 1194 (s), 1179 (m), 1160 (sh), 1146 (vs), 1089 (m), 1017 (s), 884 (w), 844 (m), 836 (w), 794 (w), 732 (m), 675 (w), 647 (w), 625 (w), 592 (w), 519 (w), 485 (w), 458 (w), 428 (w) cm^{-1}.

2e: 3330 (m), 3249 (m), 3083 (m), 1636 (m), 1607 (s), 1582 (m), 1527 (s), 1493 (s), 1436 (w), 1406 (m), 1326 (vs), 1299 (sh), 1229 (s), 1202 (s), 1152 (s), 1130 (s), 1112 (sh), 1067 (s), 1019 (s), 962 (w), 886 (w), 852 (s), 830 (w), 801 (w), 761 (m), 713 (s), 692 (w), 630 (w), 601 (w), 590 (sh), 519 (w), 408 (w) cm^{-1}.

3a: 3199 (s), 3123 (s), 3027 (s), 2846 (w), 1705 (s), 1675 (m), 1641 (w), 1604 (s), 1584 (m), 1509 (m), 1457 (m), 1430 (m), 1408 (s), 1317 (m), 1266 (s), 1210 (vs), 1186 (m), 1158 (s), 1030 (m), 989 (w), 852 (w), 835 (m), 751 (w), 723 (w), 689 (w), 651 (m), 631 (w), 573 (m), 518 (w), 505 (w), 415 (w) cm^{-1}.

3b: 3185 (m), 3085 (m), 2960 (m), 2925 (m), 2854 (w), 1698 (s), 1637 (m), 1609 (m), 1528 (w), 1515 (w), 1428 (m), 1399 (m), 1316 (w), 1292 (w), 1213 (s), 1193 (sh), 1158 (vs), 1122 (w), 1037 (w), 1019 (w), 998 (w), 848 (w), 827 (m), 731 (m), 674 (w), 652 (w), 637 (w), 594 (w), 567 (w), 516 (w), 498 (w), 468 (w), 420 (w) cm^{-1}.

3c: IR 3203 (s), 3098 (s), 1694 (vs), 1637 (m), 1602 (w), 1528 (w), 1499 (w), 1450 (m), 1415 (m), 1305 (w), 1212 (s), 1193 (m), 1154 (s), 1028 (w), 1002 (w), 933 (w), 843 (w), 795 (w), 783 (w), 724 (w), 696 (m), 659 (w), 603 (w), 591 (m), 515 (w), 502 (w), 426 (w) cm^{-1}.

3d: 3199 (s), 3103 (s), 3020 (m), 1697 (s), 1637 (m), 1593 (m), 1523 (w), 1491 (w), 1459 (w), 1421 (m), 1394 (m), 1310 (w), 1282 (w), 1223 (s), 1210 (vs), 1190 (m), 1162 (s), 1091 (m), 1013 (w), 848 (w), 805 (w), 738 (w), 697 (w), 661 (w), 637 (m), 593 (w), 519 (w), 493 (w), 470 (w), 412 (w) cm^{-1}.

3e: 3187 (s), 3105 (s), 3021 (s), 1705 (s), 1643 (m), 1541 (w), 1517 (w), 1429 (m), 1402 (w), 1327 (vs), 1302 (w), 1226 (s), 1212 (s), 1191 (m), 1164 (s), 1131 (s), 1120 (s), 1068 (s), 1016 (m), 858 (m), 812 (w), 761 (w), 699 (m), 668 (w), 624 (m), 595 (w), 514 (w), 463 (w), 415 (w) cm^{-1}.

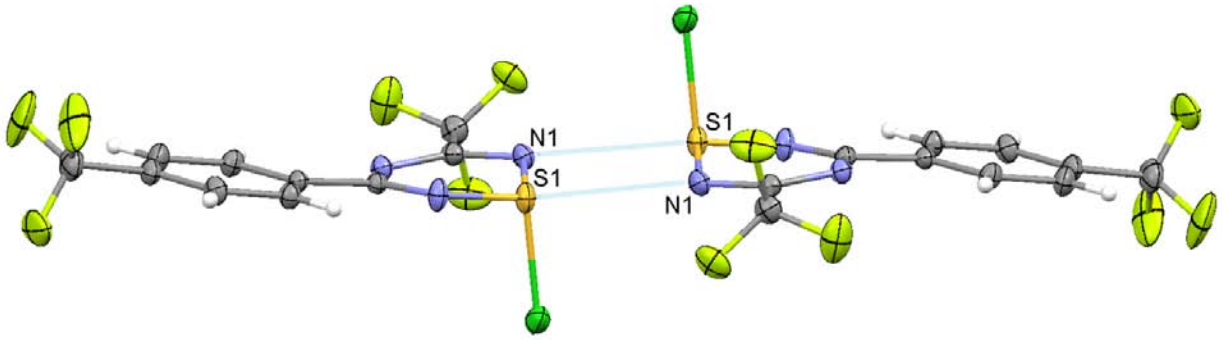

Figure S5: Thermal ellipsoids (30%) plot showing the short intermolecular S(δ^+)–N(δ^-) interactions in **4e** within the crystal lattice at −100(2) °C. The S1···N1 distance is 3.043(1) Å. Intermolecular short-contacts of this type are very common in thiazyl chemistry. Interestingly, the strength of such interactions - as measured from the interatomic distances - are very similar for the S(IV) chlorothiatriazines and the S(III) thiatriazinyls (see main text and figures below.)

Table S4. ^{1}H NMR spectral data for the 1-chlorothiatriazines

	cmpd	H_1	H_2	J_{AB} (Hz)	R
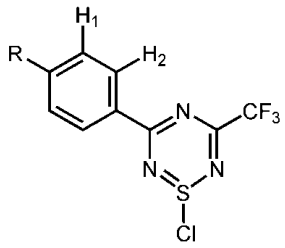	**4a**	7.02	8.45	9.0	3.94
	4b	7.35	8.37	8.2	2.49
	4c	m 7.52 – 7.58	m 8.45 – 8.48	—	m 7.67 – 7.74
	4d	7.53	8.41	8.9	—
	4e	7.82	8.59	8.5	—

Crystal structure of N-Sulfurylchloride-N,N'-benzamidine

Hydrolysis product **6** was obtained as colorless blocks suitable for X-ray analysis (Figure S6). This is the first chlorosulfonyl derivative of a primary amidine to have been structurally characterized. In all, fifteen structures with chlorosulfonyl groups attached to nitrogen have been reported.[5] The structure of **6** is stabilized by a complex network of H-bonding involving all the nitrogen and oxygen atoms (see Figures S7, S8 and Table S5). The structure of $[ClSO_2NPCl_2NH]_2BCl$ is the most comparable reported in the literature.[5c]

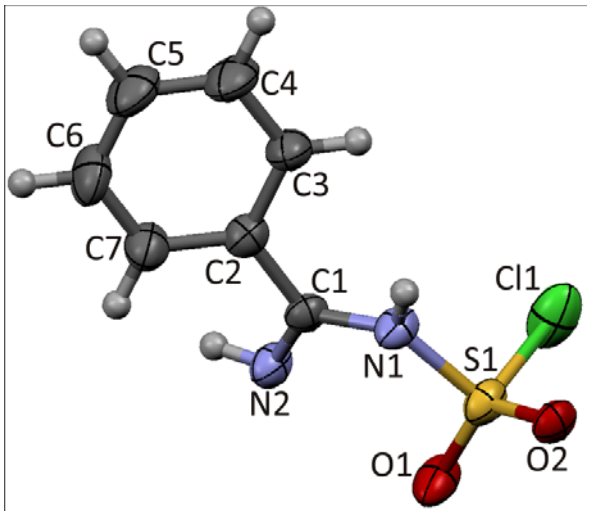

Figure S6. Thermal ellipsoids (30%) plot with atom numbering scheme showing the molecular structure of **6** as found within the crystal lattice at −100(2) °C.

Table S5. Hydrogen bonds and short contacts [Å] and angles [°] for **6**.

Bond Type	D–H...A	d(D...A)	<(DHA)
Inter	N2–H2...O2#1	2.763(3)	153(4)
Inter	N1–H1...O1#2	2.675(4)	151(4)
Intra	O1...N2	2.762(4)	
Intra	N2...O2#3	2.930(3)	

Symmetry transformations used to generate equivalent atoms:
#1 -y+1/2,x-1/2,z+1/4 #2 -x+1/2,y+1/2,-z+1/4 #3 -x+1/2,-y+1/2,-z+1/4

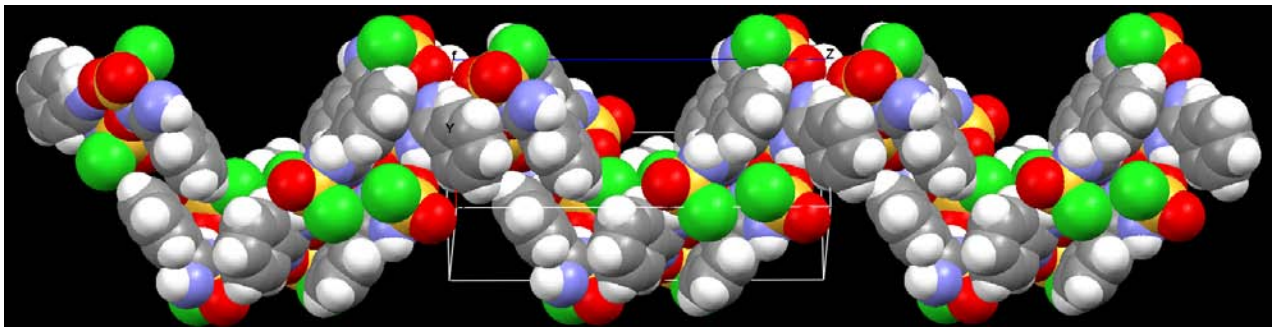

Figure S7. A packing diagram for **6** showing the double-layer "W"-shaped chain of molecules along the four-fold *c* axis of the tetragonal unit cell. The sheets defined by H-bonding as discussed in Figure S6 are clearly visible.

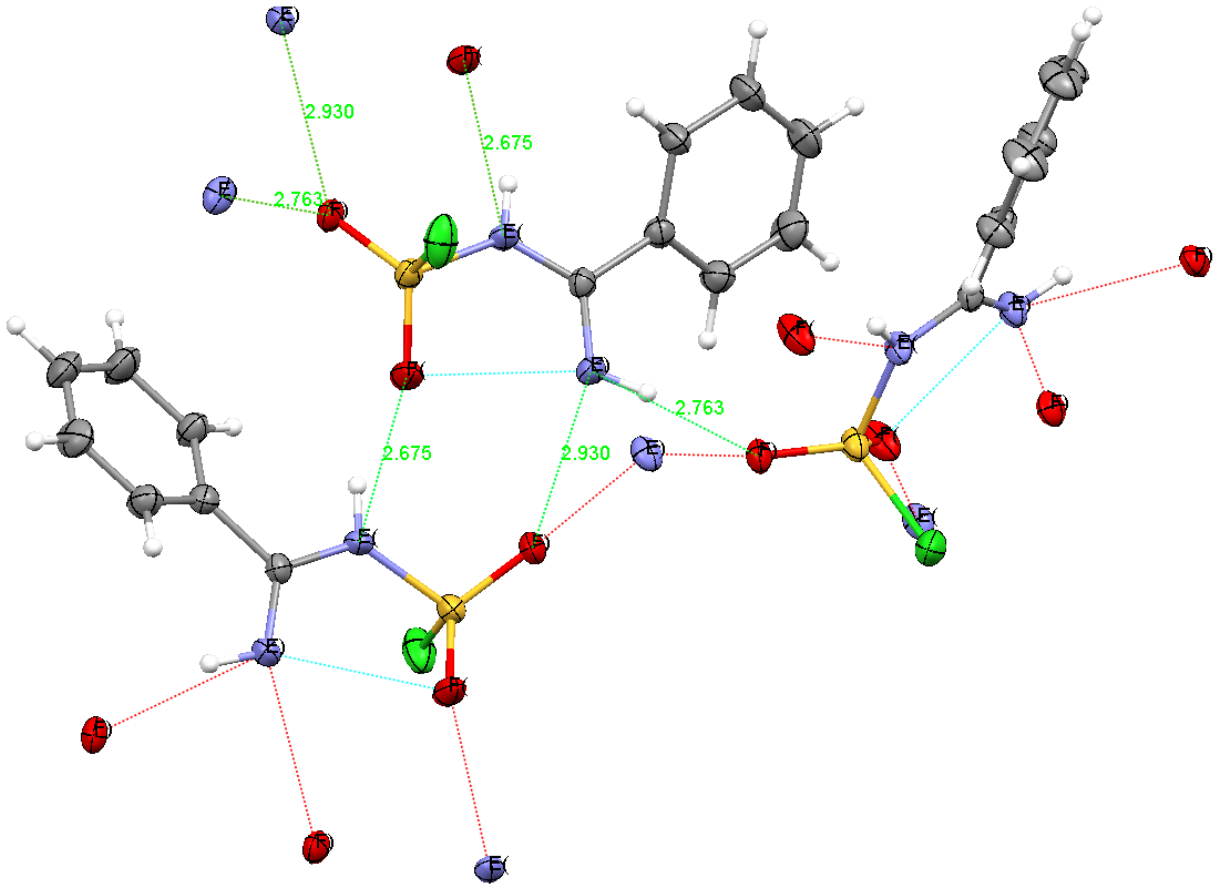

Figure S8. The complex network of hydrogen bonds in the crystal structure of **6** and short contacts that form (a) through N1-H1...O1 a chain of face-to-tail chelates vertically in the page at the l.h.s. and (b) through N2-H2...O2 a second direction directed out of the page at the r.h.s. Short contacts are also induced intra-molecularly between O1...N2 and inter-molecularly between N2...O3. The two intertwined H-bonded sheets define planes with approximate Miller indices of (24 2 -42) and (-1 12 -20). The view is approximately perpendicular to the former. The lattice contains two further sheets of molecules with approximate Miller indices of (9 0 15) and (0 16 28). Only two other known sulfonylchlorides bonded to N have been reported which also contain H-bond donors. Refcode GIVWEN contains a single type of N-H...O=S contact of 2.858(4) Å.[6] Refcode GIVXAK is the most comparable structure, containing a U-shaped chelate ring bridged by an H-bond (N-H...H 2.81(1) Å) and chain forming link between the backbone N and a neighboring chlorosulfonyl oxygen (N-H...O=S 2.96(1) Å).[7]

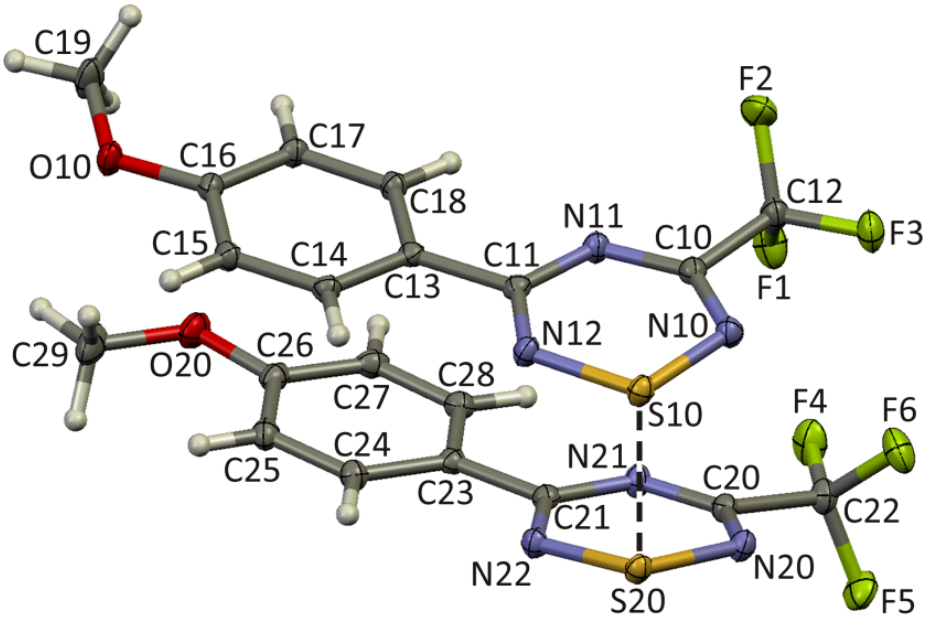

Figure S9: Thermal ellipsoids (30%) plot with atom numbering scheme showing the molecule **5a** found within the crystal lattice at −100(2) °C. The S10···S20 distance is 2.6370(3) Å.

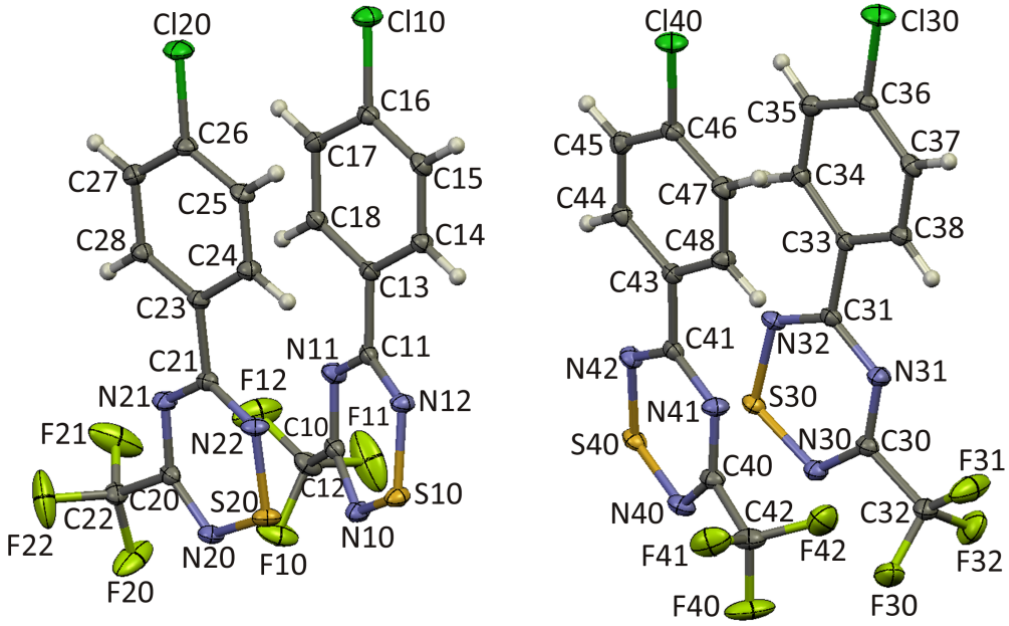

Figure S10: Thermal ellipsoids (30%) plot with atom numbering scheme showing the molecule **5d** found within the crystal lattice at −100(2) °C. The S10···S20 distance is 2.659(1) Å and the S30···S40 distance is 2.635(1) Å.

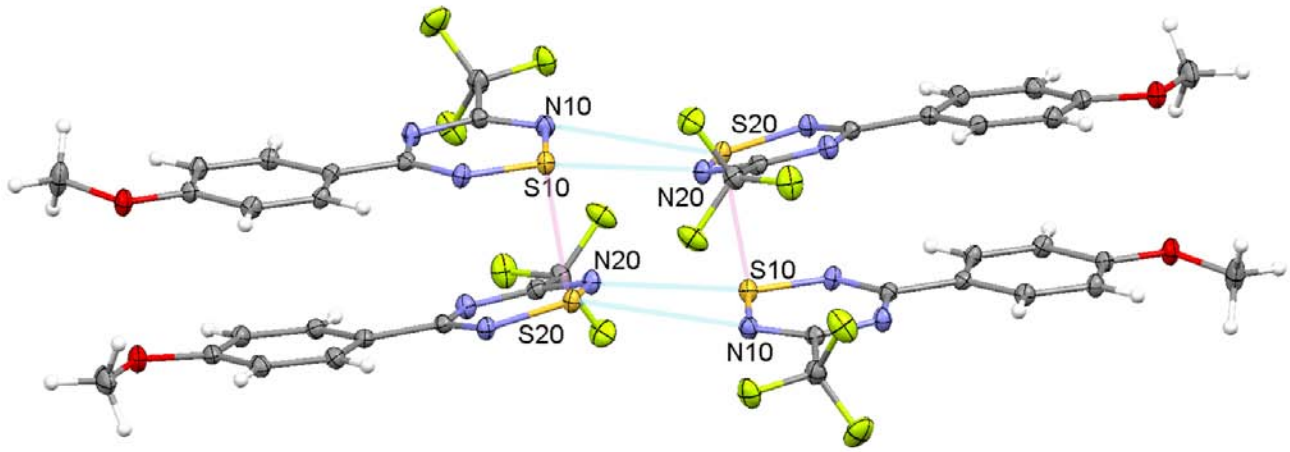

Figure S11: Thermal ellipsoids (30%) plot showing the short intermolecular and inter-dimer contacts in **5a** within the crystal lattice at −100(2) °C. The S10···N20 distance is 2.941(1) Å and the S20···N10 distance is 3.341(1) Å. Thus the shortest contacts are between the two "top" and "bottom" rings of approximately co-planar dimers of thiatriazinyls. The dimers are centrosymetrically arranged.

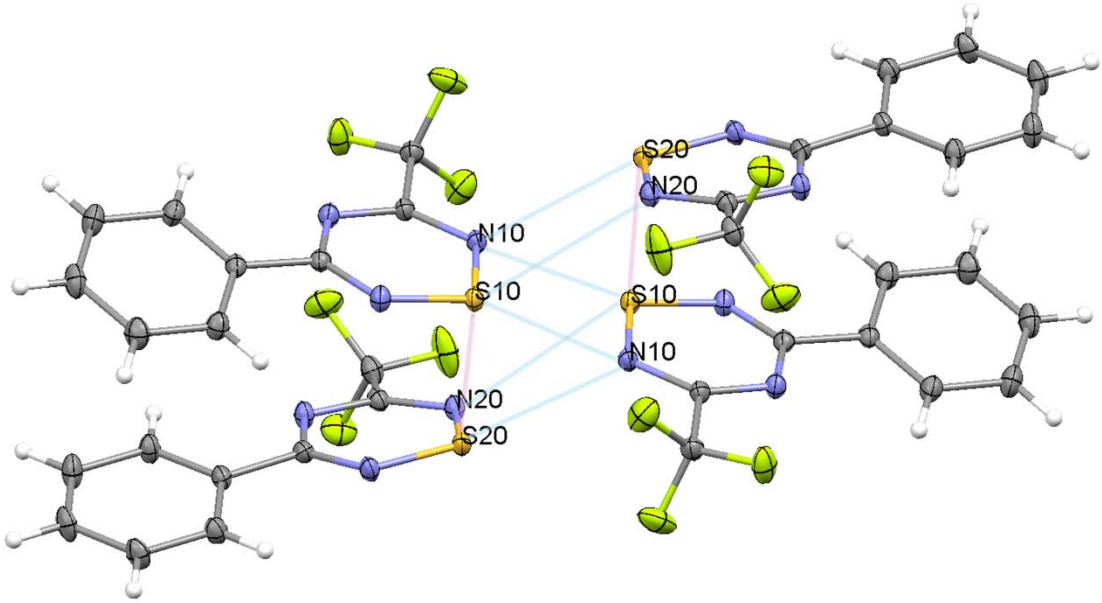

Figure S12. Thermal ellipsoids (30%) plot showing the short intermolecular and inter-dimer contacts in **5c** within the crystal lattice at −100(2) °C. The S10···N20 distance is 3.297(2) Å, the S20····N10 distance is 3.025(2) S Å and the S10···N10 distance is 3.108(2) S Å. Thus the two pairs of thiatriazinyl dimers are almost equally out of register and, though still centrosymmetrical, form a less-compact pair than that found in **5a** (Figure S9).

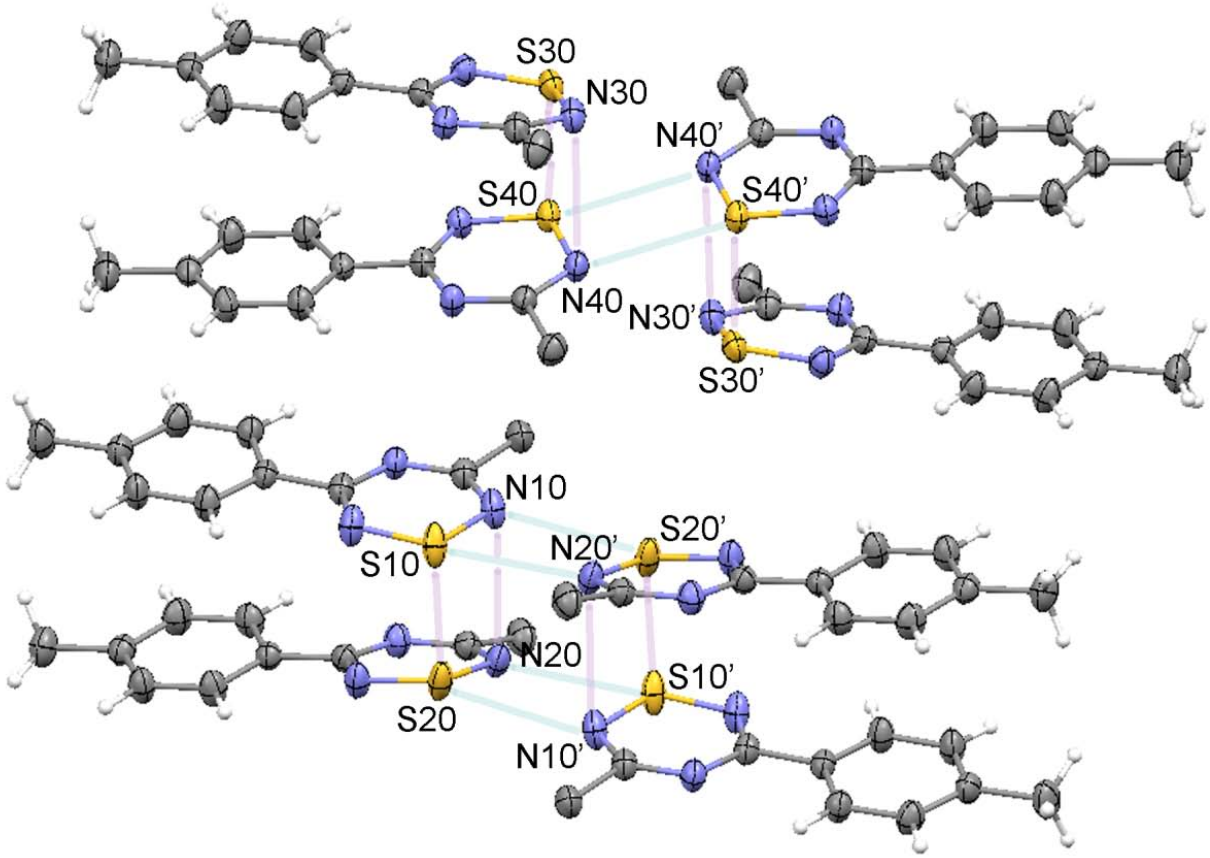

Figure S13. Thermal ellipsoids (30%) plot showing the short intermolecular and inter-dimer contacts in **5b** within the crystal lattice at 23(2) °C (fluorine atoms omitted for clarity). Here are found two distinct arrangements for the two pairs of dimers. That relating the S10,N10-S20,N20 pair forms approximately co-planar arrangements very similar to that observed for **5a**. (The S10···N20' distance is 3.085(2) Å and the S20···N10' distance is 3.088 (2) Å.) The second dimer pair is out of register in an arrangement very similar to that found in the structure of **4c** with S40···N40' at 3.108(1) Å and S30···N40' at 3.277 (2) Å.

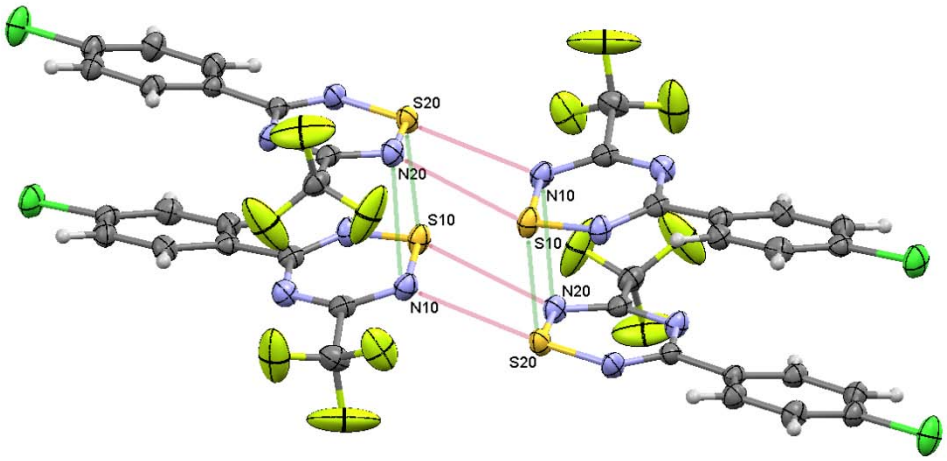

(a)

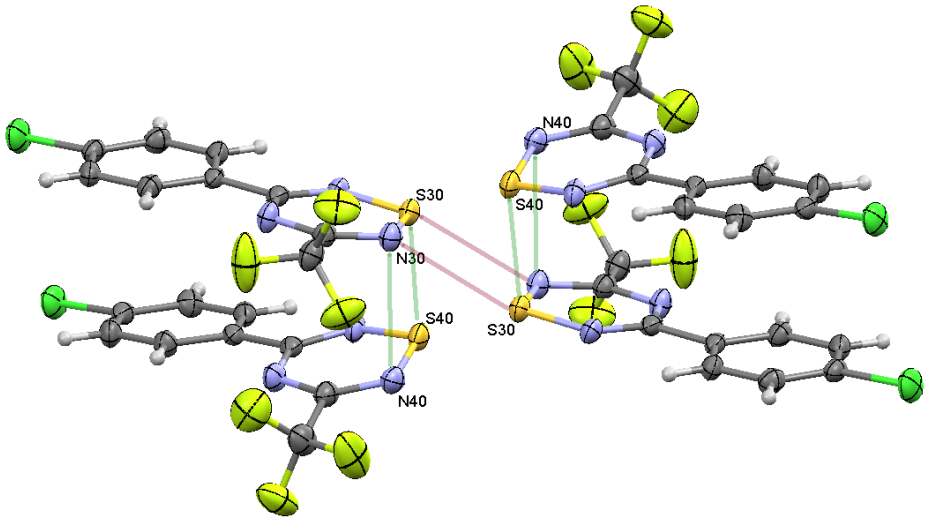

(b)

Figure S14. Thermal ellipsoids (30%) plot showing the short intermolecular and inter-dimer contacts in **5d** within the crystal lattice at −100(2) °C. Like **5b**, there are two distinct arrangements for the two pairs of dimers. (a) The S10,N10-S20,N20 pair forms an intermediate arrangment between that of **5a** and **5c**, with the S10···N20' distance at 3.123(2) Å and S20···N10' at 3.035(2) Å.) (b) The second dimer pair is strongly out of register in an arrangement very similar to that found in the structure of **4c** with S30···N30' at 3.087(2) Å. Here the S40···N30' and S30···N40' distances are very long at 3.407(3) and 3.756(3) Å, respectively.

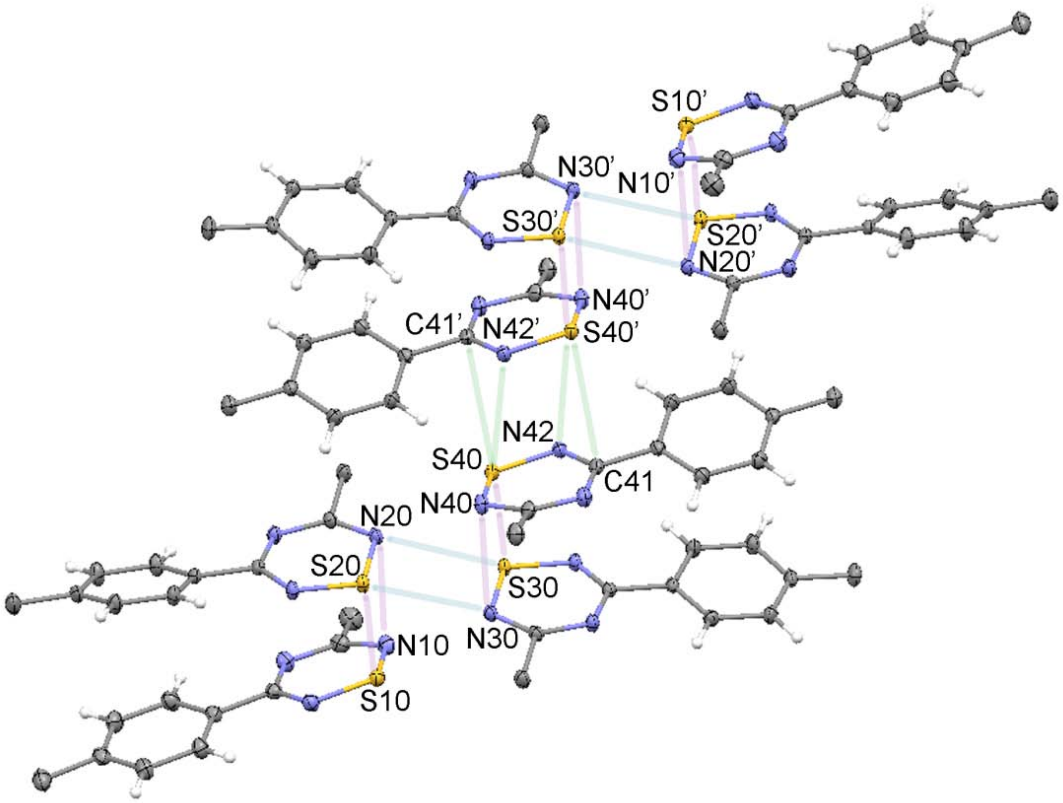

Figure S15. Thermal ellipsoids (30%) plot showing the short intermolecular and inter-dimer contacts in **5e** within the crystal lattice at −100(2) °C. Apart from the interactions within the tetramer shown in Figure 8, there are short "stacking" interactions between S40 with C41' and C41 with S40' of 3.447(2) Å.

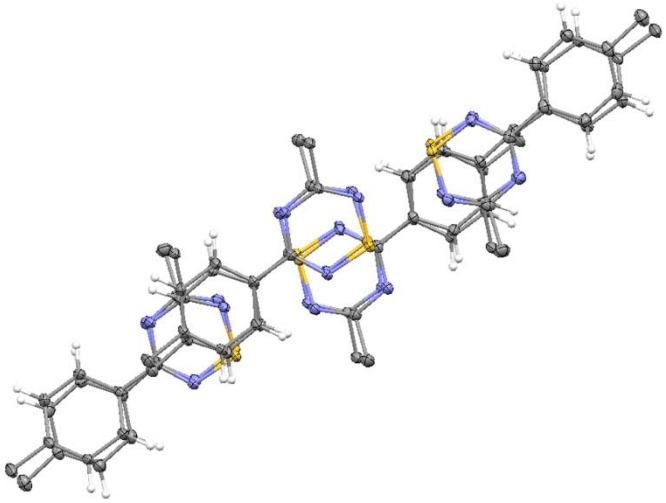

Figure S16. Stacking between two layers of thiatriazinyl dimers in **5e** leading to short S40 with C41' and C41 with S40' of 3.447(2) Å. This is the strongest interaction ever detected among multiple thiatriazinyl rings, but the stacking does not extend beyond the eight associated monomers shown in this bird's eye view approximately down the crystallographic *c* axis.

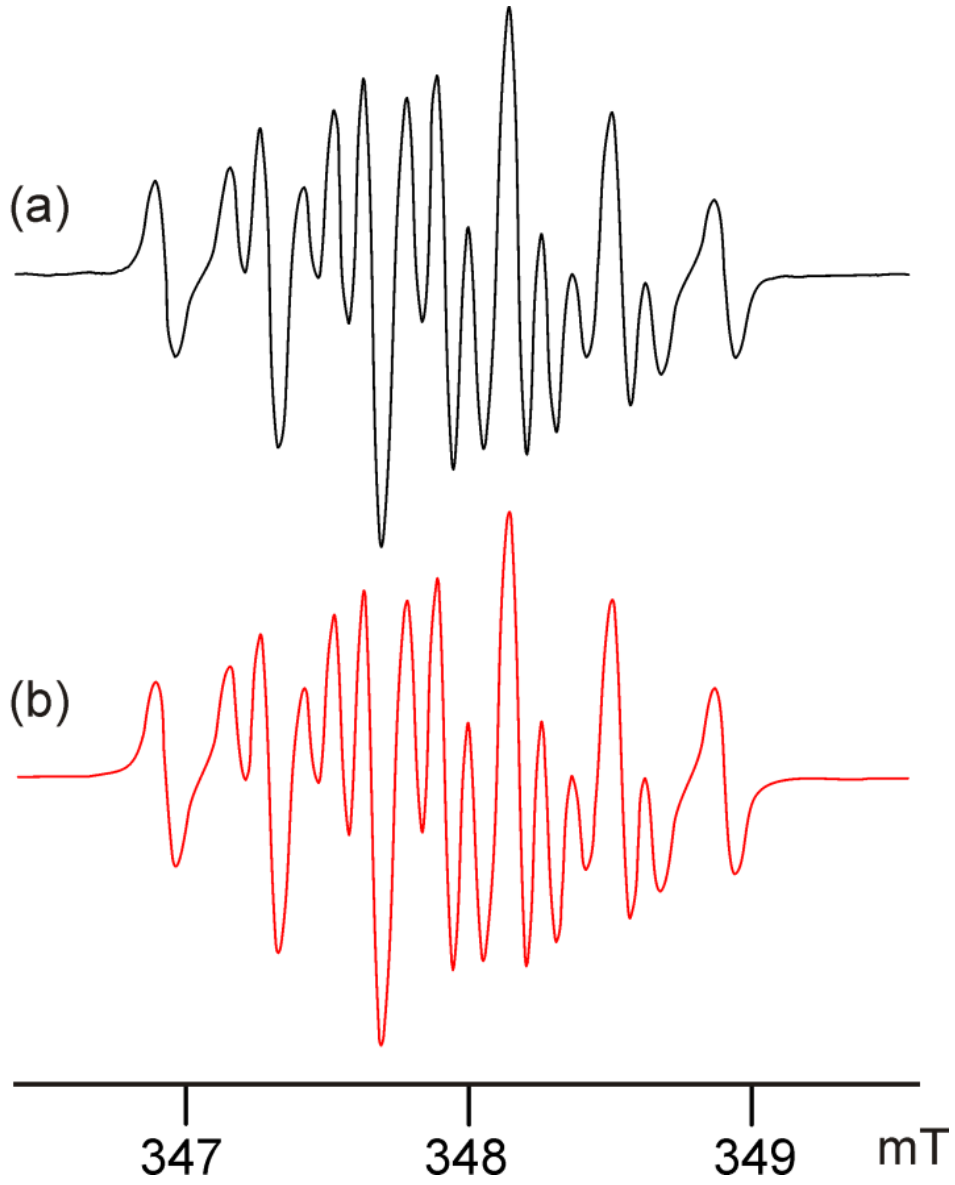

Figure S17. (a) Experimental and (b) simulated EPR spectra of **5a** in CH_2Cl_2 at 18 °C, modulation amplitude 0.005 mT, modulation frequency 100 kHz, 100% Lorentzian lineshape.

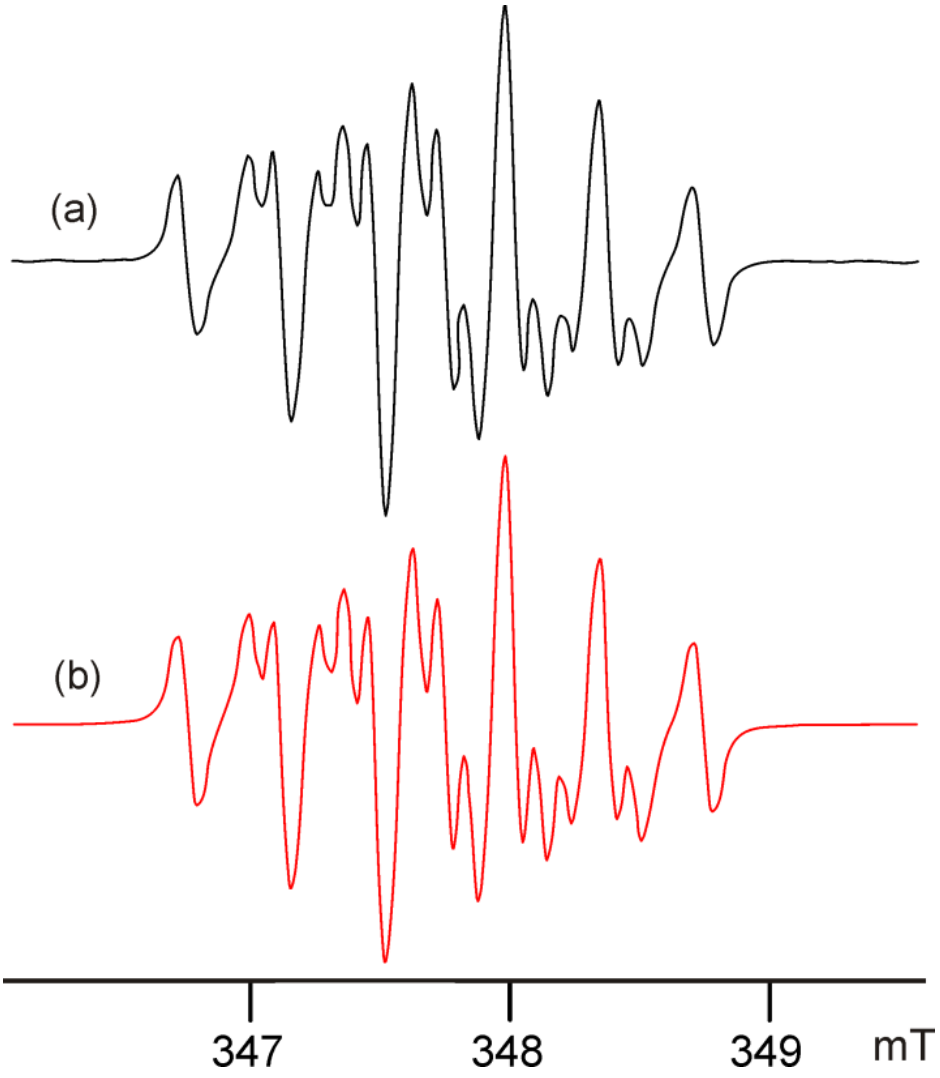

Figure S18 (a) Experimental and (b) simulated EPR spectra of **5b** in CH_2Cl_2 at 18 °C, modulation amplitude 0.01 mT, modulation frequency 100 kHz, 100% Lorentzian lineshape.

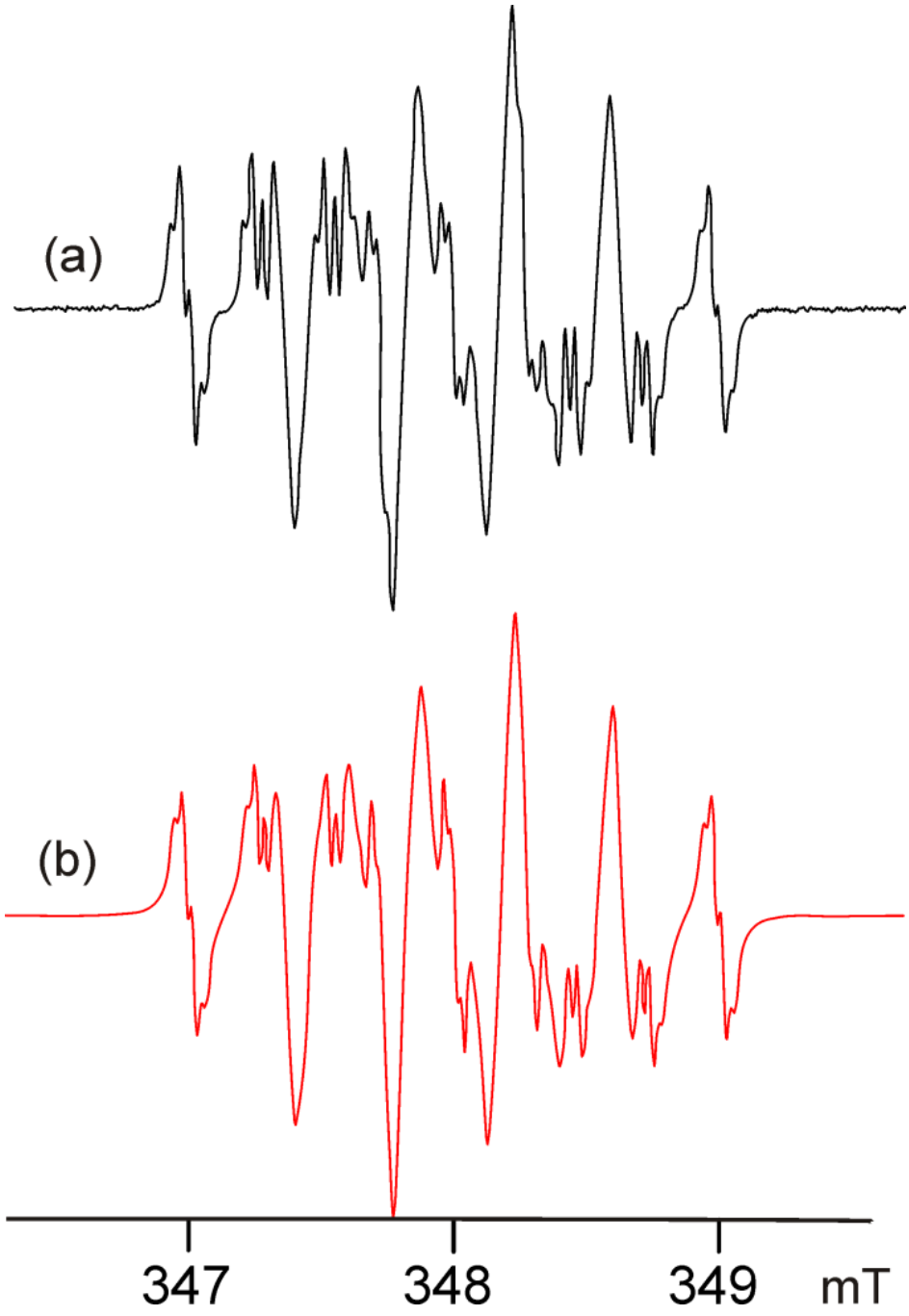

Figure S19. (a) Experimental and (b) simulated EPR spectra of **5c** in CH_2Cl_2 at 18 °C, modulation amplitude 0.01 mT, modulation frequency 100 kHz, 100% Lorentzian lineshape.

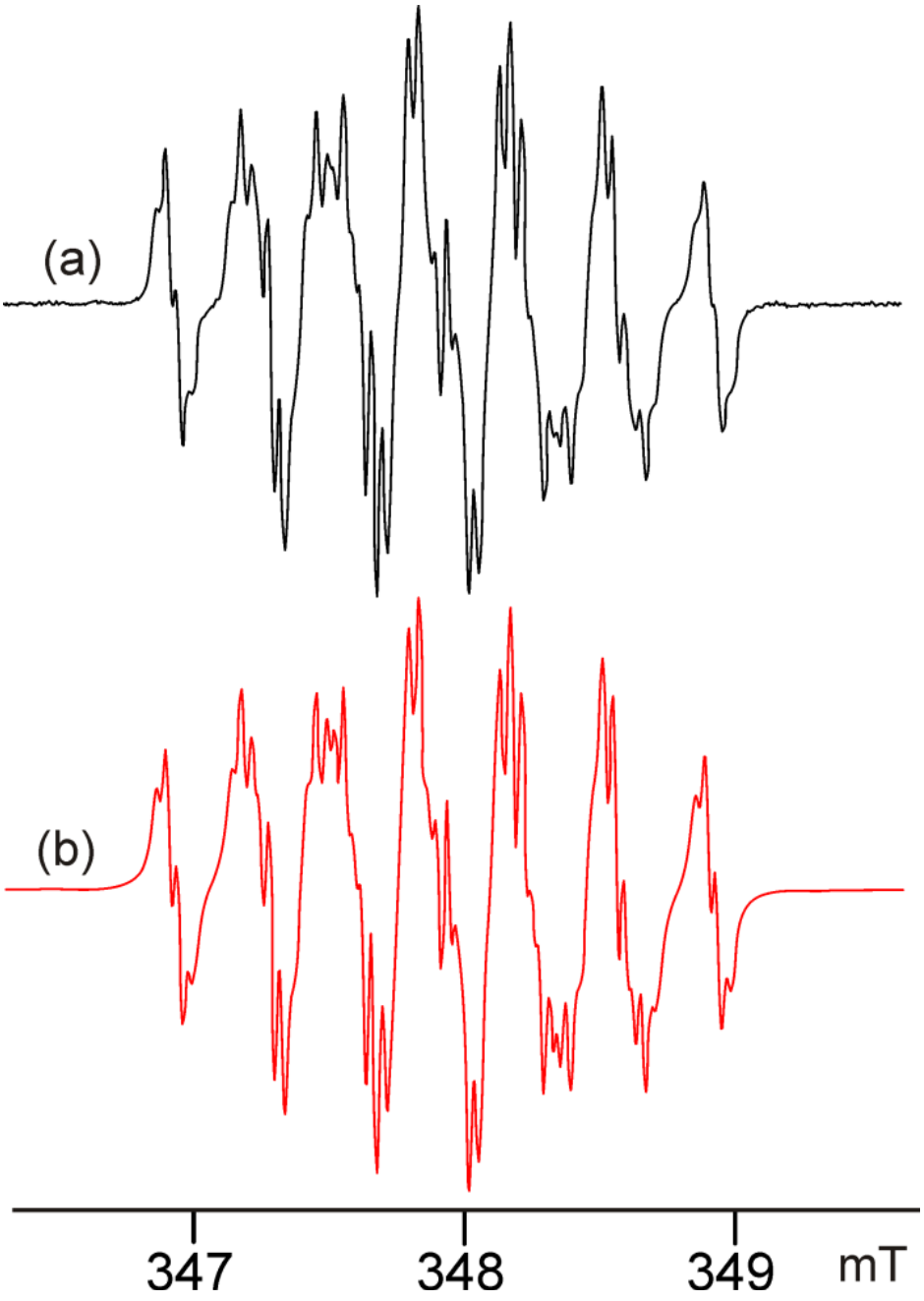

Figure S20. (a) Experimental and (b) simulated EPR spectra of **5e** in CH_2Cl_2 at 18 °C, modulation amplitude 0.01 mT, modulation frequency 100 kHz, 100% Lorentzian lineshape.

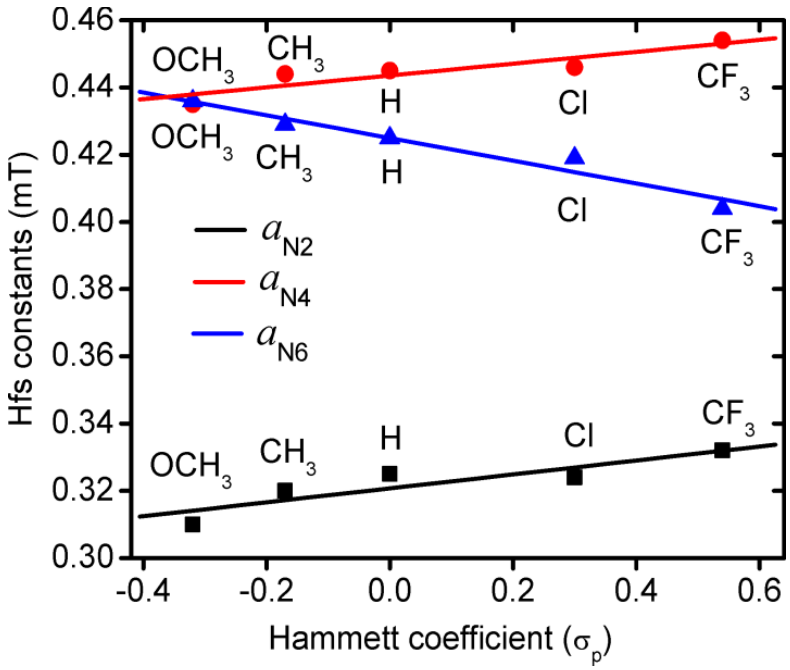

Figure S21. Plot of the Hammett coefficients (σ_p) versus the hyperfine splitting constants (mT) of **5a–e** as measured by EPR spectroscopy in CH_2Cl_2. More strongly electron donating substituents appear to increase spin density on the NSN portion of the ring, in particular on N6, but that increase is almost exactly compensated-for by decreased spin density on N2,4. Blue line (N6) R= 0.976, red line (N4) R= 0.910, black line (N2) R= 0.896.

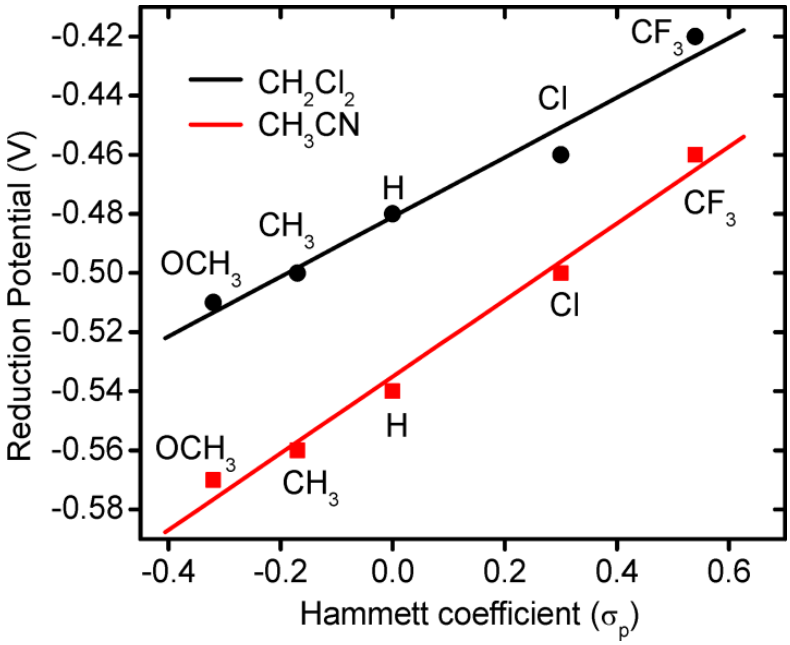

Figure S22. Plot of the Hammett coefficients (σ_p) versus the reduction peak potentials (V) at low concentrations of **5a–e** as measured by CV in both CH_2Cl_2 (black line, R = 0.993) and CH_3CN (red line, R = 0.986).

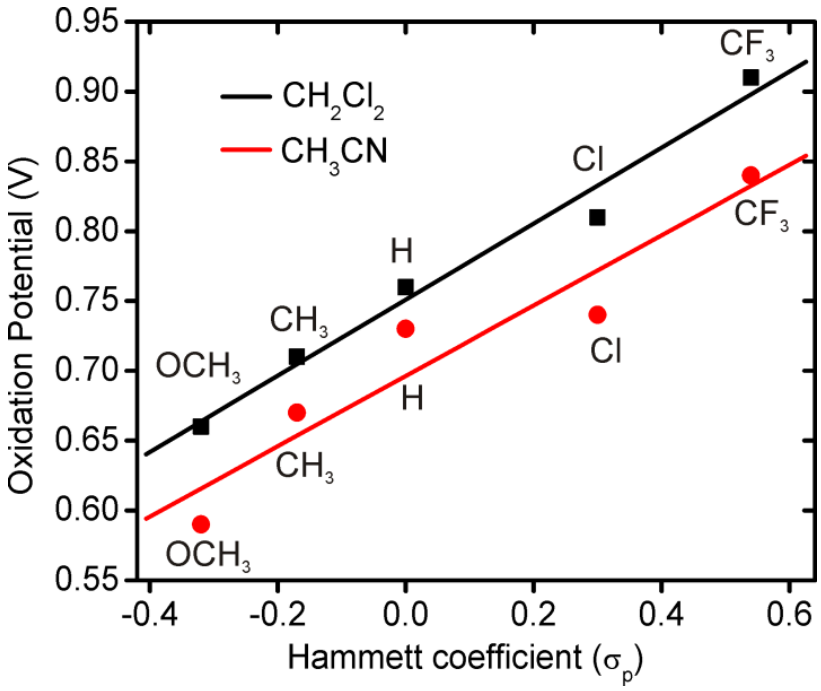

Figure S23. Plot of the Hammett coefficients (σ_p) versus the oxidation peak potentials (V) at low concentrations of **5a–e** as measured by CV in both CH_2Cl_2 (black line, R = 0.989) and CH_3CN (red line, R = 0.953).

References

1. Barker, J.; Kilner, M. *Coord. Chem. Rev*. **1994**, *133*, 219–300.

2. (a) Barker, J.; Phillips, P. R.; Wallbridge, M. G. H.; Powell, H. R. *Acta Cryst.* **1996**, *C52*, 2617–2619. (b) Jokić, M.; Bajić, M.; Žinić, M.; Perić, B.; Kojić-Prodić, B. *Acta Cryst.* **2001**, *C57*, 1354–1355.

3. (a) Häfelinger, G.; Kuske, K. H. *The chemistry of the amidines and imidates*; John Wiley & Sons Ltd.: Chichester, 1991, Vol. 2, Ch. 1, pp. 1–100. (b) Boeré, R. T.; Klassen, V.; Wolmershäuser, G. *J. Chem. Soc., Dalton Trans.* **1998**, 4147–4154.

4. Greenwood, N. N.; Earnshaw, A. *Chemistry of the Elements, 2nd Edition*; Reed Educational and Professional Publishing Ltd.: Oxford, 1997; p 60.

5. (a) Zak, Z.; Ruzicka, A.; Vlckova, M.; Frohlichova, L. *Main Group Chem*. **1997**, *2*, 155–160. (b) Taraba, J.; Zak, Z. *Inorg. Chem*. **2006**, *45*, 3695–3700. (c) Novotny, D.; Prihoda,

J.; Zak, Z.; Marek, J. *Main Group Chem*. **1997**, *2*, 117–122. (d) Lang, R.; Herzog, C.; Stangl, R.; Brunn, E.; Braun, M.; Christl, M.; Peters, E.-M.; Peters, K.; von Schnering, H. G. *Chem. Ber*. **1990**, *123*, 1193–1207. (e) Folkerts, H.; Nusshar, D.; Weller, F.; Dehnicke, K.; Magull, J.; Hiller, W. *Z. Anorg. Allg. Chem*. **1994**, *620*, 1986–1991. (f) Furst, G.T.; Wachsman, M.A.; Pieroni, J.; White, J.G.; Moriconi E.J. *Tetrahedron* **1973**, *29***,** 1675-1677. (g) Berredjem, M.; Winum, J.-Y.; Toupet, L.; Masmoudi, O.; Aouf, N.-E.; Montero, J.-L. *Synth.Commun.* **2004**, *34***,** 1653–1662. (h) Paquette, L.A.; Lau, C.J.; Rogers, R.D. *J.Am.Chem.Soc.* **1988***, 110***,** 2592–2600. (i) Ibbett, A.J.; Watkin, D.J.; Jones, J.H. *Acta Crystallogr.,Sect.C:Cryst.Struct.Commun.* **1994***, 50***,** 1283–1284. (j) Kraiem, J.; Grosvalet, L.; Perrin, M.; Hassine, B.B. *Tetrahedron Lett.* **2001***, 42***,** 9131–9133.

6. Zak, Z.; Ruzicka, A.; Vlckova, M.; Frohlichova, L. *Main Group Chem*. **1997**, *2*, 155–160.
7. Novotny, D.; Prihoda, J.; Zak, Z.; Marek, J. *Main Group Chem*. **1997**, *2*, 117–122.

Gaussian 98 Calculations output, by compound and charge

MeO CF_3 radical 5a

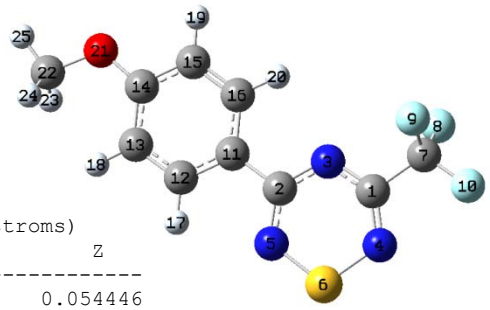

Geometry

Center Number	Atomic Number	Atomic Type	Coordinates (Angstroms) X	Y	Z
1	6	0	-0.004731	0.038994	0.054446
2	6	0	0.017608	-0.057372	2.384469
3	7	0	0.682354	0.074853	1.206238
4	7	0	-1.290232	-0.112908	-0.176238
5	7	0	-1.299921	-0.228323	2.536393
6	16	0	-2.251715	-0.292894	1.179445
7	6	0	0.879630	0.208285	-1.186422
8	9	0	1.518050	1.392861	-1.139588
9	9	0	1.812032	-0.761941	-1.226657
10	9	0	0.171974	0.157682	-2.320817
11	6	0	0.829868	-0.007433	3.610141
12	6	0	0.234187	-0.127123	4.875172
13	6	0	0.997381	-0.081274	6.036529
14	6	0	2.388422	0.086874	5.945852
15	6	0	2.995595	0.207991	4.683477
16	6	0	2.227028	0.161886	3.534056
17	1	0	-0.840427	-0.257176	4.941646
18	1	0	0.508282	-0.176020	6.998910
19	1	0	4.072099	0.337182	4.637580
20	1	0	2.691482	0.255354	2.559319
21	8	0	3.227860	0.144311	7.009396
22	6	0	2.682552	0.030845	8.318333
23	1	0	1.975710	0.843030	8.529233
24	1	0	2.181543	-0.934753	8.461041
25	1	0	3.531289	0.102901	8.999973

Isotropic Fermi Contact Couplings

	Atom	a.u.	MegaHertz	Gauss	10(-4) cm-1
1	C(13)	-0.01482	-16.65818	-5.94405	-5.55657
2	C(13)	-0.01706	-19.18077	-6.84418	-6.39802
3	N(14)	0.04375	14.13567	5.04396	4.71515
4	N(14)	0.03175	10.25948	3.66084	3.42220
5	N(14)	0.04930	15.93020	5.68429	5.31374
6	S(33)	0.05592	19.20841	6.85404	6.40724
7	C(13)	0.00008	0.08493	0.03031	0.02833
8	F(19)	-0.00078	-3.26301	-1.16432	-1.08842
9	F(19)	-0.00076	-3.20770	-1.14459	-1.06998
10	F(19)	-0.00003	-0.11743	-0.04190	-0.03917
11	C(13)	0.00118	1.32394	0.47241	0.44162
12	C(13)	-0.00188	-2.11816	-0.75581	-0.70654
13	C(13)	0.00081	0.90688	0.32360	0.30250
14	C(13)	-0.00132	-1.48193	-0.52879	-0.49432
15	C(13)	0.00144	1.61817	0.57740	0.53976
16	C(13)	-0.00219	-2.45986	-0.87774	-0.82052
17	H	0.00024	1.05894	0.37786	0.35323
18	H	-0.00006	-0.28718	-0.10247	-0.09579
19	H	-0.00018	-0.78459	-0.27996	-0.26171
20	H	0.00022	0.99449	0.35486	0.33173
21	O(17)	-0.00052	0.31665	0.11299	0.10562
22	C(13)	0.00004	0.04078	0.01455	0.01360
23	H	-0.00002	-0.09740	-0.03475	-0.03249
24	H	-0.00002	-0.09743	-0.03477	-0.03250
25	H	0.00000	0.01835	0.00655	0.00612

Tolyl CF_3 radical 5b

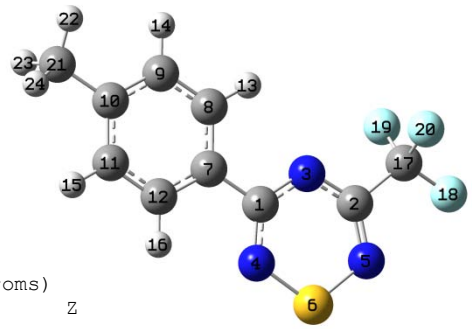

Geometry

Center Number	Atomic Number	Atomic Type	Coordinates (Angstroms) X	Y	Z
1	6	0	-0.604199	-0.070878	-0.359056
2	6	0	-0.643596	-0.116427	1.971626
3	7	0	0.050968	0.000009	0.829413
4	7	0	-1.916161	-0.242522	-0.532409
5	7	0	-1.929371	-0.293989	2.181382
6	16	0	-2.880621	-0.392743	0.810071
7	6	0	0.220278	0.051716	-1.578087
8	6	0	1.610737	0.218605	-1.477973
9	6	0	2.386710	0.332068	-2.626864
10	6	0	1.807806	0.281313	-3.902718
11	6	0	0.415948	0.119502	-3.992688
12	6	0	-0.369370	0.004282	-2.852851
13	1	0	2.066670	0.259409	-0.495522
14	1	0	3.462019	0.463250	-2.533281
15	1	0	-0.055353	0.084811	-4.972046
16	1	0	-1.443564	-0.119680	-2.935220
17	6	0	0.226737	-0.002815	3.229108
18	9	0	-0.470092	-0.239651	4.346260
19	9	0	1.245404	-0.879320	3.172001
20	9	0	0.750135	1.235699	3.311804
21	6	0	2.657253	0.372188	-5.146593
22	1	0	3.596712	0.899975	-4.953971
23	1	0	2.914958	-0.628396	-5.519211
24	1	0	2.131597	0.892132	-5.954590

Isotropic Fermi Contact Couplings

	Atom	a.u.	MegaHertz	Gauss	10(-4) cm-1
1	C(13)	-0.01711	-19.22983	-6.86168	-6.41438
2	C(13)	-0.01556	-17.49585	-6.24296	-5.83599
3	N(14)	0.04480	14.47509	5.16507	4.82837
4	N(14)	0.04743	15.32518	5.46841	5.11193
5	N(14)	0.03313	10.70340	3.81924	3.57027
6	S(33)	0.05588	19.19410	6.84894	6.40246
7	C(13)	0.00121	1.35546	0.48366	0.45213
8	C(13)	-0.00232	-2.61307	-0.93241	-0.87163
9	C(13)	0.00140	1.57425	0.56173	0.52511
10	C(13)	-0.00160	-1.80212	-0.64304	-0.60112
11	C(13)	0.00105	1.18395	0.42246	0.39492
12	C(13)	-0.00183	-2.05461	-0.73314	-0.68535
13	H	0.00025	1.10103	0.39288	0.36726
14	H	-0.00016	-0.70408	-0.25123	-0.23486
15	H	-0.00010	-0.45637	-0.16284	-0.15223
16	H	0.00022	0.98920	0.35297	0.32996
17	C(13)	0.00020	0.22511	0.08032	0.07509
18	F(19)	-0.00003	-0.12090	-0.04314	-0.04033
19	F(19)	-0.00077	-3.24140	-1.15661	-1.08121
20	F(19)	-0.00087	-3.67655	-1.31188	-1.22636
21	C(13)	0.00036	0.40007	0.14276	0.13345
22	H	-0.00007	-0.33445	-0.11934	-0.11156
23	H	-0.00038	-1.67757	-0.59860	-0.55958
24	H	-0.00012	-0.55250	-0.19715	-0.18429

Ph CF_3 radical 5c

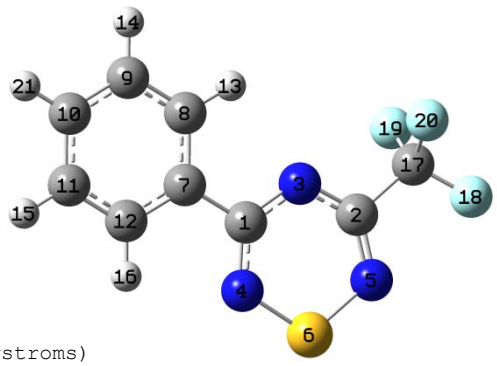

Geometry

Center Number	Atomic Number	Atomic Type	Coordinates (Angstroms) X	Y	Z
1	6	0	-0.591396	0.574450	-0.000498
2	6	0	1.689429	0.092089	-0.011874
3	7	0	0.417068	-0.335630	-0.002072
4	7	0	-0.462570	1.901483	-0.001765
5	7	0	2.186018	1.309151	-0.017225
6	16	0	1.065772	2.550321	-0.009308
7	6	0	-1.970016	0.036038	0.001305
8	6	0	-2.181156	-1.352355	-0.018059
9	6	0	-3.477460	-1.861343	-0.019644
10	6	0	-4.572058	-0.993929	-0.000925
11	6	0	-4.367440	0.388960	0.019183
12	6	0	-3.075029	0.903933	0.019892
13	1	0	-1.322923	-2.013996	-0.032807
14	1	0	-3.633650	-2.936244	-0.035748
15	1	0	-5.217382	1.065367	0.034134
16	1	0	-2.906367	1.974964	0.034817
17	6	0	2.716112	-1.047006	0.003298
18	9	0	3.969271	-0.595923	-0.120027
19	9	0	2.623621	-1.728719	1.161234
20	9	0	2.473903	-1.905567	-1.003209
21	1	0	-5.582711	-1.393384	-0.002083

Isotropic Fermi Contact Couplings

	Atom	a.u.	MegaHertz	Gauss	10(-4) cm-1
1	C(13)	-0.01720	-19.34019	-6.90106	-6.45119
2	C(13)	-0.01578	-17.73903	-6.32973	-5.91710
3	N(14)	0.04521	14.60825	5.21259	4.87279
4	N(14)	0.04683	15.13081	5.39905	5.04710
5	N(14)	0.03350	10.82333	3.86203	3.61027
6	S(33)	0.05593	19.21119	6.85503	6.40816
7	C(13)	0.00123	1.38184	0.49308	0.46093
8	C(13)	-0.00233	-2.61787	-0.93412	-0.87323
9	C(13)	0.00134	1.50116	0.53565	0.50073
10	C(13)	-0.00156	-1.75230	-0.62527	-0.58451
11	C(13)	0.00109	1.23028	0.43899	0.41038
12	C(13)	-0.00186	-2.09347	-0.74700	-0.69831
13	H	0.00025	1.10995	0.39606	0.37024
14	H	-0.00015	-0.67969	-0.24253	-0.22672
15	H	-0.00011	-0.50105	-0.17879	-0.16713
16	H	0.00023	1.00688	0.35928	0.33586
17	C(13)	0.00024	0.26497	0.09455	0.08839
18	F(19)	-0.00003	-0.11427	-0.04078	-0.03812
19	F(19)	-0.00089	-3.75477	-1.33980	-1.25246
20	F(19)	-0.00079	-3.31083	-1.18139	-1.10437
21	H	0.00019	0.86439	0.30844	0.28833

Cl CF_3 radical 5d

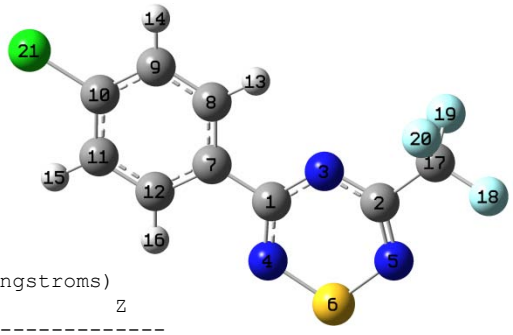

Geometry

Center Number	Atomic Number	Atomic Type	Coordinates (Angstroms) X	Y	Z
1	6	0	0.222479	0.742785	0.001135
2	6	0	2.421429	-0.027356	-0.011564
3	7	0	1.104436	-0.289426	-0.000258
4	7	0	0.517156	2.042438	-0.000400
5	7	0	3.067257	1.117231	-0.017680
6	16	0	2.116025	2.491577	-0.008392
7	6	0	-1.212659	0.384198	0.002826
8	6	0	-1.600637	-0.965019	-0.012837
9	6	0	-2.947555	-1.313482	-0.014691
10	6	0	-3.911507	-0.304351	0.000113
11	6	0	-3.548573	1.044575	0.016611
12	6	0	-2.200444	1.382753	0.017502
13	1	0	-0.836497	-1.733356	-0.024671
14	1	0	-3.250275	-2.354831	-0.027886
15	1	0	-4.313453	1.813347	0.028292
16	1	0	-1.901718	2.424955	0.029662
17	6	0	3.295075	-1.287764	0.002028
18	9	0	4.594558	-0.999297	-0.124541
19	9	0	3.118288	-1.951124	1.160605
20	9	0	2.942120	-2.107920	-1.003546
21	17	0	-5.610396	-0.736472	-0.002480

Isotropic Fermi Contact Couplings

	Atom	a.u.	MegaHertz	Gauss	10(-4) cm-1
1	C(13)	-0.01724	-19.37533	-6.91360	-6.46291
2	C(13)	-0.01565	-17.59287	-6.27758	-5.86835
3	N(14)	0.04523	14.61526	5.21509	4.87512
4	N(14)	0.04639	14.98858	5.34830	4.99965
5	N(14)	0.03350	10.82271	3.86181	3.61007
6	S(33)	0.05620	19.30454	6.88834	6.43930
7	C(13)	0.00123	1.38231	0.49324	0.46109
8	C(13)	-0.00227	-2.55031	-0.91002	-0.85069
9	C(13)	0.00135	1.51847	0.54183	0.50651
10	C(13)	-0.00173	-1.94651	-0.69456	-0.64928
11	C(13)	0.00109	1.22525	0.43720	0.40870
12	C(13)	-0.00190	-2.13801	-0.76289	-0.71316
13	H	0.00024	1.06877	0.38136	0.35650
14	H	-0.00016	-0.70500	-0.25156	-0.23516
15	H	-0.00011	-0.49685	-0.17729	-0.16573
16	H	0.00023	1.04075	0.37137	0.34716
17	C(13)	0.00020	0.22597	0.08063	0.07538
18	F(19)	-0.00002	-0.10040	-0.03582	-0.03349
19	F(19)	-0.00087	-3.66492	-1.30774	-1.22249
20	F(19)	-0.00078	-3.26254	-1.16416	-1.08827
21	Cl(35)	-0.00028	-0.12442	-0.04440	-0.04150

CF_3 CF_3 radical 5e

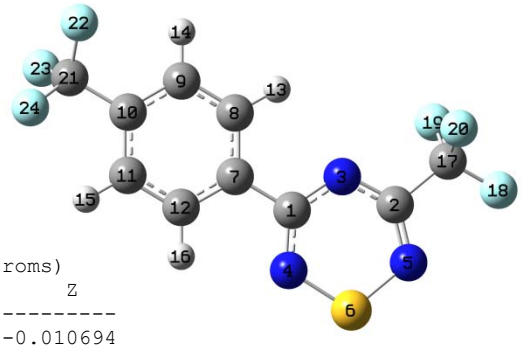

Geometry

Center Number	Atomic Number	Atomic Type	Coordinates (Angstroms) X	Y	Z
1	6	0	0.871536	0.793984	-0.010694
2	6	0	3.036831	-0.064302	0.014311
3	7	0	1.709816	-0.273089	-0.007905
4	7	0	1.216272	2.079517	-0.000718
5	7	0	3.726865	1.053638	0.030849
6	16	0	2.832103	2.465744	0.021412
7	6	0	-0.580882	0.492636	-0.023650
8	6	0	-1.019868	-0.840313	-0.018857
9	6	0	-2.380824	-1.128744	-0.027374
10	6	0	-3.314104	-0.088723	-0.041590
11	6	0	-2.884381	1.242053	-0.049844
12	6	0	-1.524962	1.531570	-0.040983
13	1	0	-0.285834	-1.637171	-0.009722
14	1	0	-2.718830	-2.159581	-0.029685
15	1	0	-3.613116	2.045137	-0.070418
16	1	0	-1.182833	2.560142	-0.049654
17	6	0	3.859168	-1.358917	0.002099
18	9	0	5.168480	-1.122769	0.132792
19	9	0	3.469702	-2.163922	1.006131
20	9	0	3.658491	-2.012933	-1.157556
21	6	0	-4.787374	-0.401752	0.010850
22	9	0	-5.074848	-1.566040	-0.609751
23	9	0	-5.220798	-0.516458	1.287136
24	9	0	-5.527086	0.565917	-0.572565

Isotropic Fermi Contact Couplings

	Atom	a.u.	MegaHertz	Gauss	10(-4) cm-1
1	C(13)	-0.01736	-19.51666	-6.96403	-6.51006
2	C(13)	-0.01603	-18.01733	-6.42903	-6.00993
3	N(14)	0.04586	14.81752	5.28726	4.94259
4	N(14)	0.04533	14.64676	5.22633	4.88563
5	N(14)	0.03417	11.03962	3.93921	3.68242
6	S(33)	0.05617	19.29405	6.88460	6.43580
7	C(13)	0.00128	1.43593	0.51238	0.47897
8	C(13)	-0.00227	-2.54731	-0.90894	-0.84969
9	C(13)	0.00127	1.42988	0.51022	0.47696
10	C(13)	-0.00155	-1.74434	-0.62242	-0.58185
11	C(13)	0.00119	1.33839	0.47757	0.44644
12	C(13)	-0.00193	-2.16447	-0.77234	-0.72199
13	H	0.00024	1.07337	0.38300	0.35804
14	H	-0.00014	-0.64378	-0.22972	-0.21474
15	H	-0.00012	-0.55495	-0.19802	-0.18511
16	H	0.00023	1.03450	0.36914	0.34507
17	C(13)	0.00026	0.29547	0.10543	0.09856
18	F(19)	-0.00002	-0.08337	-0.02975	-0.02781
19	F(19)	-0.00080	-3.38069	-1.20632	-1.12768
20	F(19)	-0.00090	-3.79826	-1.35531	-1.26696
21	C(13)	0.00038	0.42429	0.15140	0.14153
22	F(19)	-0.00007	-0.31323	-0.11177	-0.10448
23	F(19)	-0.00040	-1.68151	-0.60000	-0.56089
24	F(19)	-0.00008	-0.32978	-0.11767	-0.11000

MeO CF_3 cation 5a

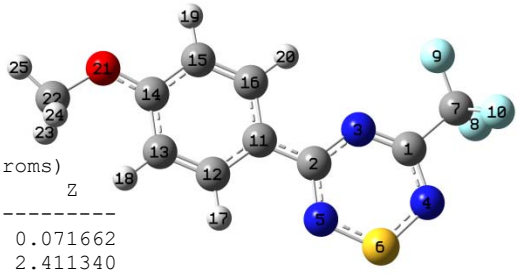

Geometry

Center Number	Atomic Number	Atomic Type	Coordinates (Angstroms) X	Y	Z
1	6	0	0.066438	0.092940	0.071662
2	6	0	0.085435	0.005010	2.411340
3	7	0	0.726788	0.085279	1.194180
4	7	0	-1.292384	0.033473	-0.113135
5	7	0	-1.284748	-0.080017	2.512457
6	16	0	-2.170640	-0.071367	1.205418
7	6	0	0.859192	0.201947	-1.243829
8	9	0	0.589004	1.387546	-1.804135
9	9	0	2.165417	0.102933	-1.017505
10	9	0	0.470864	-0.773822	-2.070131
11	6	0	0.852837	0.008770	3.605188
12	6	0	0.222106	-0.072926	4.879565
13	6	0	0.964258	-0.065421	6.037902
14	6	0	2.377949	0.025438	5.960693
15	6	0	3.019896	0.106668	4.694419
16	6	0	2.276143	0.098468	3.543641
17	1	0	-0.858431	-0.141662	4.935810
18	1	0	0.466115	-0.128299	6.997404
19	1	0	4.102060	0.174355	4.672972
20	1	0	2.761692	0.160158	2.576798
21	8	0	3.187452	0.041862	7.006689
22	6	0	2.665879	-0.033555	8.348944
23	1	0	2.015516	0.821781	8.554011
24	1	0	2.127546	-0.974301	8.496721
25	1	0	3.541533	0.000575	8.994845

Tolyl CF_3 cation 5b

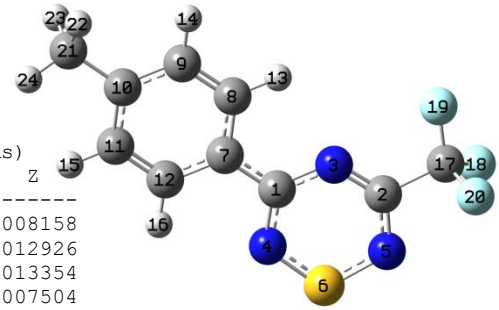

Geometry

Center Number	Atomic Number	Atomic Type	Coordinates (Angstroms) X	Y	Z
1	6	0	0.207739	0.629363	-0.008158
2	6	0	-2.035390	-0.037213	-0.012926
3	7	0	-0.764612	-0.338332	-0.013354
4	7	0	-0.093756	1.971744	-0.007504
5	7	0	-2.605219	1.207118	-0.002914
6	16	0	-1.602995	2.438779	-0.001462
7	6	0	1.581865	0.244092	-0.004053
8	6	0	1.932968	-1.132803	-0.005531
9	6	0	3.262534	-1.502336	0.003782
10	6	0	4.290994	-0.532487	0.012316
11	6	0	3.934847	0.833665	0.015508
12	6	0	2.611010	1.224531	0.006062
13	1	0	1.150950	-1.883163	-0.011553
14	1	0	3.526301	-2.555731	0.005978
15	1	0	4.716791	1.586712	0.027223
16	1	0	2.352165	2.277288	0.009669
17	6	0	-3.061862	-1.186596	-0.000605
18	9	0	-3.937718	-0.997369	-0.991052
19	9	0	-2.456125	-2.359117	-0.153824
20	9	0	-3.706683	-1.161506	1.171577
21	6	0	5.730516	-0.951264	-0.005749
22	1	0	5.890255	-1.863247	0.577917
23	1	0	6.041260	-1.172631	-1.036990
24	1	0	6.388712	-0.165183	0.373365

Ph CF_3 cation 5c

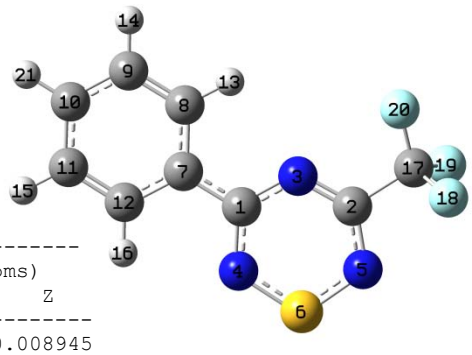

Geometry

Center Number	Atomic Number	Atomic Type	Coordinates (Angstroms) X	Y	Z
1	6	0	-0.636275	0.513189	-0.008945
2	6	0	1.653409	0.033018	-0.013833
3	7	0	0.408602	-0.370053	-0.014005
4	7	0	-0.447232	1.874677	-0.007625
5	7	0	2.117031	1.317930	-0.001359
6	16	0	1.019060	2.465467	0.001012
7	6	0	-1.979888	0.014613	-0.005419
8	6	0	-2.209211	-1.385925	-0.007622
9	6	0	-3.508001	-1.866425	-0.001373
10	6	0	-4.587193	-0.969115	0.006680
11	6	0	-4.371389	0.416997	0.008234
12	6	0	-3.079224	0.914014	0.002232
13	1	0	-1.365581	-2.066112	-0.014584
14	1	0	-3.690389	-2.935944	-0.002939
15	1	0	-5.215207	1.098897	0.014229
16	1	0	-2.901805	1.983357	0.003566
17	6	0	2.769100	-1.031503	-0.001039
18	9	0	3.647624	-0.750859	-0.966031
19	9	0	3.382047	-0.979514	1.186843
20	9	0	2.260820	-2.243588	-0.191992
21	1	0	-5.603172	-1.353106	0.011589

Cl CF_3 cation 5d

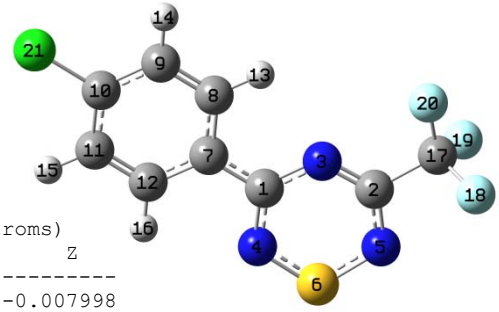

Geometry

Center Number	Atomic Number	Atomic Type	Coordinates (Angstroms) X	Y	Z
1	6	0	0.163776	0.684306	-0.007998
2	6	0	2.376948	-0.072665	-0.011617
3	7	0	1.094022	-0.321905	-0.012380
4	7	0	0.516107	2.012244	-0.004998
5	7	0	2.994369	1.147923	-0.002314
6	16	0	2.043745	2.419957	0.000853
7	6	0	-1.227484	0.352398	-0.006390
8	6	0	-1.627587	-1.010093	-0.011471
9	6	0	-2.968237	-1.339995	-0.007914
10	6	0	-3.931830	-0.313656	0.000860
11	6	0	-3.556403	1.042641	0.005627
12	6	0	-2.216223	1.372818	0.001879
13	1	0	-0.874320	-1.789233	-0.018524
14	1	0	-3.285257	-2.376798	-0.011860
15	1	0	-4.318892	1.813304	0.012309
16	1	0	-1.917435	2.414846	0.005711
17	6	0	3.356748	-1.262806	0.000471
18	9	0	4.230418	-1.114027	-0.998186
19	9	0	4.010445	-1.255503	1.167420
20	9	0	2.702013	-2.409981	-0.140483
21	17	0	-5.602331	-0.726550	0.005713

CF_3 CF_3 cation 5e

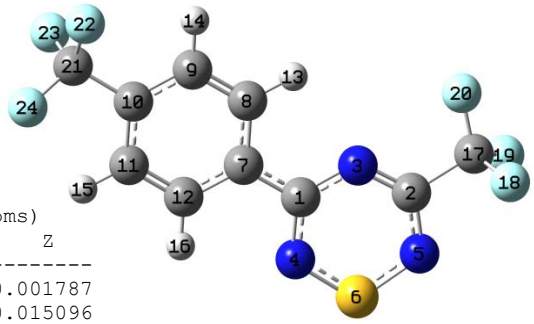

Geometry

Center Number	Atomic Number	Atomic Type	Coordinates (Angstroms) X	Y	Z
1	6	0	0.813607	0.737777	-0.001787
2	6	0	2.994512	-0.105376	0.015096
3	7	0	1.699329	-0.301790	0.004208
4	7	0	1.216243	2.050035	0.004888
5	7	0	3.656442	1.088065	0.015773
6	16	0	2.759555	2.398946	0.011597
7	6	0	-0.596469	0.459514	-0.014549
8	6	0	-1.045461	-0.884606	-0.018635
9	6	0	-2.403318	-1.154671	-0.032177
10	6	0	-3.325234	-0.096886	-0.039694
11	6	0	-2.892853	1.236739	-0.040329
12	6	0	-1.537596	1.519966	-0.026959
13	1	0	-0.323596	-1.692680	-0.012325
14	1	0	-2.757073	-2.179596	-0.042753
15	1	0	-3.620354	2.040236	-0.057389
16	1	0	-1.196334	2.548712	-0.028139
17	6	0	3.924939	-1.336057	0.003529
18	9	0	4.568472	-1.359770	-1.168247
19	9	0	4.809992	-1.216831	0.995165
20	9	0	3.222731	-2.452530	0.155216
21	6	0	-4.812395	-0.404125	0.006735
22	9	0	-5.086346	-1.547617	-0.641333
23	9	0	-5.206567	-0.540601	1.284975
24	9	0	-5.528062	0.585391	-0.550932

MeO CF_3 anion 5a

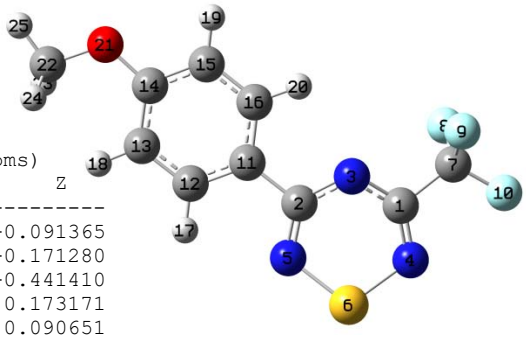

Geometry

Center Number	Atomic Number	Atomic Type	Coordinates (Angstroms) X	Y	Z
1	6	0	2.452266	0.036891	-0.091365
2	6	0	0.265317	0.779439	-0.171280
3	7	0	1.166236	-0.218780	-0.441410
4	7	0	3.102907	1.128255	0.173171
5	7	0	0.465603	2.043017	0.090651
6	16	0	2.124462	2.556368	-0.121420
7	6	0	3.259006	-1.245638	0.108062
8	9	0	2.824602	-1.952353	1.184346
9	9	0	3.149755	-2.072351	-0.962225
10	9	0	4.578749	-1.030707	0.295662
11	6	0	-1.164114	0.327861	-0.116732
12	6	0	-2.204735	1.231467	0.124935
13	6	0	-3.536665	0.815104	0.172656
14	6	0	-3.845650	-0.535139	-0.031182
15	6	0	-2.816892	-1.450913	-0.279657
16	6	0	-1.494252	-1.022123	-0.318331
17	1	0	-1.949576	2.274988	0.278255
18	1	0	-4.315972	1.545288	0.366011
19	1	0	-3.077021	-2.494699	-0.435145
20	1	0	-0.680985	-1.715635	-0.501521
21	8	0	-5.123663	-1.056109	-0.007588
22	6	0	-6.188042	-0.168493	0.254536
23	1	0	-6.092048	0.309263	1.240558
24	1	0	-6.264932	0.619823	-0.508711
25	1	0	-7.100171	-0.771521	0.237190

Tolyl CF_3 anion 5b

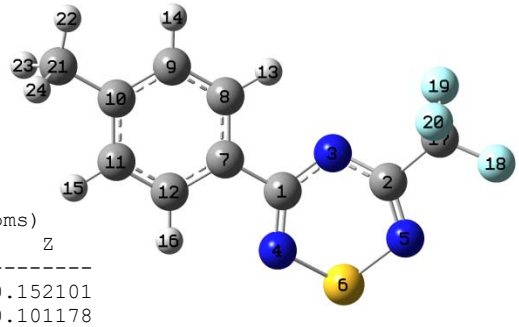

Geometry

Center Number	Atomic Number	Atomic Type	Coordinates (Angstroms) X	Y	Z
1	6	0	0.106855	0.776627	-0.152101
2	6	0	-2.081004	0.034351	-0.101178
3	7	0	-0.790375	-0.222081	-0.432155
4	7	0	-0.096681	2.041188	0.102000
5	7	0	-2.735074	1.125924	0.154169
6	16	0	-1.752365	2.554314	-0.127374
7	6	0	1.537051	0.327893	-0.076515
8	6	0	1.869936	-1.018498	-0.267776
9	6	0	3.200221	-1.438930	-0.208916
10	6	0	4.237397	-0.535851	0.045697
11	6	0	3.897688	0.813337	0.239140
12	6	0	2.575168	1.239344	0.176417
13	1	0	1.060613	-1.715106	-0.456988
14	1	0	3.436182	-2.491856	-0.360195
15	1	0	4.685873	1.538439	0.441519
16	1	0	2.314609	2.282299	0.324302
17	6	0	-2.891592	-1.247896	0.085065
18	9	0	-4.212910	-1.031931	0.259568
19	9	0	-2.772006	-2.070375	-0.987400
20	9	0	-2.469372	-1.959288	1.162967
21	6	0	5.679408	-0.987753	0.102501
22	1	0	5.757907	-2.078938	0.037973
23	1	0	6.271935	-0.566516	-0.721954
24	1	0	6.167456	-0.673951	1.035018

Ph CF_3 anion 5c

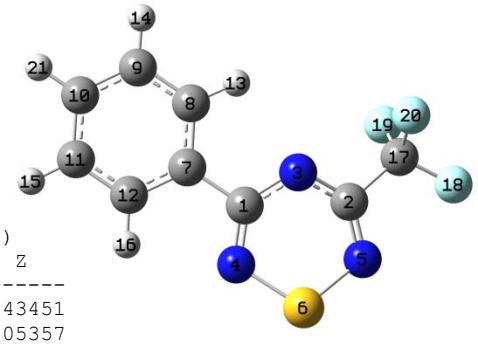

Geometry

Center Number	Atomic Number	Atomic Type	Coordinates (Angstroms) X	Y	Z
1	6	0	-0.554889	0.659572	-0.143451
2	6	0	1.692311	0.121939	-0.105357
3	7	0	0.428223	-0.253960	-0.424946
4	7	0	-0.466830	1.938795	0.102030
5	7	0	2.244969	1.270581	0.138717
6	16	0	1.132808	2.601108	-0.142488
7	6	0	-1.938408	0.081145	-0.054923
8	6	0	-2.141030	-1.294262	-0.237488
9	6	0	-3.424649	-1.839076	-0.169825
10	6	0	-4.526203	-1.020399	0.086172
11	6	0	-4.331871	0.352905	0.270365
12	6	0	-3.051747	0.898051	0.197870
13	1	0	-1.267933	-1.908512	-0.428357
14	1	0	-3.564362	-2.909061	-0.314345
15	1	0	-5.183969	1.000421	0.470314
16	1	0	-2.883596	1.961187	0.335155
17	6	0	2.619011	-1.079144	0.081219
18	9	0	3.916111	-0.741225	0.243112
19	9	0	2.272614	-1.819429	1.166641
20	9	0	2.567066	-1.915872	-0.985586
21	1	0	-5.526880	-1.445337	0.141446

Cl CF_3 anion 5d

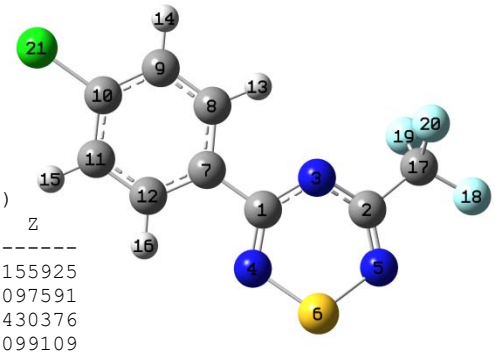

Geometry

Center Number	Atomic Number	Atomic Type	Coordinates (Angstroms) X	Y	Z
1	6	0	0.273251	0.827460	-0.155925
2	6	0	2.424112	-0.012044	-0.097591
3	7	0	1.122383	-0.211506	-0.430376
4	7	0	0.528512	2.081860	0.099109
5	7	0	3.122164	1.049903	0.161025
6	16	0	2.206265	2.523408	-0.111989
7	6	0	-1.176059	0.444246	-0.088733
8	6	0	-1.562555	-0.889383	-0.279399
9	6	0	-2.906478	-1.263495	-0.229673
10	6	0	-3.868339	-0.288532	0.018259
11	6	0	-3.515758	1.047313	0.212426
12	6	0	-2.170496	1.403598	0.154374
13	1	0	-0.780826	-1.618176	-0.462846
14	1	0	-3.202663	-2.297544	-0.377610
15	1	0	-4.282606	1.791549	0.404204
16	1	0	-1.863397	2.434007	0.298939
17	6	0	3.178037	-1.328564	0.085937
18	9	0	4.506881	-1.169591	0.257513
19	9	0	2.725847	-2.019907	1.164167
20	9	0	3.018793	-2.142960	-0.987016
21	17	0	-5.582361	-0.751626	0.087694

CF3 CF3 anion 5e

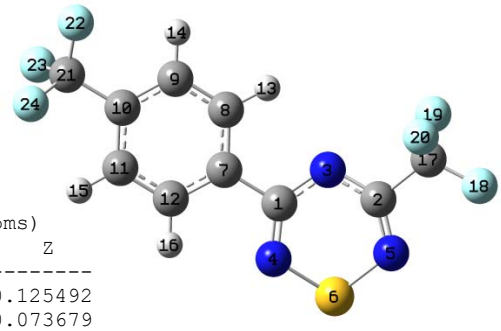

Geometry

Center Number	Atomic Number	Atomic Type	Coordinates (Angstroms) X	Y	Z
1	6	0	0.917932	0.838595	0.125492
2	6	0	3.018330	-0.042112	0.073679
3	7	0	1.717985	-0.224187	0.363710
4	7	0	1.221373	2.060940	-0.092459
5	7	0	3.711843	0.997351	-0.141207
6	16	0	2.870983	2.470484	0.105703
7	6	0	-0.551933	0.512039	0.069725
8	6	0	-0.989249	-0.795934	0.224642
9	6	0	-2.341659	-1.099707	0.180573
10	6	0	-3.270036	-0.094768	-0.023269
11	6	0	-2.842617	1.218857	-0.179448
12	6	0	-1.496730	1.517124	-0.131669
13	1	0	-0.258246	-1.564428	0.375698
14	1	0	-2.664257	-2.117430	0.298257
15	1	0	-3.560822	2.002256	-0.342561
16	1	0	-1.154545	2.525882	-0.252165
17	6	0	3.759528	-1.363565	-0.072681
18	9	0	5.059065	-1.224236	-0.264475
19	9	0	3.614103	-2.120213	1.008601
20	9	0	3.296045	-2.069001	-1.098950
21	6	0	-4.737277	-0.395225	-0.032846
22	9	0	-4.996246	-1.677838	-0.253954
23	9	0	-5.325828	-0.089103	1.121241
24	9	0	-5.386472	0.293216	-0.966459